(2)

NRL Memorandum Report 4745

Technical Analysis of a Proposed Ship-to-Ship Chemical Laser Transmission Experiment

D. H. LESLIE, P. B. ULRICH, AND G. L. TRUSTY

Applied Optics Branch
Optical Sciences Division

February 16, 1982

NAVAL RESEARCH LABORATORY
Washington, D.C.

DISCLAIMER NOTICE

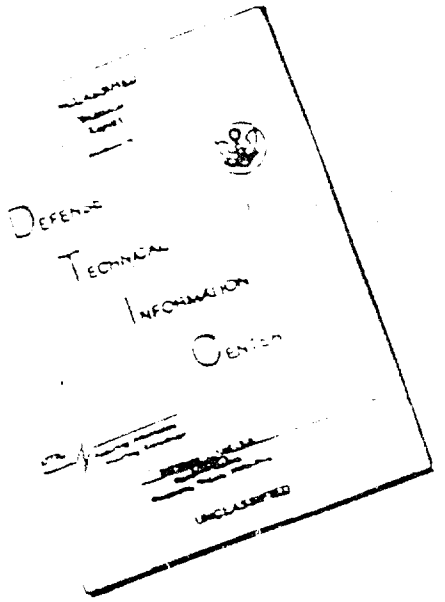

THIS DOCUMENT IS BEST QUALITY AVAILABLE. THE COPY FURNISHED TO DTIC CONTAINED A SIGNIFICANT NUMBER OF PAGES WHICH DO NOT REPRODUCE LEGIBLY.

SECURITY CLASSIFICATION OF THIS PAGE (When Data Entered)

REPORT DOCUMENTATION PAGE

READ INSTRUCTIONS BEFORE COMPLETING FORM

1 REPORT NUMBER: NRL Memorandum Report 4745	2 GOVT ACCESSION NO.: AD-A113 564
3 RECIPIENT'S CATALOG NUMBER	
4 TITLE (and Subtitle): TECHNICAL ANALYSIS OF A PROPOSED SHIP-TO-SHIP CHEMICAL LASER TRANSMISSION EXPERIMENT	5 TYPE OF REPORT & PERIOD COVERED: Interim
6 PERFORMING ORG. REPORT NUMBER	
7 AUTHOR(s): D. H. Leslie, P. B. Ulrich, and G. L. Trusty	8 CONTRACT OR GRANT NUMBER(s)
9 PERFORMING ORGANIZATION NAME AND ADDRESS: Naval Research Laboratory, Washington, D.C. 20375	10 PROGRAM ELEMENT, PROJECT, TASK AREA & WORK UNIT NUMBERS: 65-F201-0-1, 65-F201-A-1
11 CONTROLLING OFFICE NAME AND ADDRESS: NAVSEA-PMS/405-35, Washington, D.C. 20362; Naval Ocean Systems Center, San Diego, CA 92152	12 REPORT DATE: February 16, 1982
	13 NUMBER OF PAGES: 172
14 MONITORING AGENCY NAME & ADDRESS (if different from Controlling Office)	15 SECURITY CLASS (of this report): UNCLASSIFIED
	15a DECLASSIFICATION/DOWNGRADING SCHEDULE

16 DISTRIBUTION STATEMENT (of this Report)

Approved for public release; distribution unlimited.

17 DISTRIBUTION STATEMENT (of the abstract entered in Block 20, if different from Report)

18 SUPPLEMENTARY NOTES

19 KEY WORDS (Continue on reverse side if necessary and identify by block number)

Atmospheric Transmission
DF Laser
Aerosol Extinction
Molecular Absorption

20 ABSTRACT (Continue on reverse side if necessary and identify by block number)

Equipment and procedures for performing a DF laser ship-to-ship transmission experiment are described. A low-power, CW DF laser, a Fourier Transform Spectrometer, and a 32" diameter optical tracking system with 50 microradian resolution will be installed aboard the aircraft carrier USS LEXINGTON. A 60 inch-diameter tracking receiver and aerosol and meteorological equipment will be installed aboard an escort ship. Precise absolute transmittance measurements using the laser source, and high resolution infrared spectral measurements using the spectrometer, will be performed between the two ships at separations from 1 to 5 kilometers. The expected precision of

DD FORM 1 JAN 73 1473 EDITION OF 1 NOV 65 IS OBSOLETE
S/N 0102-014-6601

SECURITY CLASSIFICATION OF THIS PAGE (When Data Entered)

20 ABSTRACT (Continued)

the derived data is discussed. The contribution of the experiment results toward improving DF laser propagation model-validation is analysed in great detail. Five appendices contain discussions of tracker and optical engineering details and a discussion proposing related LIDAR measurements.

Successful completion of the project, we conclude, will provide the Navy and HEL community with a dual large aperture tracking system for performing significant atmospheric transmission measurements using a ship-based, combustion-driven DF laser.

CONTENTS

LIST OF ILLUSTRATIONS

LIST OF TABLES

EXECUTIVE SUMMARY

As a significant first step toward development of an HEL shipboard system, PMS/405 and NAVSEA/EOMET have funded NRL to perform an at-sea, ship-to-ship DF laser transmission experiment. Evaluation of the prototype equipment developed under this program, and subsequent analysis of the laser transmittance data obtained during the experiment will permit one to evaluate how realistic the modeling to date has been, and will examine near ship boundary layer problems for the first time. The specific goals of the ship-to-ship experiment are:

(1) To validate models predicting the propagation of DF laser radiation through the marine atmosphere by measuring the infrared transmittance between two ships at sea.

(2) To evaluate the utility of using current meteorological instrumentation for predicting electro-optic systems performance in the marine environment.

(3) To determine whether shipboard transmittance measurements correlate with existing land-based measurements.

(4) To demonstrate the feasibility of operating a large aperture, precision optical tracker aboard a Navy ship.

(5) To demonstrate the feasibility of operating an NF_3 combustion-driven DF laser aboard a Navy ship.

This document provides a thorough analysis of all facets of the experiment. Particular attention is given to assessing the expected quality of the measurements, and to discussing the eventual usefulness

of the results in current Navy laser transmission modeling efforts.

We provide a review of the project to date, and then immediately begin the discussion of laser transmission measurement. The *absolute transmittance* experiment involves directing a low power (100 mW), line-selectable DF laser through a converted Nike/Hercules mount and a 0.8 meter cassegrain telescope. This equipment will be mounted in the hanger deck of the aircraft carrier USS LEXINGTON, and operated during flight training operations. The laser beam receiver will be a converted 60" searchlight operated as a "light-bucket" aboard an escort ship. This receiver will also be operated as a pointable tracker. Both tracking devices are computer controlled via quad-cells and a dedicated GaAs data link. The second half of the transmittance experiment reverses the direction of propagation: a blackbody source at the focus of the 60" element is directed across the intership path and into the 32" receiver and directed into the entrance aperture of a high resolution Fourier Transform Spectrometer (FTS) tuned to operate at 2-12 μm. This is the *relative transmittance* part of the experiment, and will provide high resolution molecular spectra of the path between the ships.

In this report, we provide an extensive study of sources of transmittance error in this experiment, based on NRL experience over the past 7 years with land based transmission experiments. We discuss specific and extensive improvements for this experiment. The transmittance error in the *absolute* measurement is estimated at 2%, and the *relative* measurement transmittance error is shown to be 1%. The Beer's law relation between transmittance and extinction, $T = \exp[-(k_a + k_m) L]$, is then employed to derive a relation between the expected errors in transmittances, and the resulting expected errors in aerosol extinction, k_a, and molecular extinction, k_m. It is shown that for all atmospheric conditions likely to occur aboard LEXINGTON, and for all pathlengths greater than 1 km, high quality data on aerosol extinction and molecular absorption is obtainable. We use $\leq 10\%$ for error in k_m and $\leq 20\%$ for error in k_a as indication that the results are useful and of high quality, e.g., the precision needed to verify the various propagation codes.

Chapter three then goes into great detail to show what modeling problems in atmospheric transmission can be examined with data of the intrinsic quality as described above. In particular, the aerosol measurements will provide open-ocean data of use for validating the LOWTRAN maritime models, and as input to the Wells-Katz-Munn model relating aerosol extinction to wind speed and humidity. Near-ship effects related to aerosols such as bow vs stern wind conditions, and height above the sea surface can also be examined with aerosol extinction data of 20% accuracy. Besides the absolute transmittance data, aerosol measurements will also be made with a Knollenberg particle-size spectrometer and a nephelometer. Also an aerosol mass monitor normally used for "dry" aerosols will be tested in the marine environment. The correlation between transmission measurements and Met observables is discussed. Simple relations between extinction and Met observables are needed for Tactical Decision Aids (TDA).

The molecular absorption data, with expected error in absorption coefficient k_m of 10% or less, will address the following three problems for which complete understanding still does not exist: using the large optical depth of up to 100 torr-km to resolve the White vs Burch 3.5-4.2 μm water continuum modeling problem; using the high resolution FTS spectra to narrow the error bars on the 0.03% HDO/H_2O isotopic water vapor ratio; and providing a path-integrated water vapor concentration measurement of use to separate the water continuum and aerosol extinctions.

A more subtle, but perhaps in the long run a more serious problem of HEL propagation which this measurement addresses is: how well can open ocean DF laser *absorption* (k_m) be predicted from met observables? A thermal blooming sensitivity study is outlined, and a 10% error in knowledge of the molecular absorption is interpreted in terms of accuracy in predicting fluence vs range on an incoming target. This information is required to determine time/power on target.

In addition to the discussion outlined above, we have provided corroborative material in five appendices. *Appendix A* provides a milestone of January 11, 1982, when NRL will provide PMS/405 a

detailed report describing results of tracker at-sea-simulation studies from measurements at NRL's Chesapeake Bay Division. *Appendix B* contains two documents written by Massachusetts Manufacturing Corporation, who have been contracted by us to provide engineering work on the Nike/Hercules tracker mount. Details of design parameters in the servo-systems, optical data links, quad-cell performance parameters, infrared detector signal-to-noise calculations, and detailed analysis of the feedback systems is provided in two documents. *Appendix C* is a reprint of a published article by Richard Horton describing the design optimization involved in the final tracker telescope and relay mirror configuration. *Appendix D* contains the results of a computerized ray trace analysis of the design described in C. The calculations were performed by Research Optics, Inc., of Baltimore, Maryland, and the results indicate that (1) the tracker optical design has indeed been optimized, (2) simplification of the design is not possible without performance sacrifice, and (3) considering the constraints imposed by relaying the optical beam through the tracker mount, the final configuration is an impressive optical design achievement. *Appendix E* is authored by Prof. T. D. Wilkerson of the University of Maryland Institute of Physics and Technology. He describes what LIDAR measurements might be obtained in the ship-to-ship experiment by employing one of several established LIDAR groups. A more interesting possibility is then described - the use of a pulsed DF LIDAR to obtain water vapor concentration profiles in the wavelength region of interest. Appendix E concludes with a description of what benefit the Navy HEL program might gain from using a sophisticated, multiuse LIDAR at sea.

The impact of the DF laser ship-to-ship transmission experiment will be far-reaching. We anticipate the aerosol extinction results will require the addition of an "open-sea" aerosol model to LOWTRAN since results will probably point out additional inadequacies in the present "maritime" model for open sea predictions. Aerosol measurements will provide additional data for validation of the Wells-Katz-Munn extinction model. Water vapor continuum models and the isotopic water HDO/H_2O ratio problem will be directly addressed by the high resolution infrared spectral measurements. The accuracy of thermal blooming models will be addressed when the ability of meteorological measurements

to predict DF absorption is determined. And a final achievement will be the demonstration of the use of a dual, large aperture tracking system to perform significant atmospheric transmission measurements using a ship-based, combustion-driven chemical laser.

TECHNICAL ANALYSIS OF A PROPOSED SHIP-TO-SHIP CHEMICAL LASER TRANSMISSION EXPERIMENT

I. BACKGROUND ON THE PROBLEM

Since 1979 the Optical Sciences Division of the Naval Research Laboratory (NRL) has been supported by PMS-405 and the EOMET program, to perform absolute transmittance measurements between two ships. The spectral region of interest is 3.5 – 4.2 microns, the DF laser operating region. As originally tasked, a Xenon laser (line selectable from 2 – 12 microns) was to be employed with a Fourier Transform Spectrometer (FTS) and aerosol and meteorological equipment to obtain absolute transmittance measurements in a manner similar to that successfully used by NRL in a series of land and sea-coast measurements.[1-10] The obvious difference in the ship-to-ship measurement is the necessity for two tracking systems to keep the source and receiver in optical alignment for a period of ten minutes or so. In FY 81 the task was altered to require the use of combustion driven DF chemical laser as the calibration source, rather than the Xenon laser. The substitution of the DF source complicated planning due to safety and logistical considerations. These problems have been examined, and to a large extent solved. We believe that a successful experiment is now moving from the planning and procurement stage to the assembly and execution stage.

The purpose of this document is to closely examine the scientific justification for completing the program. The absolute transmittance measurement as now configured has a very high probability of success, will contribute valuable data on open-sea transmittance such that codes may be verified (or modified), and will have a substantial operational impact on future Navy HEL planning in the areas of thermal blooming, scaling laws, optical turbulence and its compensation, and in defining accurate micro-met requirements.

Manuscript submitted December 9, 1981.

We will first describe the details of the experiment as it is now configured. We will examine in detail the precision of transmittance measurements required to provide data of high enough quality such that meaningful conclusions regarding aerosol extinction and molecular absorption may be drawn. We will demonstrate how this data affects present Navy codes which predict laser and broad-band optical transmission in the infrared. We will detail and quantify the error in transmittance expected from several possible sources: Met parameters, turbulence, diffraction, blooming, tracker jitter, etc. The net expected error in extinction for both aerosols and molecular absorption will be derived from the expected transmittance error for assumed realistic meteorological extremes expected aboard LEXINGTON. From this analysis we can project a figure-of-merit for the transmittance data compared with model predictions. The predictive capability of codes such as LOWTRAN,[11] HITRAN,[12] and aerosol models such as the Wells-Katz-Munn (WKM) model for predicting aerosol extinction from wind speed, temperature, and humidity[13, 14] will be examined. These modeling abilities are of great value to the Navy at present for such fundamental tasks as the design of laser devices, and the design of tactical decision aids (TDA) for in-the-field use of laser devices.

The most important outcome of the ship-to-ship experiment will be the creation of a unique data base for code verification and design of future devices. We demonstrate in this document that the experiment has been properly designed such that high quality data and practical conclusions will result.

II. SHIP TO SHIP MEASUREMENT OF ABSOLUTE TRANSMITTANCE AND HIGH RESOLUTION INFRARED SPECTRAL MEASUREMENTS

The transmittance measurements involve two separate experiments which share the same optical, tracking, data reduction, and support equipment.

A. Absolute Transmittance Measurements

The absolute transmittance source is the combustion driven DF laser, which served NRL experiments well for over five years burning F_2. The device is now completing modifications at TRW to burn the safer fuel NF_3. The laser output beam is coupled through transfer optics, collimated, and sent out through a 32" Cassegrain telescope, across an intervening path of 0.5 to 5.0 km, captured by a 60" searchlight mirror (the so called light bucket) mounted on the escort ship. Details of the optical train in the trucker may be found in Appendix B. A pyroelectric detector is mounted at the focus of the 60" receiver on a turret mount. Appendix B-2 describes a preliminary estimate of the expected S/N at this detector considering a previous optical design involving a complicated triplicate mirror. We have since examined the quality of the 60" device focus (a blur circle of less than 1.5 mm). The quality was much higher than originally expected, so we have replaced the triple mirror design with a much simpler receiver. In the present configuration we estimate a S/N of 10^3 to 10^4, based solely on D*, a reasonable laser power of 100 mWatts, and simple phase sensitive detection. Hence we expect far less than 0.5% transmittance error due to noise in the detection system. The captured signal is sent back to LEXINGTON for processing via the data link described in detail in the Appendix. The signal is ratioed against a reference signal from the reflecting chopper to ratio out fluctuations in the laser power. Previous experience with ratiometers[1,15] has indicated an expected error of 0.4% or less due to the division. We note that we are considering eliminating the ratiometer in favor of a simple division of the signal and reference at the minicomputer control system. This is an example of where technology has progressed since the last NRL transmission field experiments, and where it is to our advantage to use simpler techniques and more reliable digital electronics instead of the analog system used previously.

Our previous results, however, indicated a 2% transmission accuracy over land and sea-coast paths is achievable, but only when turbulence does not cause excursions of the light beam out of the light bucket. Since we are employing the same size source and receiver optics and similar pathlengths, we expect the same situation, or far better, to obtain here, since C_n^2 values on the open sea are typically one to two orders of magnitude less than over land. Thus, we do not expect any problems from beam

wander which the tracker cannot handle. There is, however, a second order effect due to turbulence. The receiver is obscured at its center by the detector turret mount. The total obscured area is 3% of the receiver mirror area. As long as the beam does not vary in size at the receiver, no error is induced. Turbulence, however, may cause some spreading of the beam, so the central obscuration will block proportionately less of the total beam area as the pathlength is increased. Dr. A. Goroch of NEPRF (Naval Environmental Prediction Research Facility) has estimated the r.m.s. beam wander for three values of the index of refraction structure parameter C_n^2 at three ranges.[16-18] The results are presented in Table I below.

Table I — R.M.S. Beam Wander Due to Turbulence

C_n^2	0.5 km	3.0 km	5.0 km
10^{-16} m$^{-2/3}$	0.25 μrad	0.60	0.77
10^{-15}	0.77	1.90	2.40
10^{-14}	2.45	6.00	7.70

The beam spread is less than 10% of the beam wander. The most likely value of C_n^2 for our experiment is about 10^{-15} m$^{2/3}$. The results of Table I can be expected to be within 50% of correct for situations where horizontal homogeneity exists on a scale of about 10 km upwind. In addition, ocean sea-surface temperatures are more uniform than near coastal regions,[18] reinforcing our confidence in the applicability of the above estimates for our experiment.

The above values are to combined with the estimated tracking error, $(\theta_{track}^2)^{1/2} \approx 48\ \mu$rad, and the error due to diffraction at the exit aperture, $(\theta_{diff}^2)^{1/2} \approx 4.75\ \mu$rad, to obtain

$$\theta_{net} = [\theta_{track}^2 + \theta_{diff}^2 + \theta_{turb}^2]^{1/2}$$
$$= 48.8\ \mu\text{rad}$$

which is less than 2% increase above the tracking uncertainty itself. Hence we conclude that for open sea conditions we anticipate negligible error to be introduced by optical turbulence. In any case, since C_n^2 will be monitored during the tests, we can account for this effect in the data reduction.

A final possible degrading effect in transmittance may occur if the tracking system fails to achieve lock-on. This is very unlikely for our projected conditions, however, since the Nike-Hercules mount was designed to track airplanes at much higher rates and accelerations. Furthermore, we have improved its specifications as detailed in Appendix A.

Of the six possible accelerations (roll, pitch, yaw, surge, heave, sway) we concluded that only roll is of any reasonable concern here. Since the aircraft carrier training operations only take place during reasonably calm weather, we have assumed a roll amplitude of $\pm 1^0$ every 12 seconds. The 17.5 mrad amplitude will be handled by a feedback system having a gain of 400, giving 43.6 μrad accuracy as detailed in the Appendix. We point out that the $\pm 1^0$ amplitude assumption allows for a ± 87 meter vertical displacement of the escort ship at a range of 5 km. Hence we are confident that a generous design margin has been built into the system. In addition, a ring of detectors, eight or so, will circle the 60" receiver and provide a warning system in the event that the beam might wander out of the receiver.

The probable maximum errors in transmittance for the absolute transmittance experiments are listed in Table 2 below.

Table 2 — Error Sources in Absolute Transmittance

Element	Error Source		ΔT
1. Pyroelectric Detector	S/N = 10^3 to 10^4		$<<0.5\%$
2. Ratiometer	Analog Divider		$\leqslant 0.4\%$
3. Turbulence	Central Obscuration		$\leqslant 0.5\%$
		TOTAL	$\leqslant 2.0\%$

From the discussion above, and considering NRL's considerable experience with similar experiments in the 1970's we conclude that a transmittance error of 2% or less in absolute transmittance is reasonable to expect.

B. High Resolution Infrared Spectral Measurements

The second part of the transmittance experiment employs the same optics, but in the opposite direction. The turret at the 60" receiver, on the escort ship, is rotated to bring a blackbody source (500 watt tungsten filament in a quartz jacket) into position, and a mirror at the tracker transfer optics is rotated to bring the FTS entrance aperture into alignment, rather than the DF laser exit aperture. The blackbody radiation is sent across the path in a 1/2 degree beam, through the FTS, to the cooled InSb detector. This optical arrangement has been used in numerous NRL high resolution measurements, and a S/N of over 200 has been routinely obtained in the transformed spectra at pathlengths of up to 6.4 km. Typically sampling times of 5 to 15 minutes with about 100 coadded interferograms are used to obtain effective (unapodized) resolution of 0.08 cm^{-1} in the transformed spectra. We note here that the FTS part of the transmittance experiment does not propose to measure absolute transmittance, and no attempt is made to operate in the light bucket mode. Spectral information is acquired, however, and as long as a constant fraction of the blackbody source output is radiated into the entrace aperture of the FTS, quality data with S/N greater than 100 will be obtained.[19] The effect of turbulence will be to add some modulation to the interferogram, but experience has shown that this noise is normalized out by the coaddition process. Based on previous experience, we assume a maximum of 1% for the noise in the transformed spectra.

We have evaluated the two parts of the transmittance experiment and have obtained estimates of 2% accuracy for the absolute transmittance, and 1% accuracy for the relative transmittance. Both estimates have assumed that the tracking portion of the system performs as planned, i.e., 42 microradian tracking noise. Since we are attempting to keep a 32" spot inside a 60" diameter area at the longest (5 km) distance, about 140 microradian precision in tracking is required for the worst case condition. Hence we have a tracking design margin of about three.

III. THE INTRINSIC QUALITY OF THE DATA

The transmittance values themselves are raw data and further analysis is required to extract the extinction coefficients from measured values. There are two relevant mechanisms contributing to the total extinction: aerosol extinction and molecular absorption. The aerosol extinction coefficient, k_a, is the sum of two parts, the aerosol scattering coefficient k_s and the aerosol absorption coefficient k_{abs}. The two parts are related to the real and imaginary parts of the index of refraction of liquid water through Mie scattering theory and absorption efficiency functions Q_{sa} and Q_{abs}. We might also note that at 3.8 microns absorption is only a minor portion of the total aerosol extinction, whether the particles are assumed to be water or salt. Therefore for the purpose of our discussion aerosol extinction and scattering are effectively the same, and hence the total optical extinction is given by the sum of the aerosol and molecular extinction coefficients:

$$k = k_a + k_m$$

with units of reciprocal kilometers km^{-1}. Transmittance and extinction are related by the usual Beer's law relation,

$$T = \exp(-kL)$$

where L is the path length in kilometers. We now derive what probable extinction errors Δk_a and Δk_m are likely to result from the transmittance errors we estimated in Section II. We will assume atmospheric conditions which bracket those conditions most likely to be present during the experiment. Interpretation of the resulting Δk estimates in view of aerosol and molecular modeling will be made in Section IV.

From Beer's Law we get

$$|\ln T| = |kL|$$

$$\frac{\Delta T}{T} = L\,\Delta k + k\,\Delta L$$

$$\frac{\Delta T}{T} = \ln T \left| \frac{\Delta k}{k} + \frac{\Delta L}{L} \right|$$

In our experiment we plan to use a laser range finder which will give us the ship separation to better than 1%, so the fractional error in L will be negligible compared with the other fractional errors. Therefore we obtain the basic relation between extinction error, transmittance error, and transmittance:

$$\frac{\Delta k}{k} = \frac{\Delta T}{T}\left|\frac{1}{\ln T}\right|.$$

The $\ln T$ factor means that a good measurement of extinction requires that the transmittance not be close to 100%. Figure 1 gives a plot of the above relation for a series of values of T[20]. At 37%T the errors in T and k are equal, but at 90% transmission a one percent error in T gives a 10% error in k; and at 98% transmission we get 50% error in k for the same 1% measurement of T. It is for this reason that methods other than transmittance are employed to measure very small absorption coefficients in the laboratory[20] where very long pathlengths are not available. This is especially true of water vapor measurements where the finite dew-point prevents obtaining more than 15 to 20 torr of water in a closed cell at ambient temperatures. For our experiment this means that situations of very high transmittance will not necessarily provide useable data. Of course high transmission conditions are not a cause for concern to operation of the HEL beam.

Table 3 lists three probable extremes of atmospheric conditions with regard to humidity which may occur during our experiment. Intermediate values of water vapor pressure are more likely, although some extremely humid days aboard the LEXINGTON gave over 20 torr of water partial pressure in the summer of 1979, as shown in Fig. 2. We have listed molecular absorption coefficients for the DF laser $P_2(8)$ line as predicted using our HITRAN code and the 1980 AFGL Atlas of absorption line parameters.[12] In addition, we chose to use the "Burch" water vapor continuum,[21] which gives about 5-10% less absorption than the other continuum model in current use, the "White" continuum model.[22] This is not because we prefer one over the other, but for the purpose of this estimation of likely absorption we would rather underestimate than overestimate the predicted results to get highest error estimates, as discussed above. Aerosol extinction values corresponding to dry open sea,[10] humid open

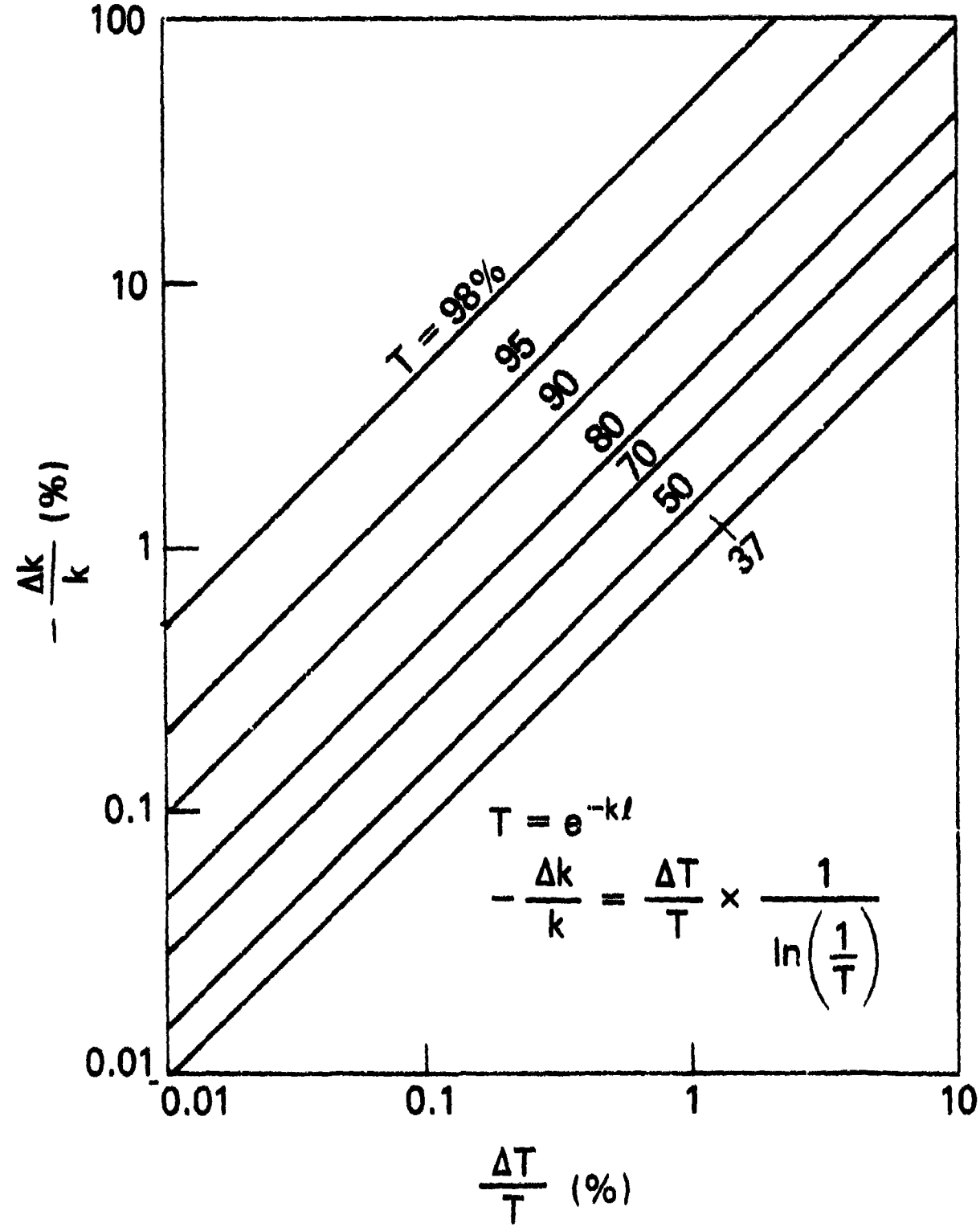

Figure 1 – Extinction coefficient error vs transmittance error for expected values of transmittance

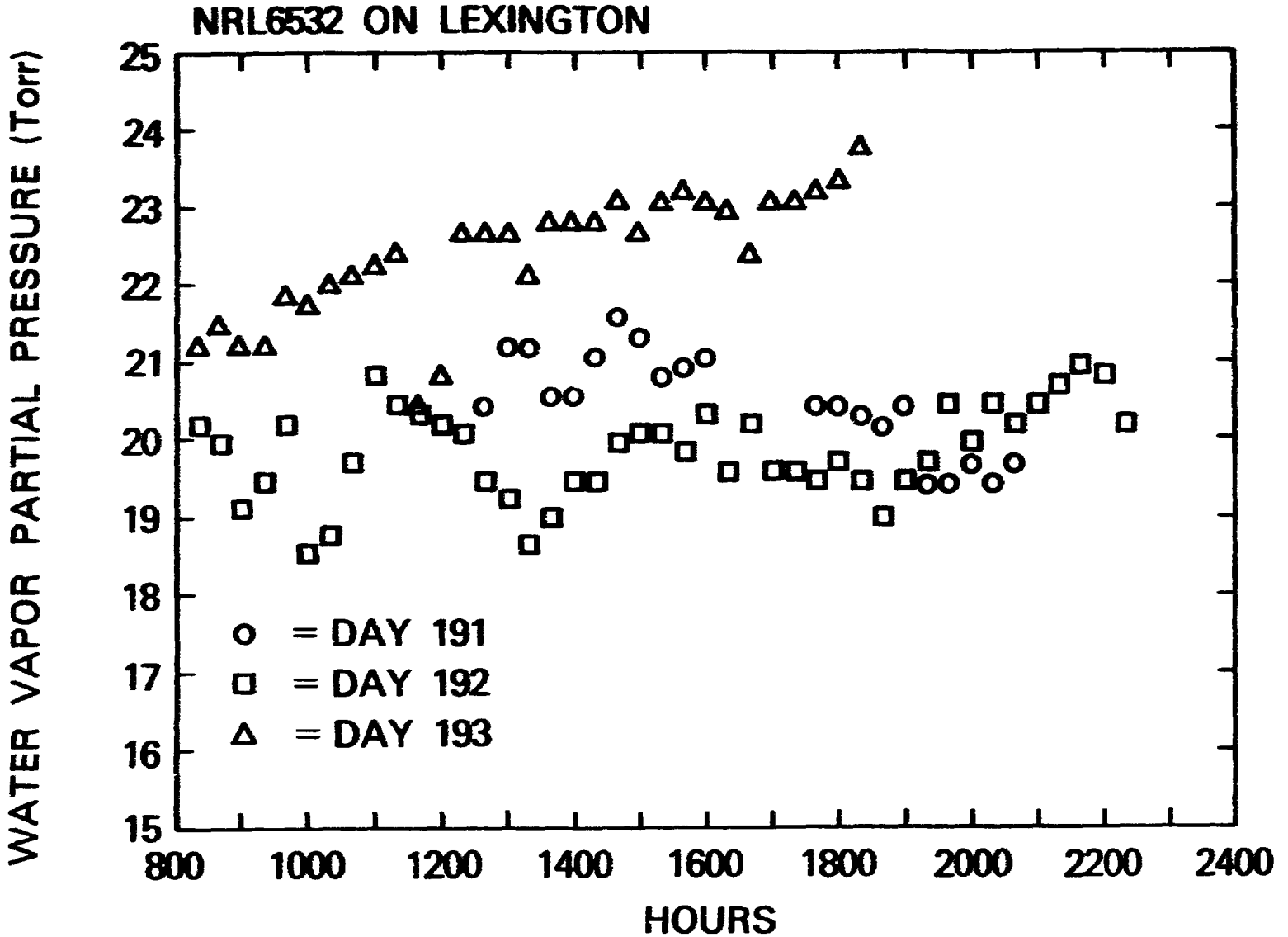

Figure 2 — Water vapor partial pressure aboard USS LEXINGTON for three days in July 1979

sea,[9] and coastal aerosol[3] extinction as calculated using a Mie algorithim and observed particle size distributions are assumed. We note that open sea aerosol extinction is somewhat less than coastal aerosol extinction at the same humidity. We will discuss this point in relation to the "maritime" model in the LOWTRAN code in Section IV, but we only point out here that NRL has access to one of the few truly "open ocean" data bases as the result of several cruises over the past few years.[9,10] Table 3 also lists the Beer's law transmittance at $P_2(8)$ for three pathlengths.

Table 3 — Range of Likely $P_2(8)$ Molecular, Aerosol, and Total Extinction and Resulting Predicted Percent Transmittance for Three Pathlengths

	Dry Open Sea 6.0 torr H_2O	Humid Open Sea 20.0 torr H_2O	Coastal 20.0 torr
k_m	.12 km^{-1}	.037 km^{-1}	.037 km^{-1}
k_a	.020	.030	.150
k_{total}	.032	.067	.187
T(0.5 km)	98.4%	96.7%	91.1%
T(3.0 km)	90.9	81.8	57.1
T(5.0 km)	85.2	71.5	39.3

The 2% estimates in ΔT for the absolute transmittance will be used to determine the likely error in aerosol extinction Δk_a and the 1% estimated error in ΔT for relative transmittance will be used to determine the resulting error in the molecular absorption coefficient Δk_m. These are calculated using the previously derived relation, or estimated using the graph in Figure 2. The results are collected in Table 4, for the three pathlengths.

Table 4 — Fractional Percent Error in Molecular $P_2(8)$ and Aerosol Extinction Coefficient for Three Atmospheric Conditions and for Three Pathlengths

	Pathlength	Dry Open Sea 6.0 torr H_2O	Humid Open Sea 20.0 torr H_2O	Humid Coastal 20.0 torr H_2O
$\Delta k_m/k_m$	0.5 km	62.0%	29.8%	10.7%
	3.0	10.5	5.0	1.8
	5.0	6.2	3.0	1.1
$\Delta k_a/k_a$	0.5 km	12.4%	59.6%	21.4%
	3.0	21.0	10.0	3.6
	5.0	12.4	6.0	2.2

The extremely high uncertainty in the very high transmittance cases are put into perspective when we realize that an inability to distinguish between 97% and 99% is truly a great uncertainty in knowledge of the extinction. The logarithmic term bears this out. Figures 3-5 are HITRAN plots of the spectral region around the $P_2(8)$ laser line, and show the expected transmittance for the parameters listed above. We again see why the short optical depth case is so hard to analyze. The immediate conclusion is that pathlengths as short as 0.5 km are very useful for obtaining information on the near-ship absorption, which may be much higher than the intervening path.

We have worked out the above results for the DF $P_2(8)$ line since it is known to be one of the more powerful lines in the emission from multiline devices, and because it is so well transmitted through the atmosphere. By contrast, the DF $P_1(8)$ line, also a line with significant strength though not as great as $P_2(8)$, is very strongly absorbed by water vapor, in particular, by a strong HDO line. Previous NRL results with the BDL DF laser[2] indicated that although only 5% of the total output power resided in $P_1(8)$, 15% of the total absorption and hence of the thermal blooming was caused $P_1(8)$. Because of the anomalously large blooming effect due to a handful of weak DF lines, some concern should be given to controlling the output power spectral distribution of the device. We therefore, thought it appropriate to repeat the $P_2(8)$ analysis for the $P_1(8)$ parameters, and this is given in Tables 5 and 6 below. Figures 6 through 8 give the corresponding molecular absorption effect on the anticipated transmittance of DF $P_1(8)$.

The above analysis has given predicted uncertainties in extinction coefficients resulting from our assumed uncertainties in transmittance for a likely range of optical depths. For the next section we will go into great detail to establish criteria for assessing the quality of our extinction measurements. Specifically, we will demonstrate that a 10% uncertainty in measured k_m and a 20% uncertainty in measured k_a will contribute substantial results in terms of current laser propagation modeling efforts. Fig-

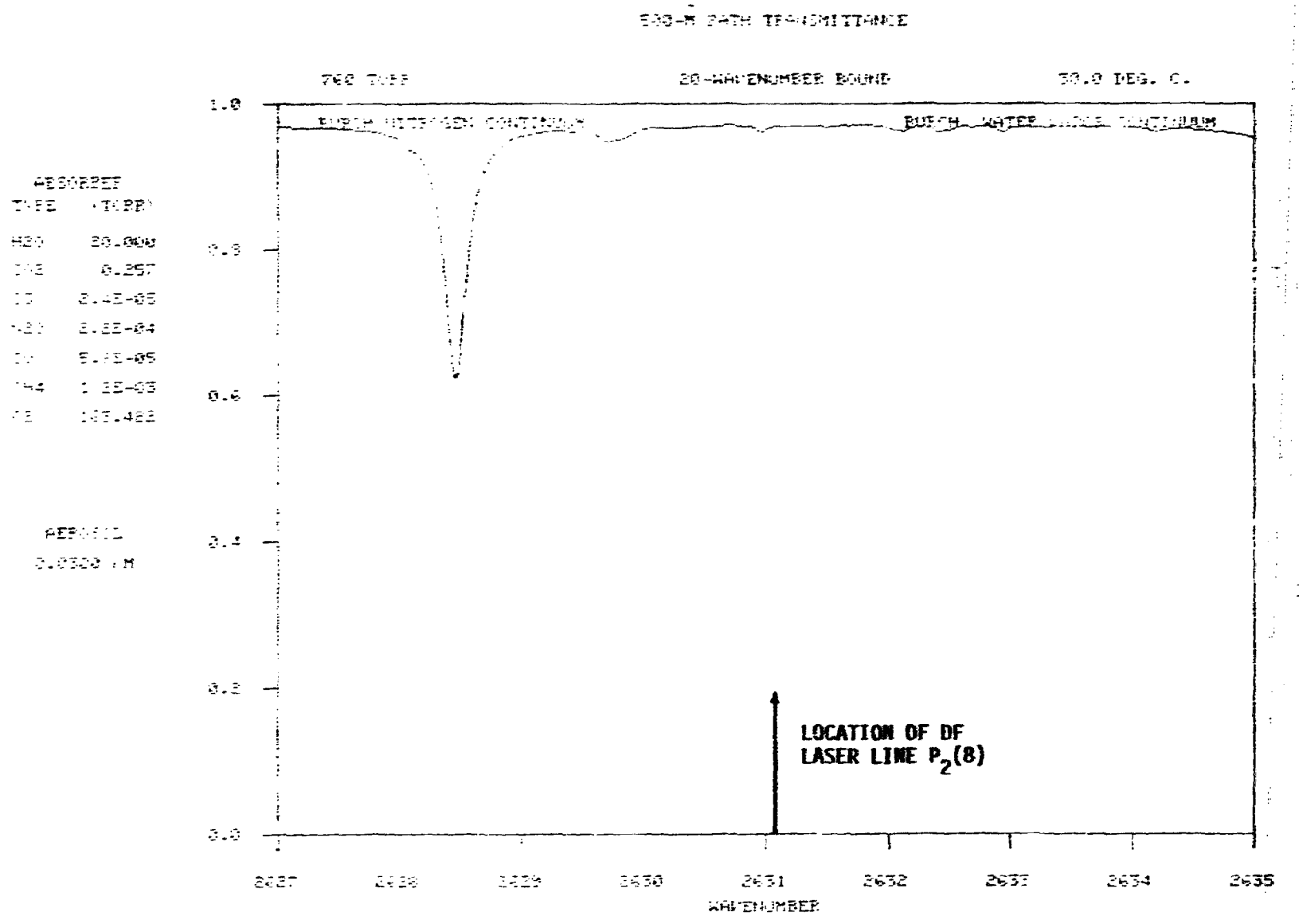

Figure 3 — Calculated transmittance near DF P_2 (8) for 20 torr H_2O and 500 meter path

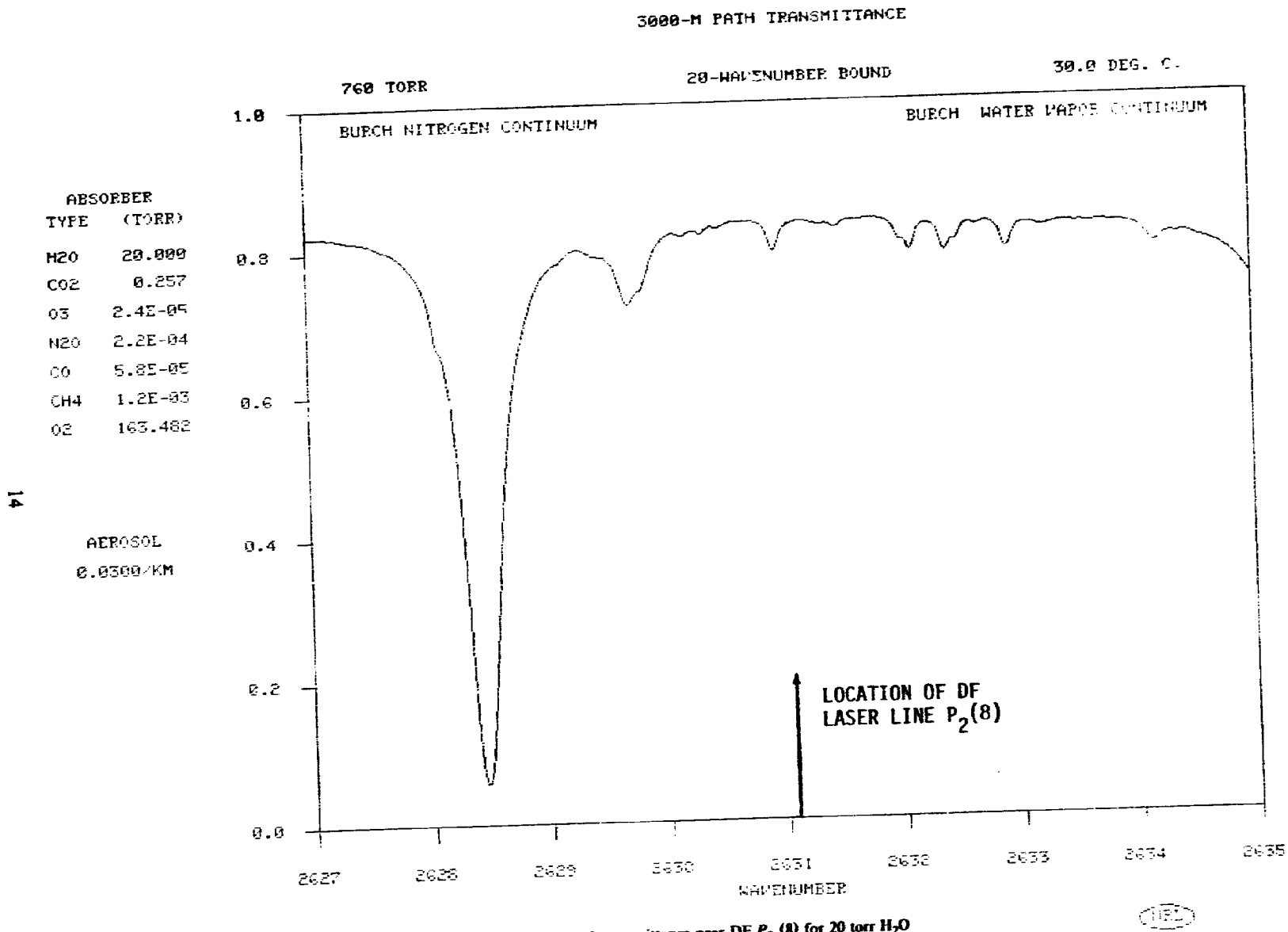

Figure 4 — Calculated transmittance near DF P_2 (8) for 20 torr H_2O and 3.0 km path

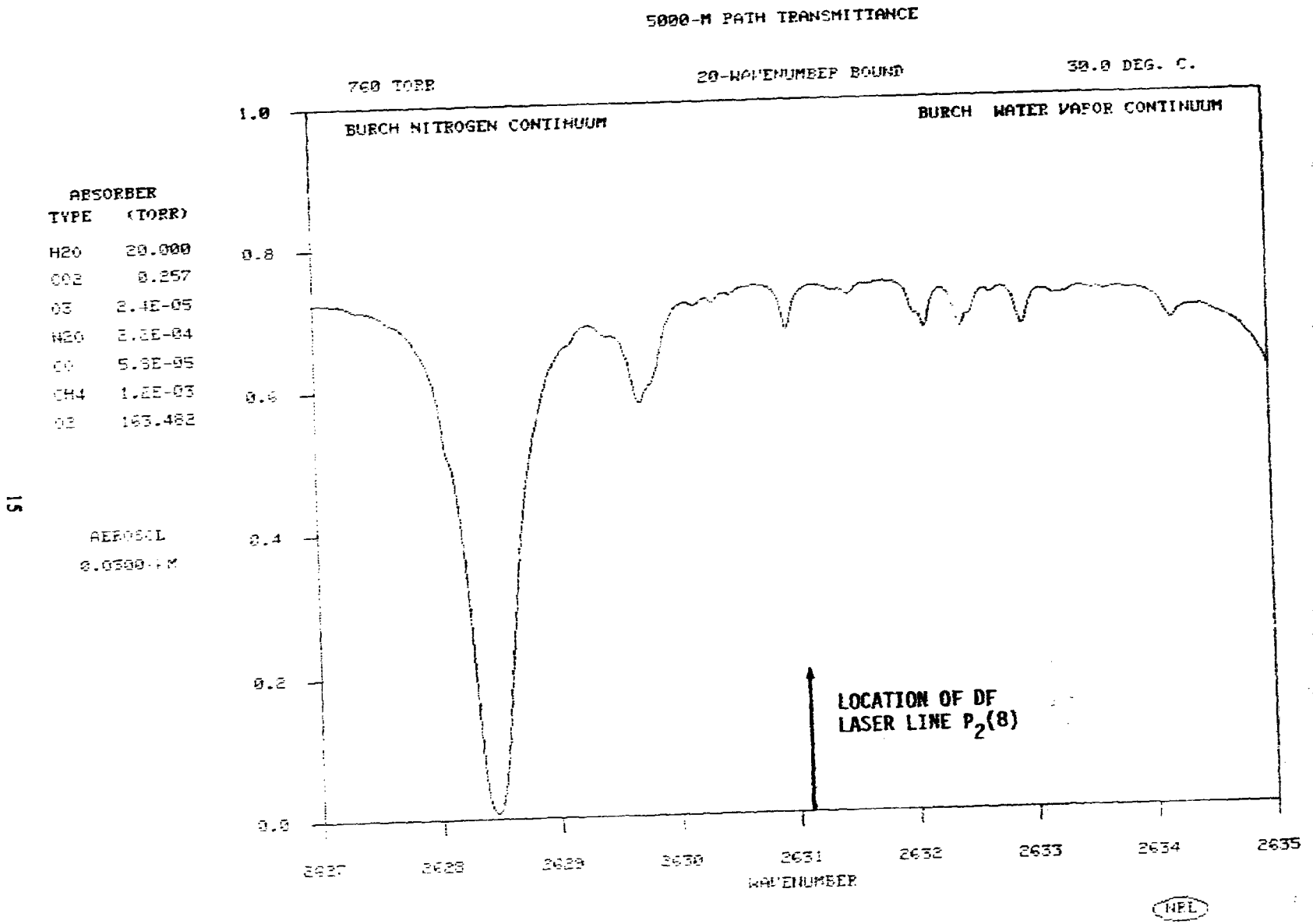

Figure 5 — Calculated transmittance near DF P_1 (8) for 20 torr H_2O and 5.0 km path

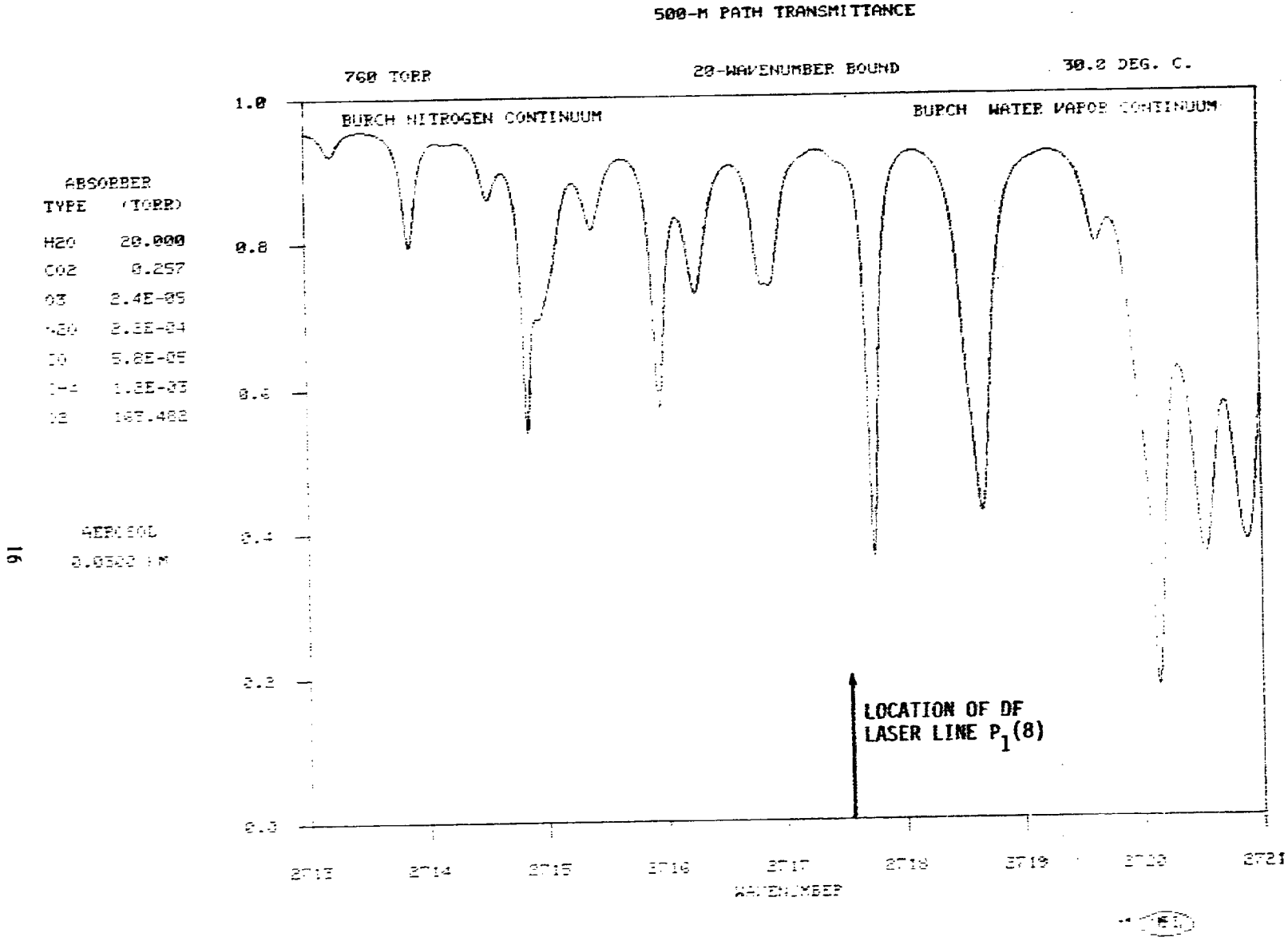

Figure 6 — Calculated transmittance near DF P_1 (8) for 20 torr H_2O and 500 meter path

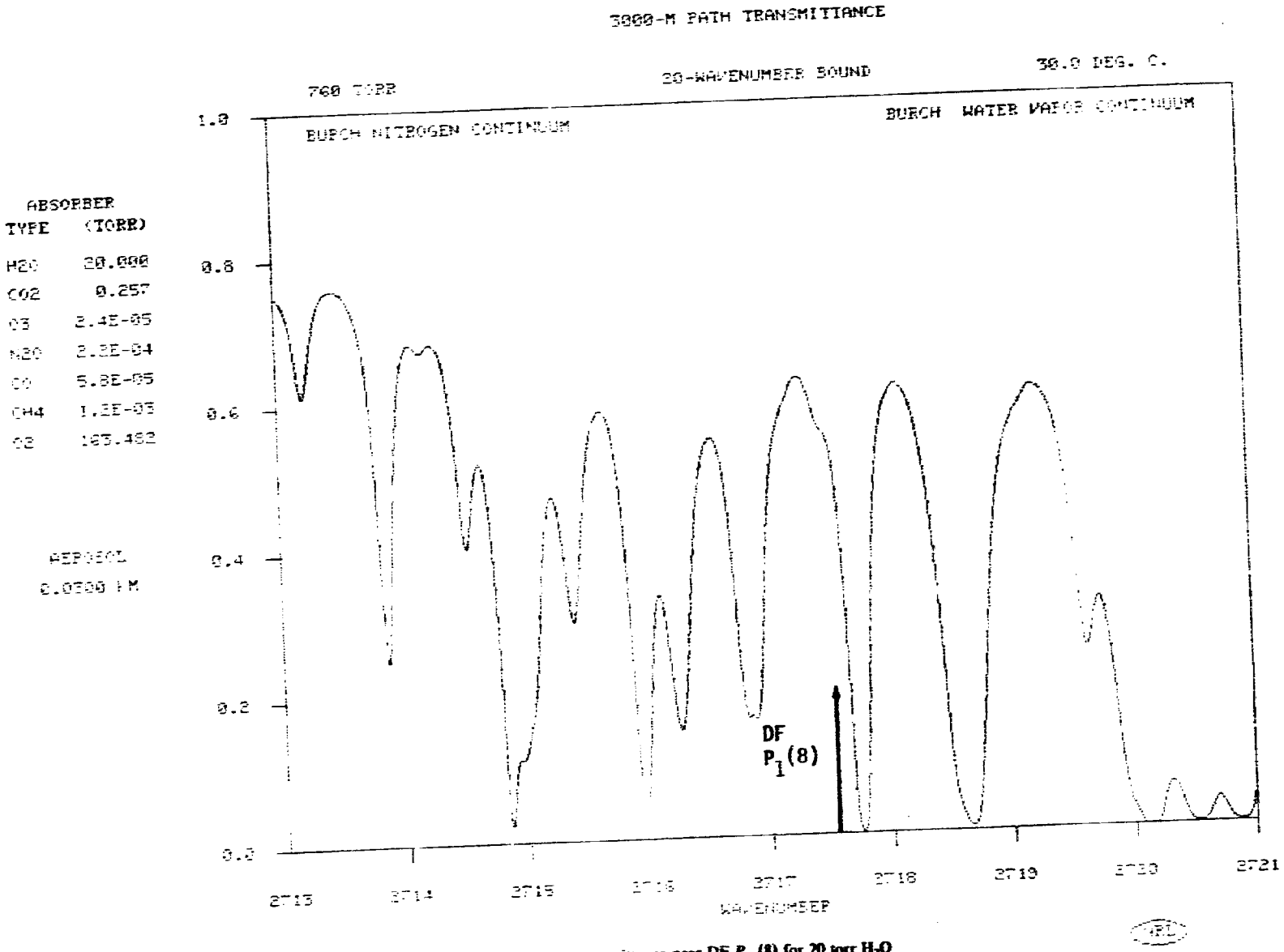

Figure 7 — Calculated transmittance near DF P_1 (8) for 20 torr H_2O and 3.0 km path

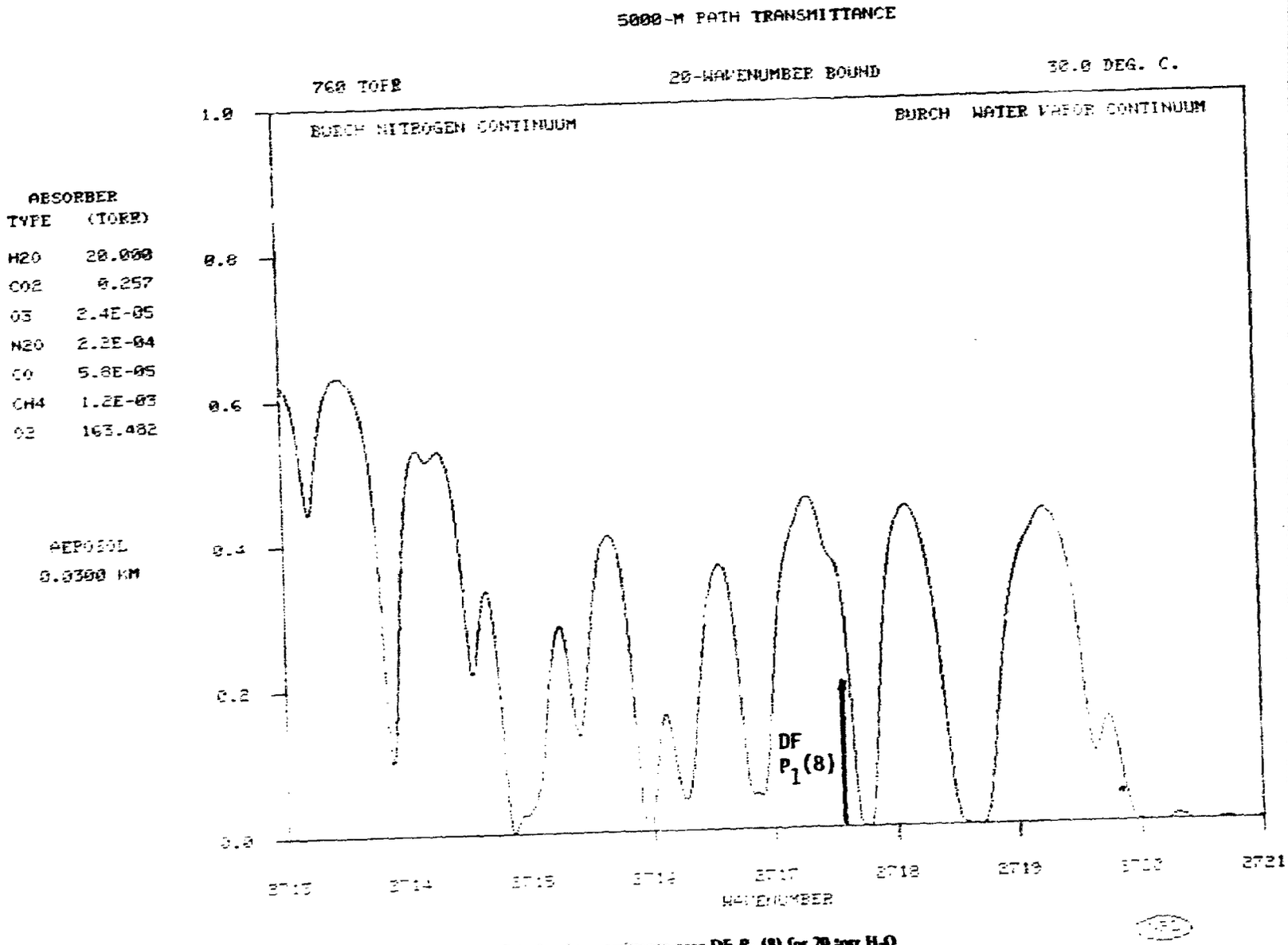

Figure 8 — Calculated transmittance near DF P_1 (8) for 20 torr H_2O and 5.0 km path

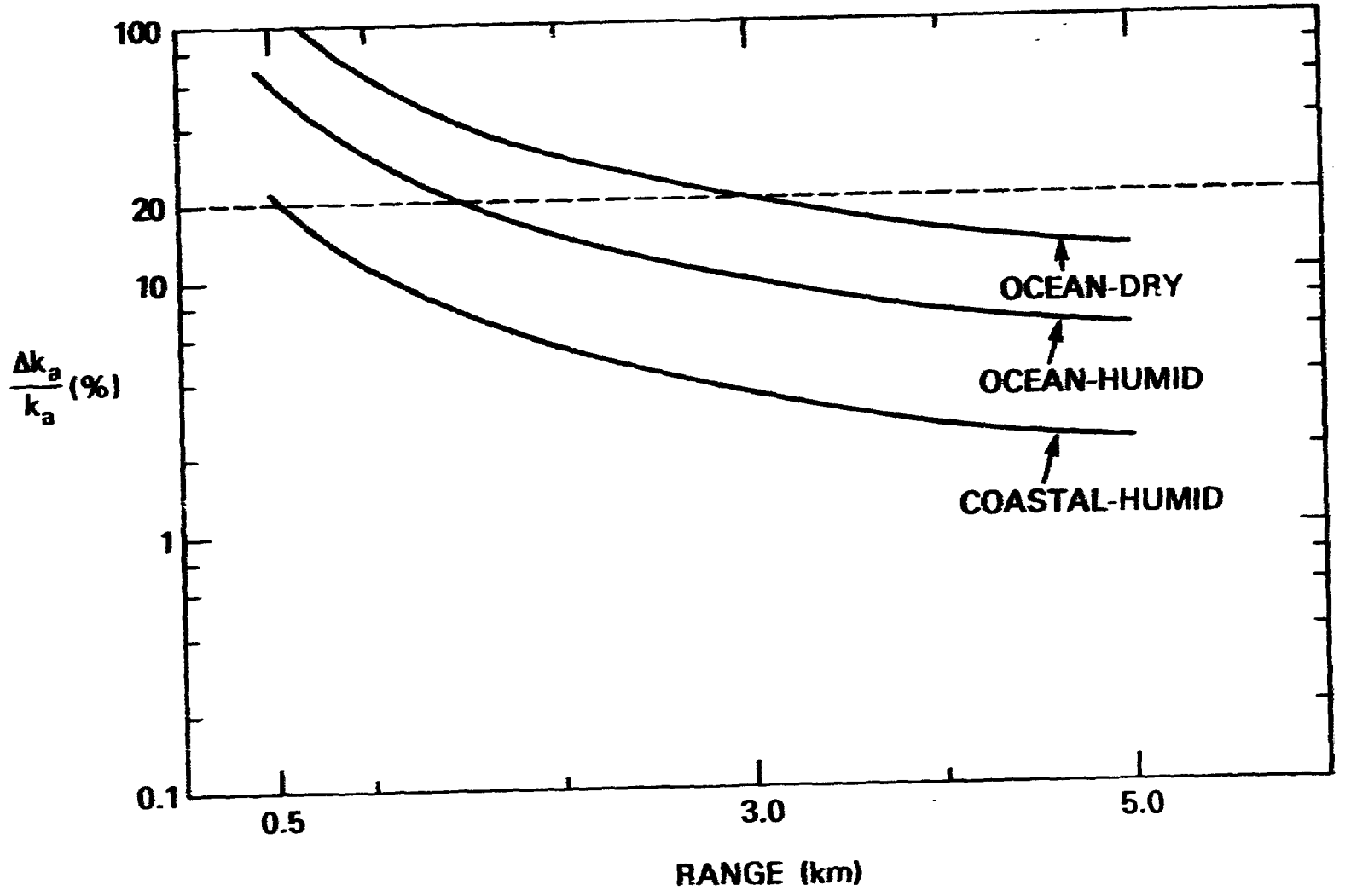

Figure 9 — Percent error in measurement of DF P_2 (8) aerosol extinction vs range for three atmospheric conditions

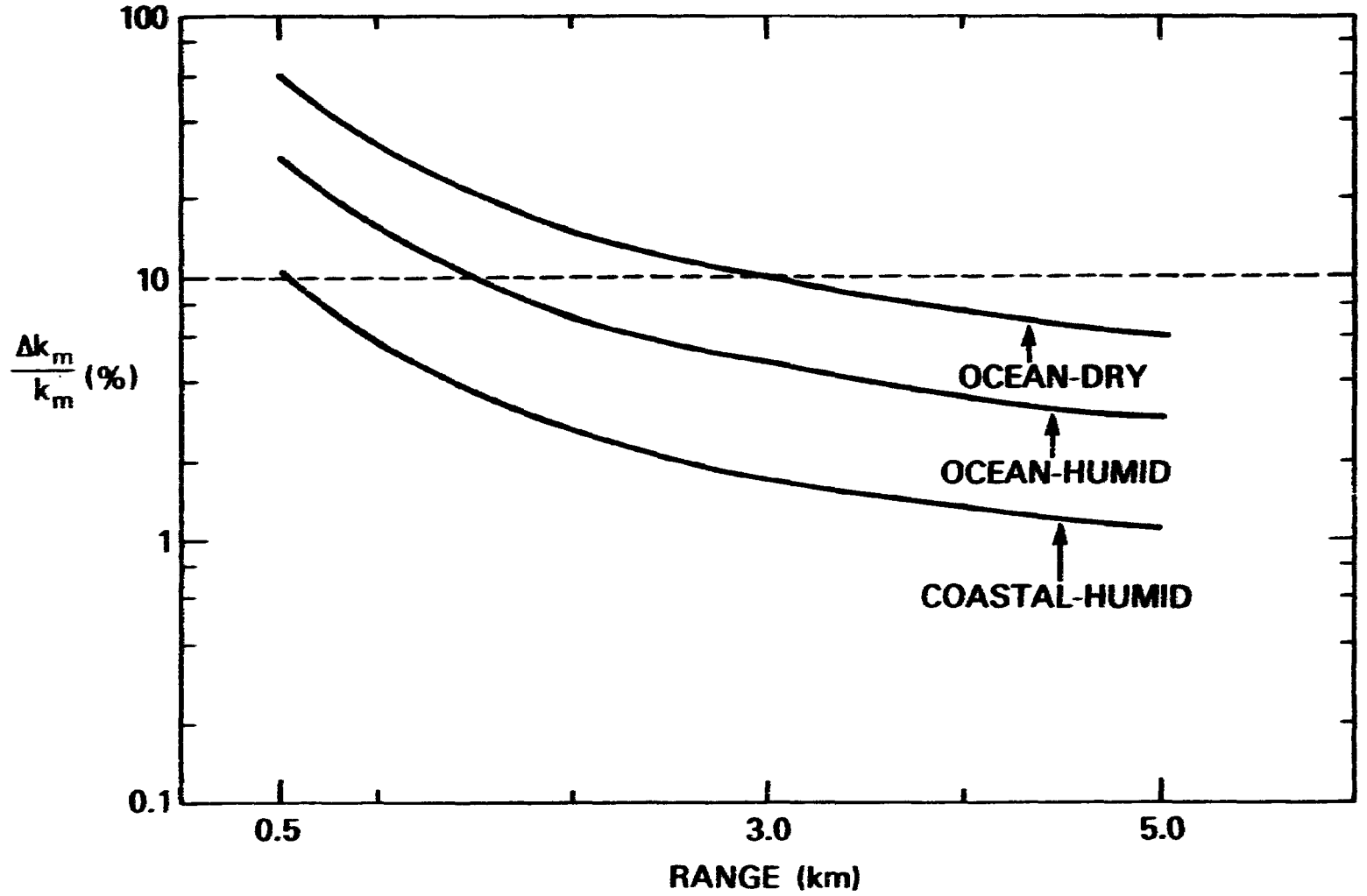

Figure 10 — Percent error in measurement of DF P_2 (B) molecular absorption vs range for three atmospheric conditions

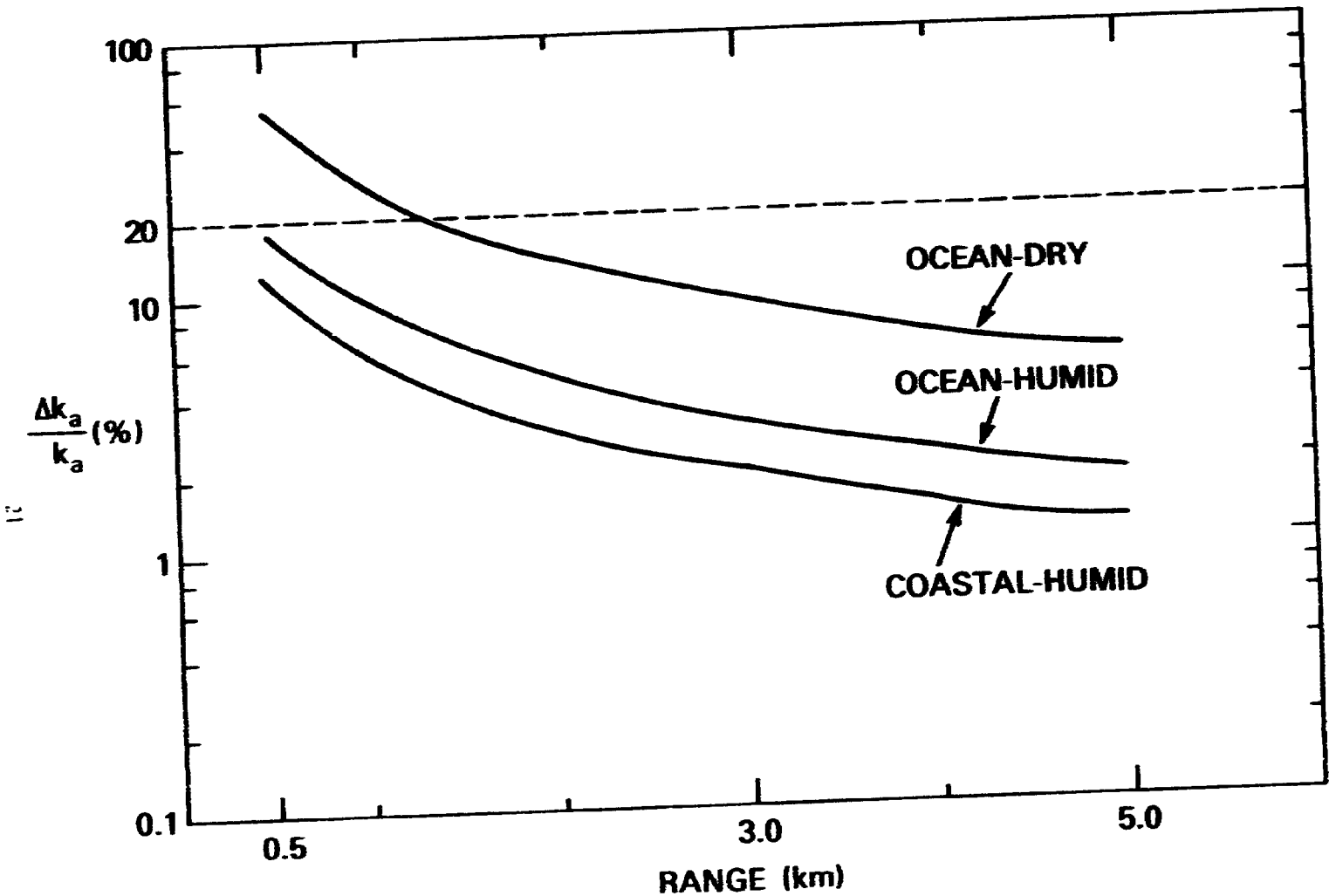

Figure 11 — Percent error in measurement of DF P_r (8) aerosol extinction vs range for three atmospheric conditions

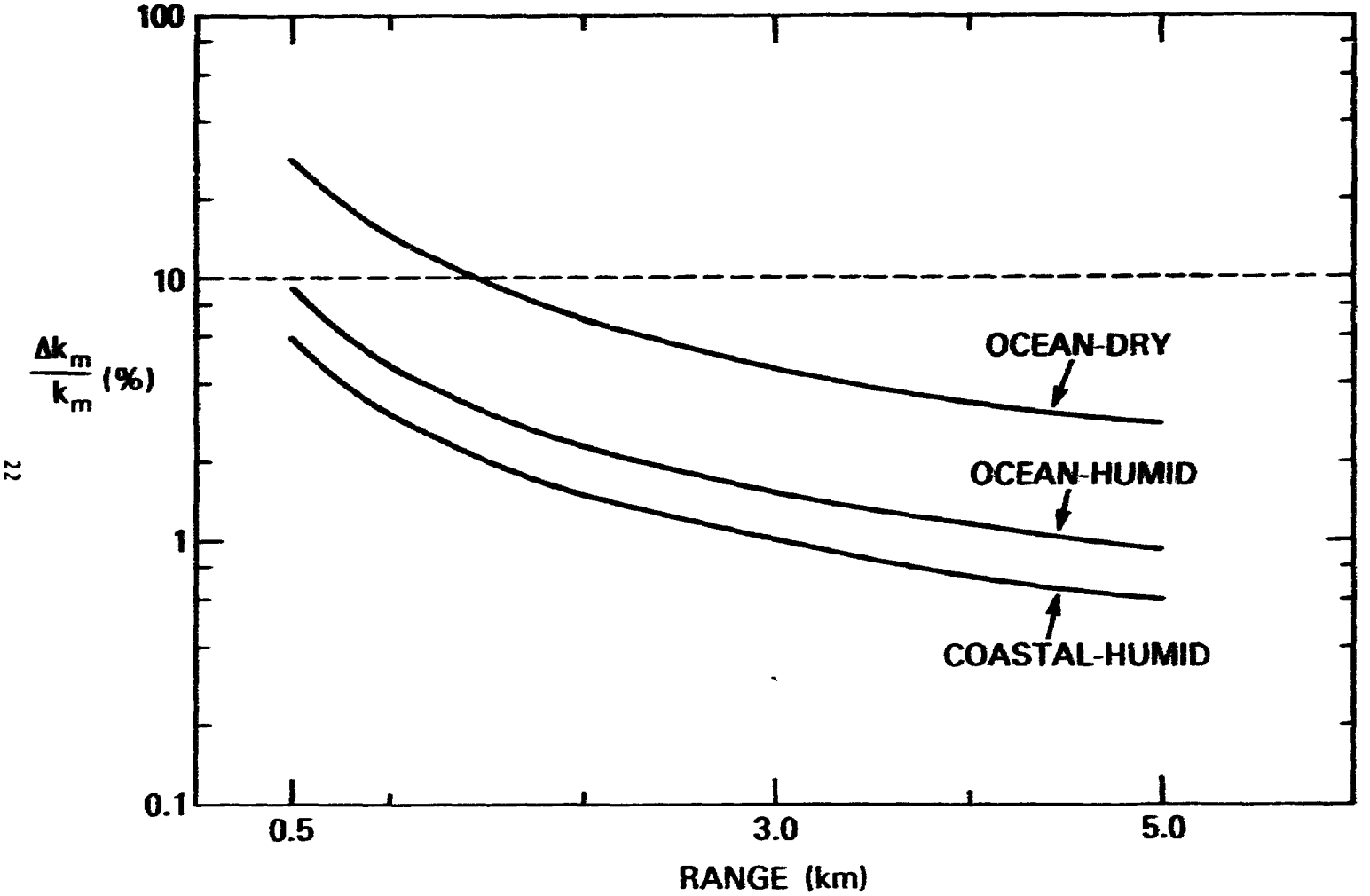

Figure 12 — Percent error in measurement of DF P_1 (8) molecular absorption vs range for three atmospheric conditions

Table 5 — Range of Likely $P_1(8)$ Molecular, Aerosol, and Total Extinction and Resulting Predicted Percent Transmission for Three Distances

	Dry Open Sea 6.0 torr H_2O	Humid Open Sea 20.0 torr	Humid Coastal 20.0 torr
k_m	.054 km^{-1}	.189 km^{-1}	.189 km^{-1}
k_a	.020	.030	.150
k_{total}	.074	.219	.339
T(0.5km)	96.4%	89.6%	84.4%
T(3.0km)	80.1	51.8	36.2
T(5.0km)	69.1	33.5	18.4

Table 6 — Fractional Percent Error in Molecular $P_1(8)$ and Aerosol Extinction Coefficient for Three Atmospheric Conditions and for Three Pathlengths

	Pathlength	Dry Open Sea 6.0 torr H_2O	Humid Open Sea 20.0 torr H_2O	Coastal 20.0 torr H_2O
$\Delta k_m/k_m$	0.5 km	27.8%	9.1%	5.9%
	3.0	4.5	1.5	1.0
	5.0	2.7	0.9	0.6
$\Delta k_a/k_a$	0.5 km	54.0	18.2	11.8
	3	9.0	3.0	2.0
	5.0	5.4	1.8	1.2

ures 9-12 plot the expected measurement uncertainties in DF $P_1(8)$ and DF $P_2(8)$ molecular absorption and aerosol extinction measurements. The dashed lines at 10% and 20% indicate the "useful data" criteria. We see from the above tables, and their results as presented in Figures 9-12, that these criteria can be met and exceeded under almost all atmospheric conditions and ship separations likely to occur during the experiment. In view of this, we list the most important conclusions of the analysis of measurement procedures *per se*:

1. Data at 0.5 km will be useful for establishing internal calibration and for near-ship effect assessment, but little high quality spectral information will be acquired at this short optical depth.

2. The $P_1(8)$ DF laser line should be used as well as $P_2(8)$ so both "weak" and "strong" absorption by water vapor can be examined.

3. The equipment described here is capable of creating an extremely useful scientific data base.

IV. IMPACT OF THIS EXPERIMENT ON THE MODELING OF HEL TRANSMISSION

A. Introduction to Current Modeling of Atmospheric Transmission

The Navy, and in-fact the entire DoD, has been actively involved in the development of computer codes for the prediction of broadband and laser transmission. Here we concentrate on the infrared and only mention that many of the same atmospheric parameters also impact transmission prediction of the entire spectrum for radio waves to ultraviolet. Many codes are unrestricted in the sense of time or computer size. One example of a large code is FASCODE (Fast Atmospheric Signature Code), developed by AFGL.[23] It predicts atmospheric transmission and/or radiance for a variety of atmospheric and aerosol scenarios including slant paths from sea level to the upper atmosphere, and it requires a very large computing ability. An opposite case is REALTRAN,[24] which predicts transmission at selected wavelengths from "look up tables" and is driven by a HP9825 desk top calculator and interfaced in real time to temperature, pressure, and dewpoint meters. Desktop or hand held calculators will in the near future play important roles as TDA (Tactical Decision Aids) for laser weapons systems. LOWTRAN[11] and HITRAN[12] codes are available in several forms and generally are used in low resolution (5-20 cm^{-1}) and high resolution (laser) transmission problems respectively. The AFGL ATLAS of 160,000 atmospheric absorption lines is used by programs like HITRAN and LASER[25] as input. LOWTRAN is unique in its ability to also predict aerosol extinction using look-up tables for six model atmospheres: 1962 US Standard, Tropical (15°N), Midlatitude Summer (45°N, July), Midlatitude Winter (45°, January), Subartic Summer (60°N, July) and Subartic Winter (60°N, January), which support rural, urban, *maritime*, and fog tropospheric aerosol models. Variations in aerosol effects with humidity are also included in the most recent version of LOWTRAN-5 and the reader is referred there for more detail.[11] We expect that one important result of our ship-to-ship experiment will be the ac-

quisition of high quality "open-sea" aerosol data and we anticipate the need for comparison with the "maritime" model.

A second model which predicts open ocean aerosol extinction from MET observables (temperature, humidity, wind speed) is the Wells, Katz, Munn (WKM) model.[13,14,26] We expect our open-sea data will be very useful for validating this model. The HITRAN Code for predicting high resolution (i.e., laser) absorption requires high quality laboratory data where aerosols are not an interference in measurements, and we expect our results will not have much impact on the HITRAN data base. Two related areas may be affected however: the H_2O continuum absorption, and the fractional population of deuterated atmospheric water vapor (HDO/H_2O ratio). The effect of the errors in each is less than 10% in absorption coefficient. The H_2O continuum is described by two models: One attributable to K. O. White of the U.S. Army Atmospheric Sciences Laboratory at WSMR, the "White" continuum,[22] and one to D. E. Burch of Ford Aerospace.[21] Previous analysis by J. Dowling of NRL's Florida data base was unsuccessful at distinguishing between the two models.[4] The open ocean data which may be obtained under very humid conditions (20 torr or greater) may involve sufficient optical depth to distinguish between these two models. The HDO/H_2O ratio problem is based on sketchy upper atmosphere data,[27] which purports to show evidence of large excursions from the commonly accepted value of 0.03%. The FTS data obtainable in the ship-to-ship experiment should add to the growing body of evidence (at sea level) that no significant (i.e., ~10% of nominal .03%) variations are seen in high quality measurements.

We have given this brief review to introduce the reader to some of the computer codes and models available for predicting atmospheric transmission in a variety of situations. Additional information can be obtained from the original sources, and much of the current state-of-the-art relating meteorology to laser transmission may be found in the recently published proceedings of the NRL-directed LIDAR review conference[28] cosponsored by OUSDRE and the EOMET program.

The value of the data obtained in the ship-to-ship experiment is that it will provide accurate laser extinction, FTS, and aerosol data related to Met observables, and therefore will be useful to many people in the DoD community. We now proceed to describe the equipment and procedures used to acquire the data, we assess its intrinsic quality, and we show how the results of a ship-to-ship open-sea experiment contribute to validating and improving current modeling.

B. Aerosol Extinction Results and Models

LOWTRAN and the WKM model are the two codes/models most likely to be directly affected by the aerosol-related results of the proposed transmittance experiment. We now demonstrate why the $\frac{\Delta k_a}{k_a} \approx 20\%$ figure-of-merit for aerosol extinction will provide useful input to the models. The aerosol measurements are performed with four instruments, plus Met support. These are (1) the Knollenberg particle spectrometers that measure the aerosol particle size distribution dn/dr vs particle radius, (2) an aerosol mass monitor which given the mass of aerosols present in μgrams per cubic meter, (3) a nephelometer which gives a total scattering coefficient in km $^{-1}$, and (4) the transmittance experiment which gives the difference between the total extinction and the molecular absorption contribution. The list of the aerosol related measurement equipment is given in Table 7.

Table 7 — Aerosol Monitoring Equipment

Apparatus	Output	Point or Path Integrated	Process	Error
Knollenberg Counter	$\frac{dn}{dr}$ vs r	Point	$k_{sc} + k_a = \int \frac{dn}{dr}(\pi r^2)\,dr$	20%–50%
Mass Monitor	Micrograms/m^3	Point	M and $\int \frac{dn}{dr}(\frac{4}{3}\pi r^3)\,dr$	To be determined
Nephelometer	0.5 μ m scattering	Point	$k_{sc}(0.5\mu) - k_{sc}(3.8\mu)$	50%
Laser Transmittance	Total 3.8μ extinction	Path-Integrated	k total $= k_{sc} + k_{abs} + k_{mol}$	20% or less
FTS Spectra	H_2O absorption spectrum	Path-Integrated	k_{abs}	10% or less
MET	H_2O concentration	2 Points	ppH_2O	2%

A note about the instrument in (2) above may be in order. So far the particle mass density vs aerosol extinction relation has been observed only by calculating the mass density and aerosol extinction using $\frac{dn}{dr}$ from particle spectrometer results, e.g., see Fig. 20 in Ref. 10. We are now investigating the use of an instrument that monitors the mass density of particles directly by weighing the particles in a known volume of air using a quartz microbalance. We have not finished analyzing the data taken with the instrument, so far, and hence the "To be determined" remark in Table 7. If this mass-monitor investigation shows promise, and the ship-to-ship measurement will certainly aid in the evaluation, then a device much simpler than the Knollenberg spectrometers may be devised for routine IR-extinction prediction. The mass density will not, however, provide good visibility information and hence the inclusion of the nephelometer (3) above.

It should be noted how the elements of Table 7 are interrelated:

- Total extinction is the sum of aerosol scattering, aerosol absorption, and molecular absorption.
- Aerosol mass concentration is related to the MIE scattering result if the particles are spherical and homogeneous.
- Visibility (0.5 μm) is related to scattering at 3.8 μm. (The relationship is nonunique, however).
- Point and path integrated measurements can be compared to extract near-ship effect.

An important result of the experiment will be analysis of the data to obtain how well the separate instruments are correlated.

Clearly one cannot expect to provide each Naval vessel with a laser transmissometer and state-of-the-art Met gear for monitoring IR atmospheric transmission. One important result will be the correlation of "simple" observables: humidity, temperature, wind speed, with laser extinction. This is where

the expected impact on programs and models such as LOWTRAN and WKM will fall.

Figure 13 provides an indication of the performance intercomparison between identical Knollenberg particle counters. Seven counters and a Barnes Transmissometer on San Nicholas island were compared[29] on a common site and a 50% spread in predicted k_a between instruments is noted. For each instrument a 20% error in repeatability is common. Figures 14 and 15 indicate two very important measurement results from previous open-sea aerosol measurements aboard the research vessel USNS HAYES in 1977.[9] Figure 14 indicates an order of magnitude decrease in the number of 2-10 μ size particles from 9 to 15 meters above the ocean surface. Figure 15 demonstrates the large influence of near-ship effects of over an order of magnitude increase in aerosol extinction between stern and bow wind conditions. Such near-ship effects will be examined in our data since we will be able to analyze the difference between our point and path-integrated MET observations. The important change in particle size distribution toward fewer large particles in open-sea conditions is clearly shown in Figs. 16 and 17. Figure 16, which shows Mie-extinction results from open-sea measurements gave an average aerosol extinction, at 3.8 μm, of about 0.01 km $^{-1}$ for 19 days of observation in the North Atlantic.[10] By contrast, Fig. 17 shows that over an order of magnitude increase in the average 3.8 μm extinction was observed at the coast at Cape Canaveral Air Force Station, Florida.[30] Figure 18, from three days of observations aboard LEXINGTON in 1979, shows an average in between the coastal and sea distributions.[31] Clearly a 20% measurement accuracy in extinction coefficient can distinguish between these two distributions. We have shown that a 20% precision in k_a is a reasonable expectation, and data of this precision can provide valuable information on aerosol extinction, and open-ocean vs coastal particle size distributions.

C. *Molecular Absorption Results and Models*

The molecular absorption in the DF region is mostly due to HDO, H_2O, the water vapor continuum, and lesser contributions from N_2O and CH_4. The N_2O and CH_4 concentrations are expected to be

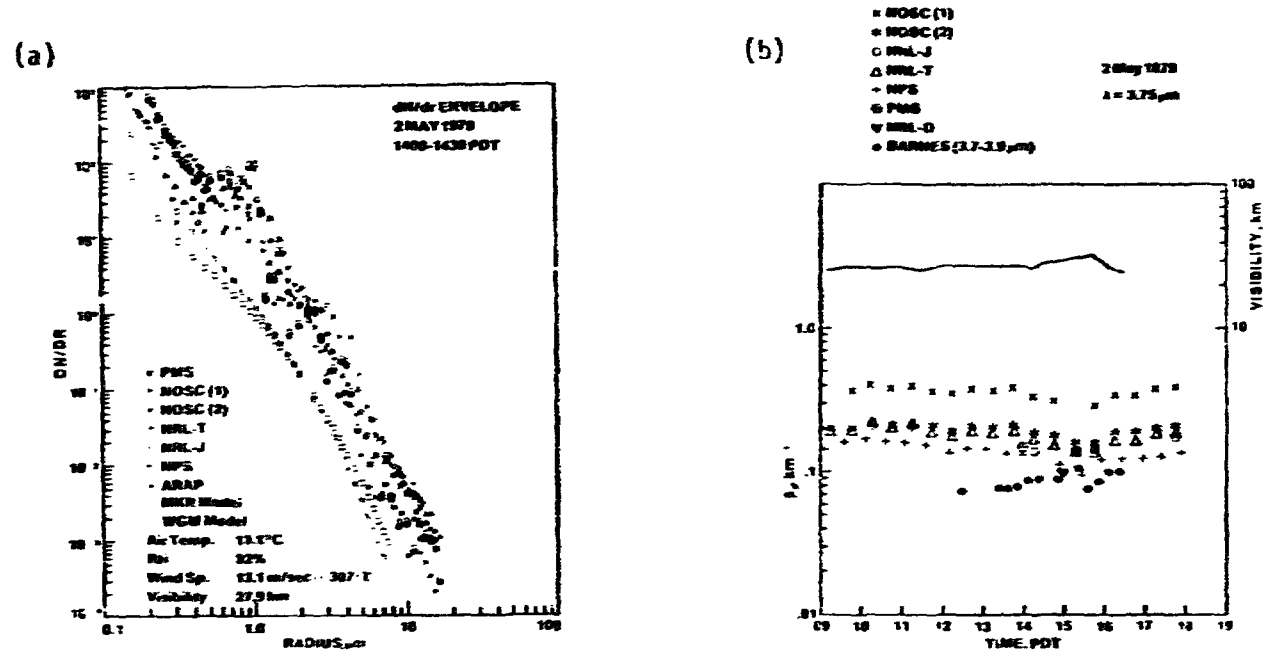

Figure 13 — Intercomparison of particle size spectrometers on San Nicholas Island (a) particle size distributions (b) 3.75 μm extinction derived from Mie calculations

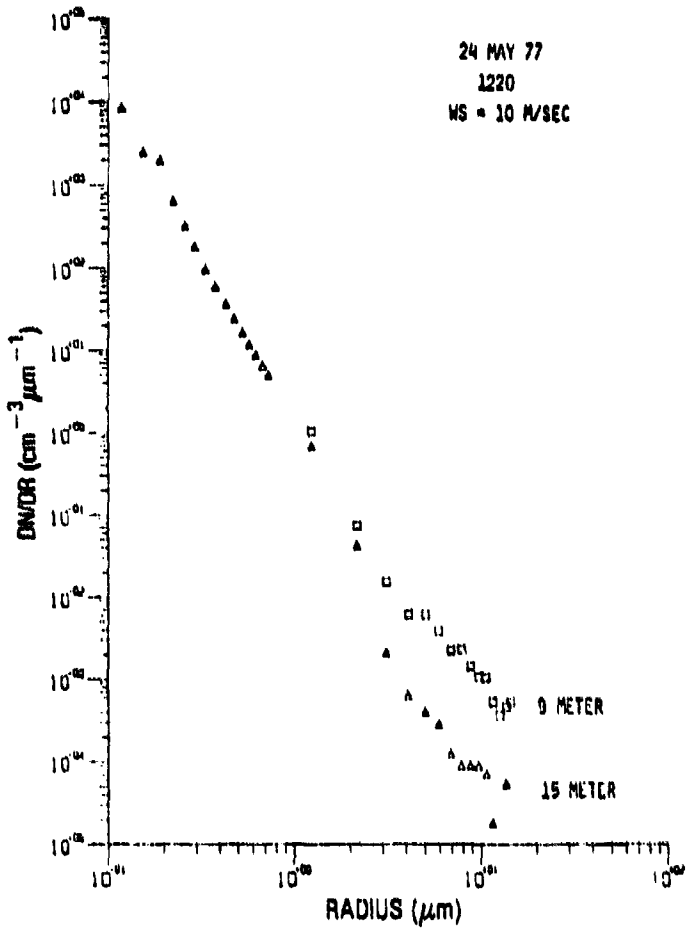

Figure 14 — Particle size distribution aboard USNS HAYES for two heights above the water surface

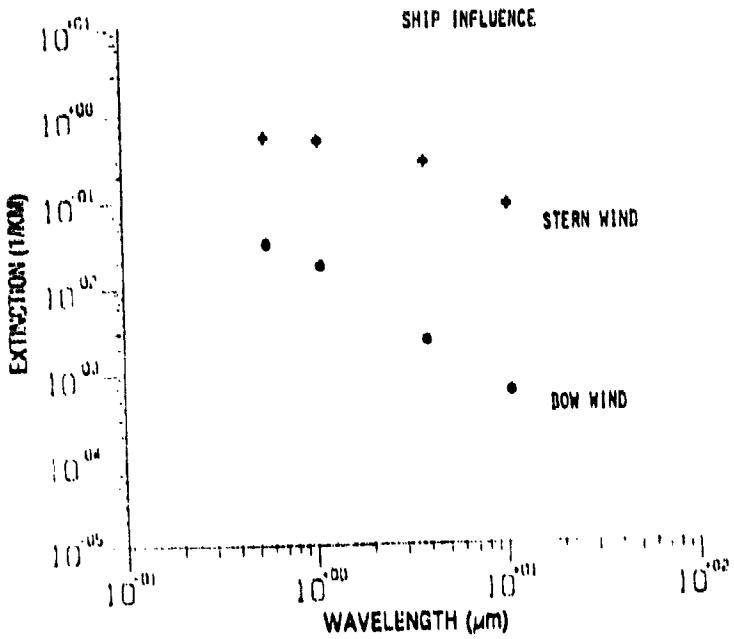

Figure 15 — Aerosol extinction derived from particle size distribution measurements vs wavelength for bow and stern wind conditions aboard USNS HAYES

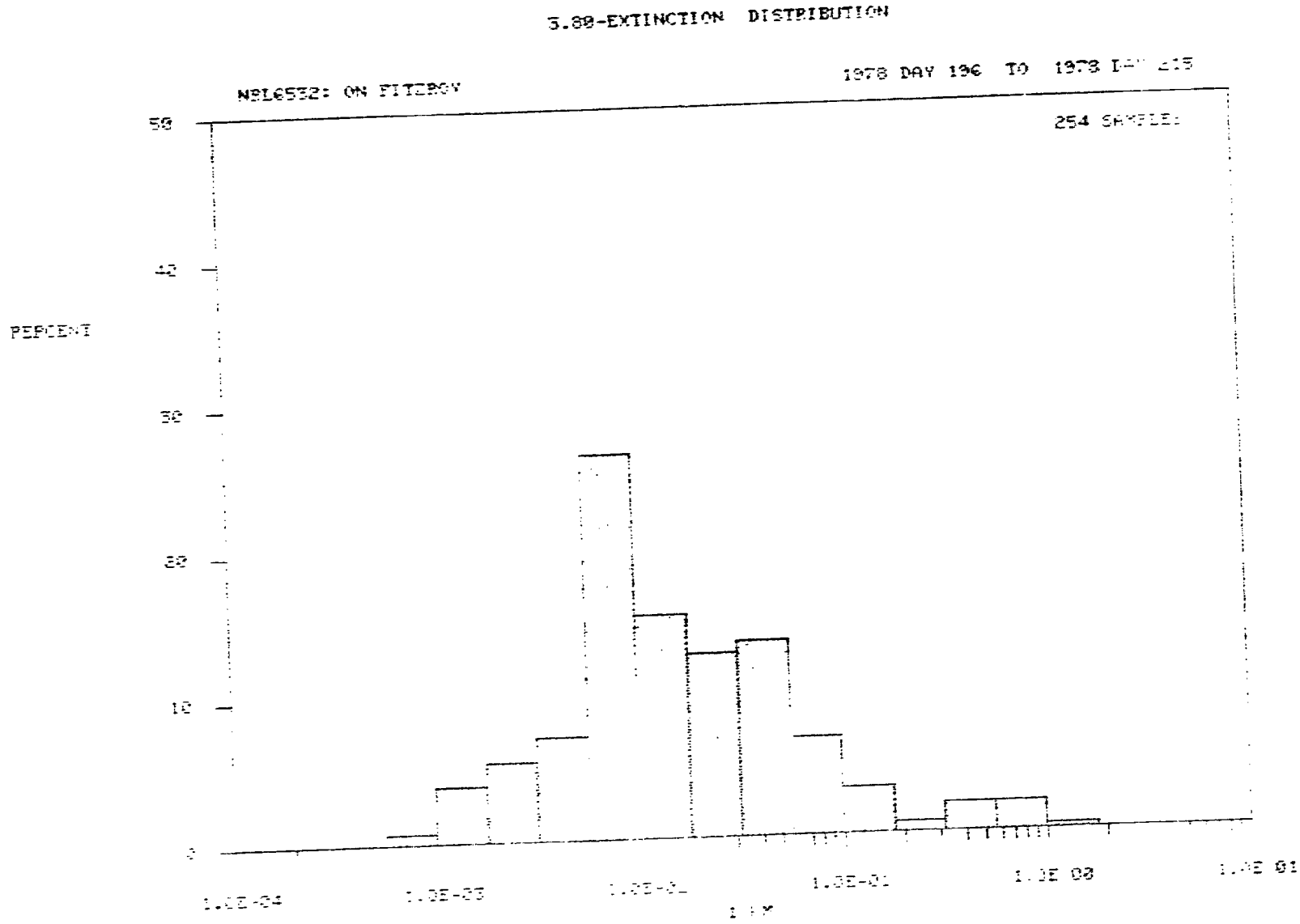

Figure 16 — Open-ocean 3.8 μm extinction distribution derived from measured particle size distributions over a 19 day period

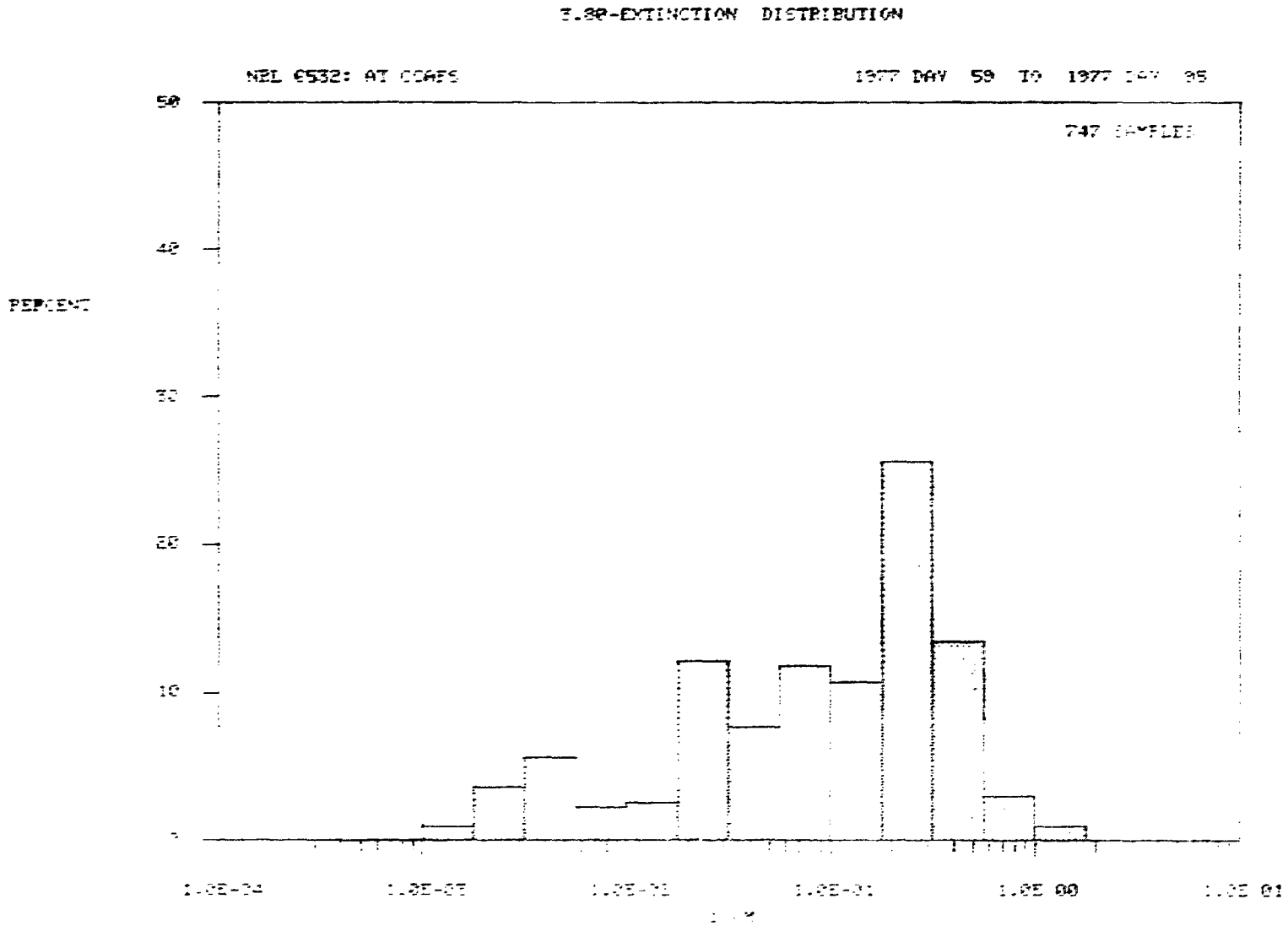

Figure 17 — Coastal 3.8 μm extinction distribution derived from measured particle size distributions over a 36 day period

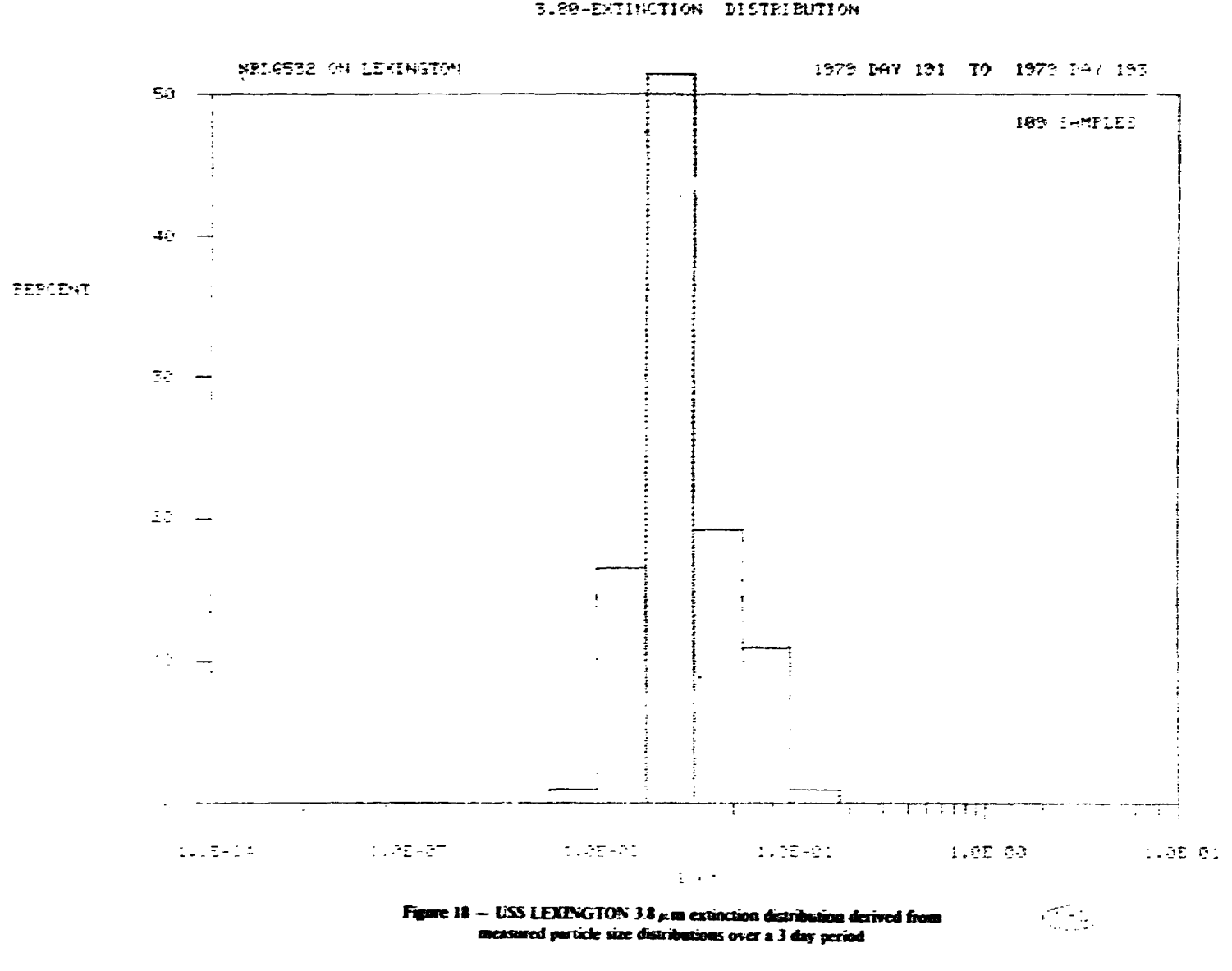

Figure 18 — USS LEXINGTON 3.8 μm extinction distribution derived from measured particle size distributions over a 3 day period

near their cannonical concentrations of 0.28 ppm and 1.6 ppm respectively. These values can be easily checked from the FTS spectra. The H_2O and HDO concentrations are related by the commonly accepted value of 0.03% HDO. Although some questions exist regarding the independence of the ratio with altitude[27] as we alluded to earlier, we can check this number with analysis of the FTS spectra. Figure 19 displays FTS spectra in the 3.94 μm region for a 6.4 km path at WSMR.[8] Note the high quality of the spectrum. The regular spacing of the N_2O lines allows simple data reduction since no overlapping is present. The N_2O data presented here yielded a value of (0.278 ± .03) ppm, very close to the accepted value of 0.28 ppm. Results also indicated no departure from 0.03% HDO/H_2O, and CH_4 concentrations were observed to be some 50% above the 1.6 ppm standard.

Figure 20 shows a plot of several closely-spaced water vapor absorption lines, two of which are HDO, near 3.66 μm. These data were replotted from archival storage of results taken during September, 1976, over a 5.12 km path at Patuxent River Naval Air Test Center, for 11.3 torr of ambient water vapor.[7] These data are of very high quality indeed, as very little noise is observable. The absorption coefficients of two of these lines can be determined to an accuracy of 5% or better. The molecular integrated line strengths are available from the 1980 AFGL Atlas[12] and are given in Table 8 below.

Table 8 — HDO and H_2O Absorption Line Parameters Near 3.66 μm

Molecule	ν	HWHM	S
HDO	2730.928 cm^{-1}	.098 cm^{-1}	2.65×10^{-24} $cm^{-1}/mol/cm^2$
H_2O	2732.493	.056	1.09×10^{-24}

Our analysis of this spectra yields a value of (0.028 ± .003)% HDO. This is an example of the high quality results available from the FTS spectra. The Pax-River case represents an optical depth of 57.86 torr-km of water vapor. In our planned experiment we can reasonably expect an optical depth of 100 torr-km or more. Figure 21 gives an indication of how measurement of the HDO/H_2O ratio impacts current HEL test results interpretation. To produce this figure we used a recent MIRACL test

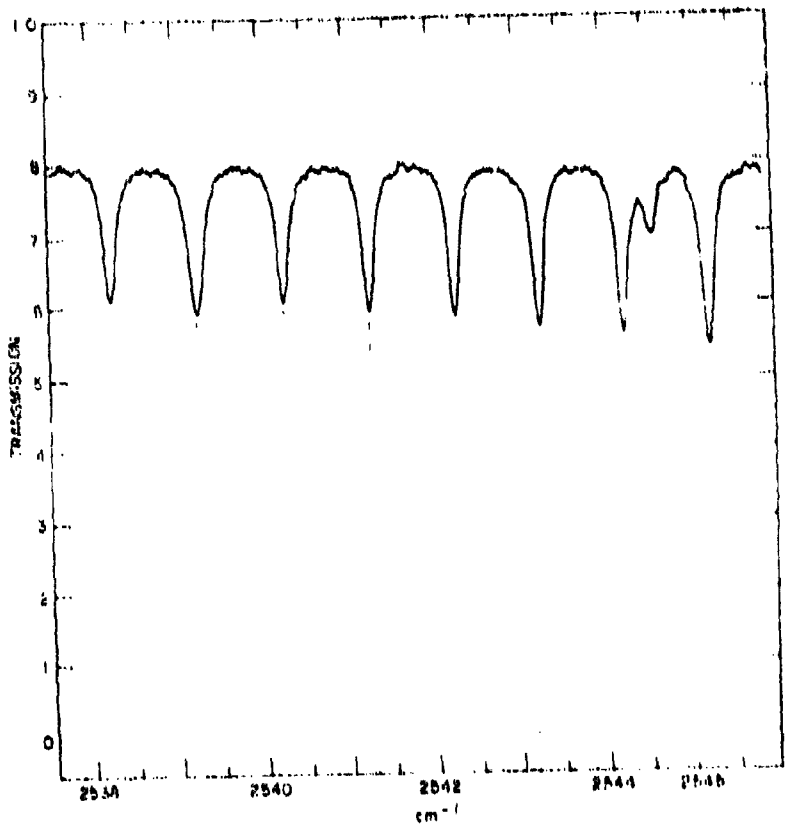

Figure 19 — N_2O absorption spectrum near 3.93 μm observed over a 6.4 km path at White Sands Missile Range, New Mexico

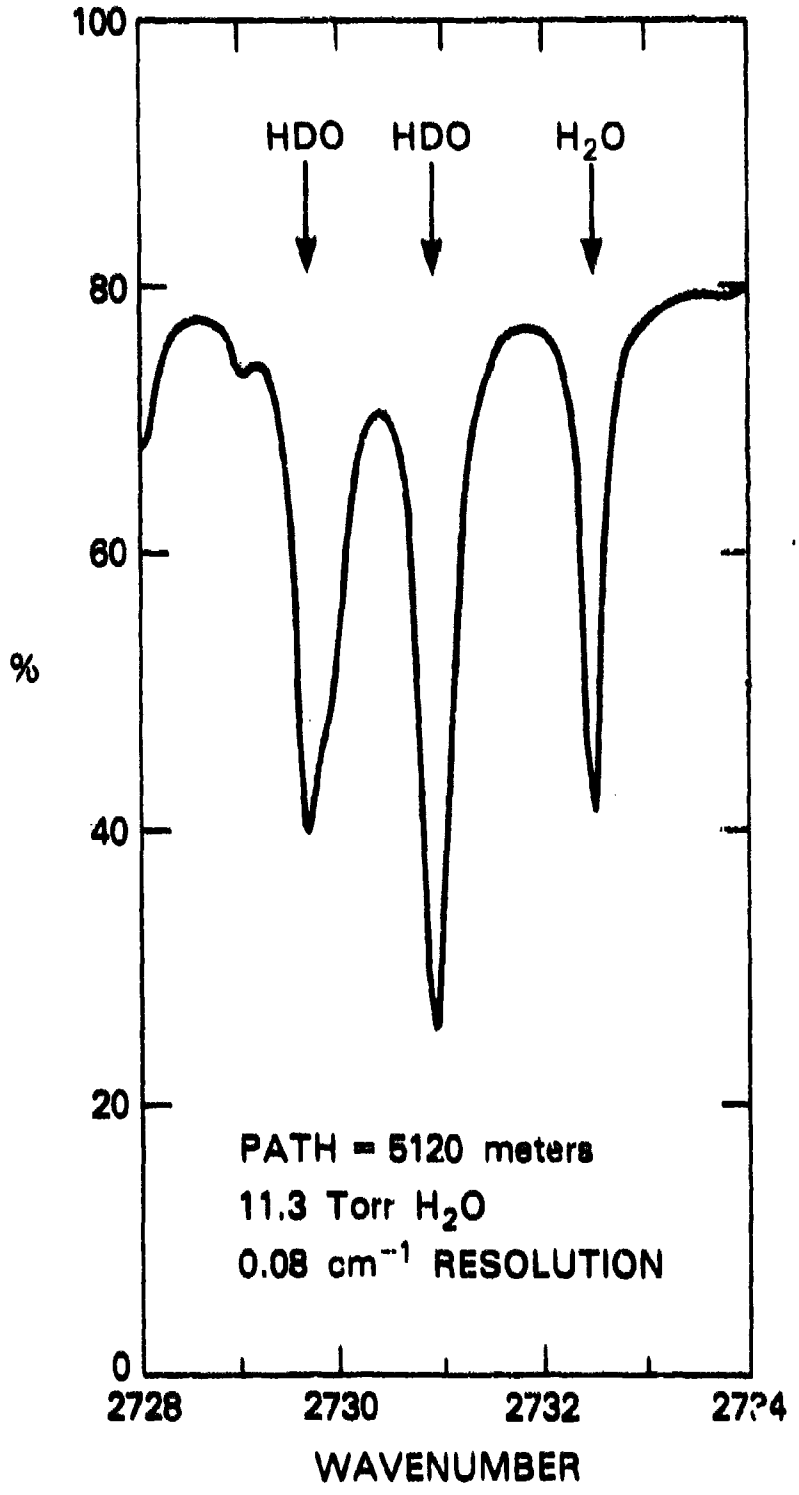

Figure 20 — HDO/H_2O absorption spectrum near 3.66 μm observed over a 5.12 km path at Patuxent River Naval Air Station, Maryland

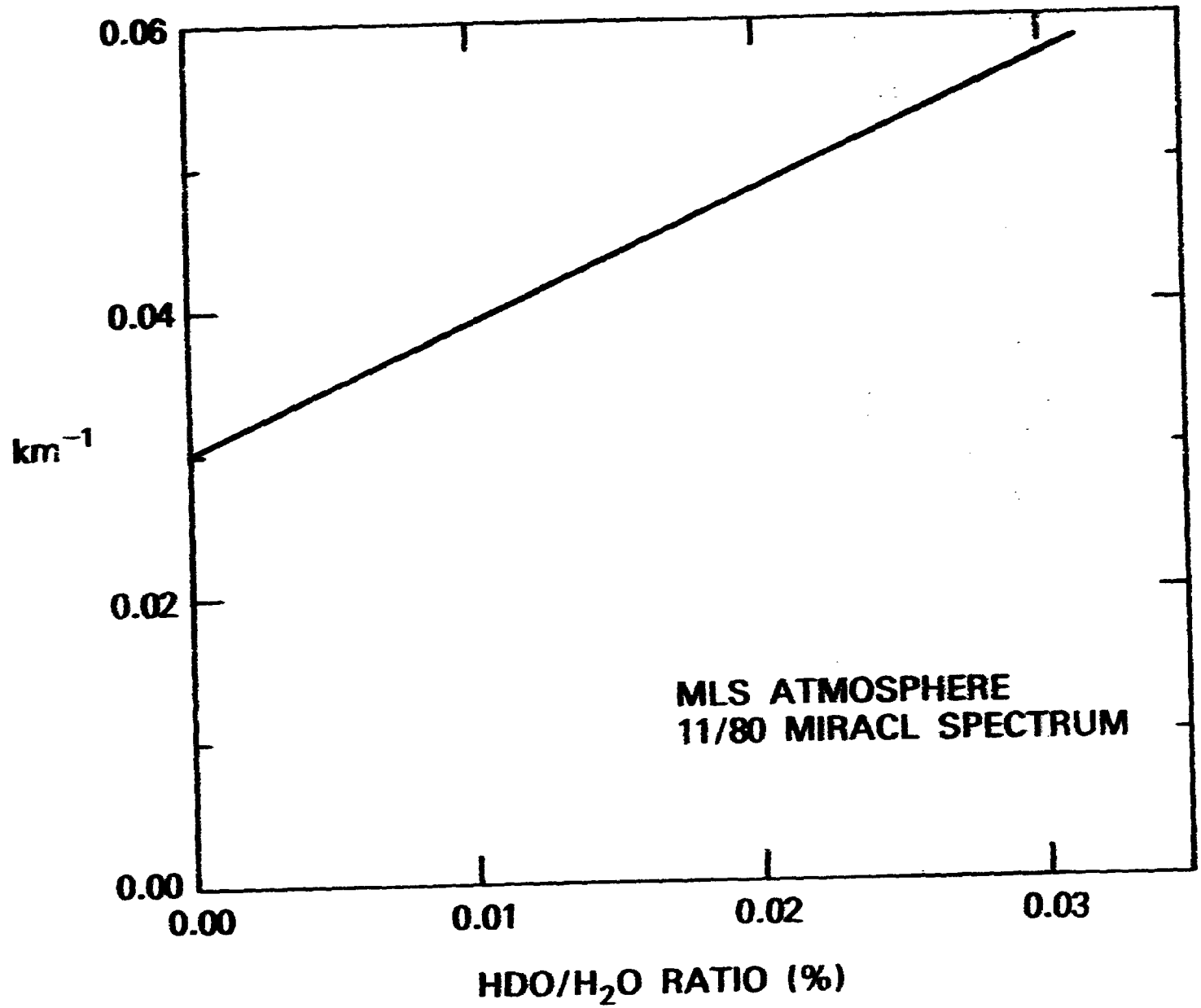

Figure 21 — DF laser absorption vs HDO/H_2O ratio averaged over a realistic multiline output power spectrum

result power spectrum, kindly supplied by Dr. J. Stregack, to fold together the weighted absorption coefficients of some 20 DF lines, and varied the result with the HDO/H_2O ratio. The result shows a very linear relation between net absorption (above the floor of .03 km^{-1} for mid-latitude summer) and HDO/H_2O ratio. The uncertainty of 10% or less may or may not be significant depending on the scenario, linear absorption, blooming, etc., and the power spectral distribution at the time. However, results of the ship-to-ship experiments are expected to narrow the error bars on the .03% ratio at sea level.

The measurement accuracy of the dew point meters (EG&G Model 110 S-M) is 1.5% (state of the art). For moderate to high humidity at expected moderate to high temperature we calculate this implies a 1.8% accuracy in measuring the H_2O partial pressure. At 5 km and ~ 20 torr H_2O this yields a transmittance uncertainty of about 0.5% and hence an error in extinction of 2% at 80% $P_2(8)$ transmittance. This is well within bounds of useful data. The accuracy will be even better at $P_1(8)$.

The high resolution molecular spectra presented above has been shown to be very useful for extracting path-integrated molecular concentrations. A second quality of great interest in the molecular spectra is the water vapor continuum. The physical origin of the water vapor continuum is probably related to the cumulative absorption of the far wings of water vapor absorption lines. Two models are in current use in the 3.5-4.2 μm region: the "Burch" model[21] and the "White" model.[22] Generally the Burch model is criticized for not predicting enough absorption where the White continuum tends to predict too much at the short wavelength end of the DF region. Both models are based on laboratory measurements in closed cells. The finite vapor pressure of water, entrance aperture size and mirror reflectivities limit the amount of optical depth available in laboratory experiments to at most 30 to 40 torr-kilometers.

At five kilometers path and 20 torr of water vapor we would see an optical depth of 100 torr-kilometers. The spectrum near $P_2(8)$ is shown in Fig. 22, and we see the two continua yield 73%

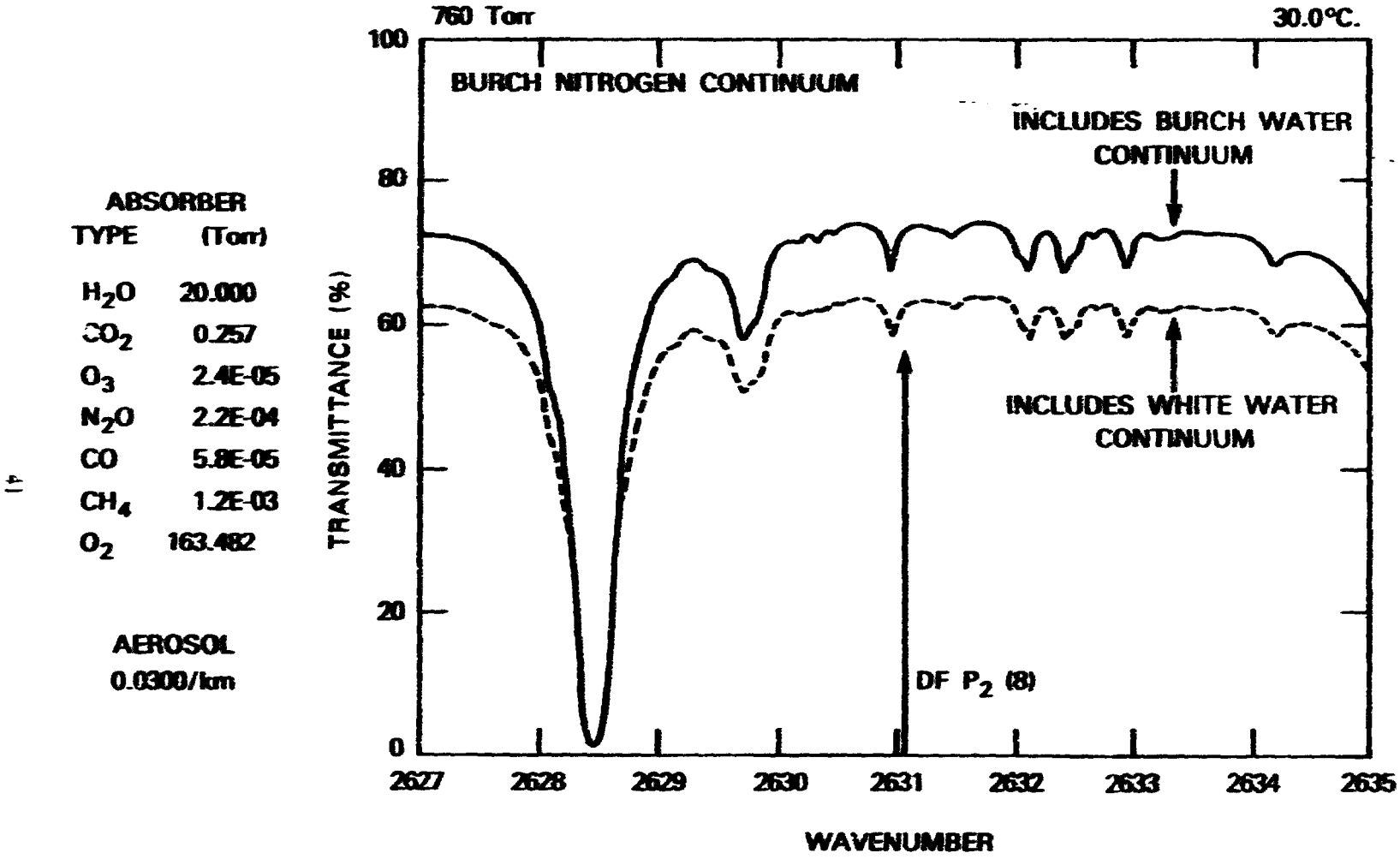

Figure 22 — 5 km transmission spectrum near DF P_2 (8) calculated for an open-ocean humid atmosphere and two H_2O continuum absorption models

transmittance for the Burch model, and 63% for the White model. At an average transmittance of 68% and an assumed error of 2% we obtain an expected error of 5.2% in molecular extinction. Allowing for an aerosol absorbance of 0.15 (0.03 km^{-1} × 5 km) analyzed at a ±20% uncertainty gives a range of aerosol absorbance of 0.12 to 0.18. The Burch and White absorbances work out to 0.13 and 0.23 respectively, each with 5% uncertainty. Considering the aerosol uncertainty, the molecular uncertainty, and the small contribution from the nitrogen continuum which we know with great certainty, we should be able to conclusively tell which model correctly predicts the observed absorption. The expected spectra as plotted in Fig. 22 demonstrates this.

The molecular absorption spectra that we have presented here have yielded absorption coefficient results well within the 10% uncertainty that we have projected for the ship-to-ship transmission experiment. Spectral data of 10% or less uncertainty will address the following important questions:

1. How well does measured dew point, measured at the path end-points, correlate with path integrated water vapor absorption?

2. Does the open ocean HDO/H_2O ratio vary significantly from 0.03%?

3. Does the measured water vapor continuum absorption distinguish between the Burch and White Models?

Considering the high quality of the high resolution data to be available from this experiment we should be able to provide quantitative and meaningful answers to these questions. Of particular concern to the Navy HEL community will be the correlation between predicted and measured absorption. This will be discussed in detail in Section V in relation to the critical thermal blooming problem.

V. IMPACT OF THIS EXPERIMENT ON NAVY HEL

In the previous chapters we have given an in-depth description of the ship-to-ship DF laser transmittance experiment. We have gone through the details of estimating the errors in transmittance, extinction coefficients, instrumental errors, and required accuracies such that the results might have significance. We now review these points and discuss how these results will impact the larger scope of Navy HEL programs. A very important aspect of this program is to examine the predictive ability of models as they relate laser propagation to meteorological observables. Thermal blooming effects in high energy laser transmission depend principally on the absorption coefficient and wind speed.[32] A previous NRL study[33] briefly examined the sensitivity of thermal blooming effects to meteorological variables. We will examine this important HEL propagation effect in relation to our experiment.

A. Model Validation

The two problems of prime concern to us are aerosol extinction and molecular absorption. In the former we expect to have a very significant impact in that we expect the data to add to the growing body of NRL evidence that an "open-sea" aerosol model is needed, and concurrent measurements of the ship's impact on the open-sea condition. Previous NRL open-sea aerosol measurements have shown a distinct order of magnitude decrease in the number of 2-10 μm size aerosols in open ocean vs coastal measurements. One likely result of the measurement is the recommendation that an "open-ocean" aerosol model option be added to LOWTRAN.

A second anticipated result is the need for study of near ship aerosol distributions. Much has been made of the requirement that a ship-based HEL weapon needs to be stern mounted, but no *extensive* aerosol studies have been made on an aircraft carrier. Particular attention needs to be paid to the variation of extinction with the height above the sea surface. Statistical models such as WKM may need to be re-examined if our data base is of the quality that we expect. Accurate prediction of aerosol

extinction based on "simple" observables (windspeed, humidity, air/water temperature) will play an ever increasing role in the development of TDA. Hence high quality data relating Met to extinction is a necessity.

The effect of our expected results on molecular absorption modeling is not likely to be as extensive as that on aerosol modeling. The HITRAN code has gone through over ten years of revisions, and has been fine tuned to state-of-the-art high resolution measurements. However, our expected contribution will be the use of HITRAN, with our field data, to relate humidity to extinction, to carefully examine the HDO/H_2O ratio question, and to provide spectroscopic support to the separation of molecular from aerosol extinction in the laser-transmittance part of the experiment.

B. HEL Sensitivity to Absorption Coefficient Measurement Accuracy

An important concern in the design of the at-sea transmission experiment is the issue of how HEL performance predictions are affected by expected errors in the derived absorption coefficients. While we have not yet undertaken a complete parametric analysis of this problem, a simple calculation was performed to illustrate the general form such a sensitivity study would take.

A set of conditions was selected to allow a complete analytic treatment without recourse to the computer. Nonlinear propagation was based on an empirical fit to a large amount of data as reported by Gebhardt.[34] This fit is of the form

$$I_p(z) = \frac{P_o\, e^{-k_m z}}{\pi a^2(z)} \frac{1}{1 + 0.0625N^2} \tag{1}$$

where I_p = peak intensity at range z, P = laser output power, k_m = absorption coefficient, $a(z)$ = beam radius at range z and N = distortion coefficient given by

$$N = \frac{-n_T k_m P z^2}{\pi n_0 \rho_0 c_p v_0 a_0^3} \tag{2}$$

where n_T = coefficient of index change with respect to temperature, n_0 = ambient refractive index,

ρ_0 = ambient atmospheric density, v_0 = wind velocity, and a_0 equal beam radius at the laser.

If we assume that a missile of velocity v_m is irradiated initially at a very large range and remains thereafter within the focal volume of the laser as it approaches, then the total accumulated fluence, $E(z)$, at any range z is given by

$$E(z) = \frac{1}{v_m} \int_{\infty}^{z} I_p(z')dz' \tag{3}$$

The beam radius $a(z)$ at focus is given by $0.45\beta\lambda z/D$ where β is a measure of the poorness of the beam quality, λ is the laser wavelength and $D = (2\sqrt{2}a_0)$ is the laser aperture diameter. Thus

$$E(z) = \frac{PD^2 e^{-k_m z}}{\pi (0.45)^2 \beta^2 \lambda^2 v_m} \int_{\infty}^{z} \frac{dz'}{(z')^2 (1 + 0.0625 N_0^2 z'^2)} \tag{4}$$

where we have assumed small absorption, $k_m z << 1$, no slewing and strong focusing, $a_0/a(z) >> 1$, so that Gebhardt's Eq. (34) applies and, thus,

$$N_0 = 8.74\, k_m P/v_0 \beta \lambda D.$$

The integration in Eq. (4) can be performed to yield the result

$$E(z) = \frac{PD^2 e^{-k_m z}.25\ N_0}{\pi (0.45)^2 \beta^2 \lambda^2 v_m} \left| \frac{\pi}{2} - \tan^{-1} \chi_0 - \frac{1}{\chi_0} \right| \tag{5}$$

where

$$\chi_0 = 0.25\ N_0 z.$$

Since

$$\tan^{-1} \chi_0 = \frac{\pi}{2} - \frac{1}{\chi_0} + \frac{1}{3} \frac{1}{\chi_0^3} + \ldots$$

we can rewrite (5) for our purposes as

$$E(z) = \frac{PD^2 e^{-k_m z}(.25\ N_0)}{\pi (0.45)^2 \beta 2\lambda^2} \frac{1}{v_m} \frac{1}{3} \left| \frac{1}{.25\ N_0 z} \right|^3$$
$$= \frac{0.11\ D^4 v_0^2}{k_m^2 P z^3} \tag{6}$$

The various influence coefficients for a sensitivity analysis are now straightforwardly obtained. Two such are given here:

(1) Delivered fluence sensitivity to errors in measured absorption coefficient at constant range:

$$\left.\frac{\Delta E}{E}\right|_{z = \text{const}} = -2\,\frac{\Delta k_m}{k_m} \tag{7}$$

(2) Sensitivity of damage threshold range to errors in absorption coefficient at constant threshold fluence:

$$\left.\frac{\Delta z}{z}\right|_{E = \text{const}} = -\frac{2}{3}\,\frac{\Delta k_m}{k_m}. \tag{8}$$

We selected some nominal values for P, v_0, D, and k_m (which will not be specified here in the interest of keeping this report unclassified). In so doing we generated a curve which represents one of a family which are possible performance curves, given our possible errors in measuring k_m, the absorption coefficient. For assumed errors, Δk_m, of $\pm 10\%$ in the at-sea transmission measurement, the envelope of these curves is shown for one case in Fig. 23. The sensitivity in range at the $z = 2\,k_m$ point is indicated on the figure for illustrated purposes.

Comments and Conclusions

(1) This simple calculation is offered only as suggestive of the sensitivity analyses which will be performed to derive a desired limit on the error which can be tolerated in the at-sea transmission measurement program. Nevertheless, we seem to be "in the ball park" for an accurate enough measurement.

(2) We anticipate that the ship's boundary layer will be so significant that any model assuming homogeneous absorption and scattering, such as the sample calculation here, will be misleading. Influence coefficients for strongly nearfield perturbed beams are an important by-product of this experiment.

(3) Worst case conditions will be during propagation through the ship's polluting plume due to both low relative wind vector and higher absorption (cf: $(v_0/k_m)^2$ term in Eq. (6). In addition this re-

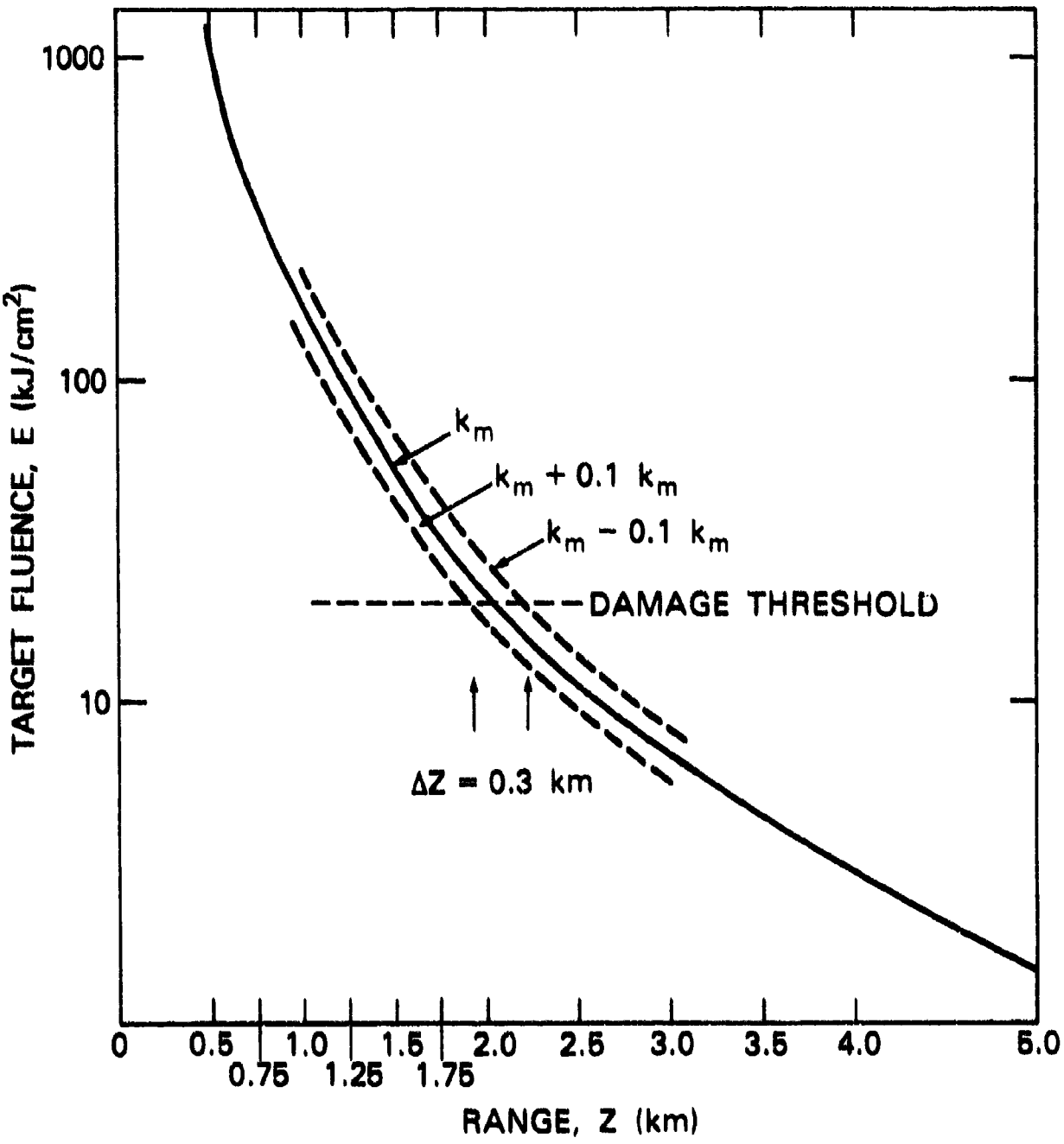

Figure 33 – Suggested sensitivity of on-target fluence to ship-to-ship measurement accuracy

gion of battlespace will be full of structure (turbulence, aerosol and sea spray discontinuities, gaseous plumes from ship and aircraft etc.). Clearly, careful analysis of this region can only be credible if backed-up by a suitably designed remote sensing (LIDAR) system.

C. Future use of the Tracker

An important issue in the HEL propagation study has not been addressed: the beam spread due to optical turbulence under at-sea conditions. Measurements of beam spread at 3.8 microns only exist for overland conditions. Just how severe IR turbulence effects are over water has not been determined. Nor has the lever-arm effect that would occur in the near-ship atmosphere been assessed. After finishing this first ship-to-ship measurement the tracker system with only slight modification could study these very important issues. And, the required equipment for the modification already exists as does the data reduction system and software expertise.

The tracker will also be a valuable asset for future DoD programs for which careful assessment of atmospheric effects is an important technical requirement. Its mobility gives it virtually unlimited access to field sites where electro-optical system tests are undertaken. Possible post-LEXINGTON projects include:

(1) Long range slant-path transmission measurements, utilizing a flying (aircraft or satellite) tracking beacon; blackbody source and laser retroreflector to study, e.g., atmospheric stratification, effects of inversion layers on E-O systems, tropopause peculiarities, ozone layer, stratospheric free radical effects, incipient cloud effects, transmission through weather fronts, etc. Potential sponsors: NAVAIR 370, DARPA, EOMET.

(2) Generation of statistical data base of near-field turbulence effects on blue-green and UV lasers in support of DARPA uplink and Navy SSC programs. These data could be taken at candidate sites for laser transmitter. Potential sponsors: DARPA.

(3) High resolution spectral, transmission data-taking in support of field tests of future EO systems e.g., IRST, laser designators, beam rider systems etc. Sponsors: Specific system sponsors.

(4) Support of other service programs in atmospheric optics including U.S. Air Force slant visibility studies for A/C landing and takeoffs and support of smoke and dust tests carried out by U.S. Army.

(5) Support of international defense programs in atmospheric optics through NATO, RSG-8, and TTCP-JAG/9.

(6) Use in LIDAR mode in support of developing programs in trace chemical/biological agent detection, vehicle emission detection, tracer detection for monitoring presence of passing ships etc.

(7) Possible role in support of actual anti-missile testing at SEALITE including real-time data gathering for aid in performance assessment, additional spectral or spatial tracking of targets, LIDAR data on path structure, especially desert plumes, wind shear and dust clouds.

Thus, we anticipate that the current NAVSEA/EOMET investment will pay dividends in future EO system support in the Navy and throughout DoD.

ACKNOWLEDGMENTS

The authors gratefully acknowledge the technical contributions of the following people: T.H. Cosden, R.A. Patten, and C.V.Acton of NRL, A.K. Goroch of NEPRF, B.S. Katz of NSWC-White Oak, J. Streguck of PMS-405, M. Douma of Massachussetts Manufacturing, V. Muffaletto of Research Optics, T. Wilkerson of the University of Maryland, and F. Gebhardt of SAI.

REFERENCES

1. J.A. Dowling, R.F. Horton, G.L. Trusty, T.H. Cosden, K.M. Haught, J.A. Curcio, C.O. Gott, S.T. Hanley, P.B. Ulrich, and W.L. Agumbar, "Atmospheric Transmission Measurement Program and Field Test Plan," NRL Report 8059, November 30, 1977.

2. J.A. Dowling, K.M. Haught, R.F. Horton, G.L. Trusty, J.A. Curcio, T.H. Cosden, S.T. Hanley, C.O. Gott, and W.L. Agumbar, "Atmospheric Extinction Measurements at Nd-YAG and DF Laser Wavelengths Performed in Conjunction with the JAN Propagation Tests, June-September 1975," NRL Report 8058, February 10, 1978.

3. T.H. Cosden, J.A. Curcio, J.A. Dowling, C.O. Gott, D.H. Garcia, S.T. Hanley, K.M. Haught, R.F. Horton, G.L. Trusty, and W.L. Agumbar, "Atmospheric Transmission Measurement Program Report for 1 July through 30 September 1976 (TQ1976)," NRL Report 8104, September 1, 1977.

4. J.A. Dowling, R.F. Horton, S.T. Hanley, and K.M. Haught, "High Resolution Field Measurement of Atmospheric Transmission," SPIE Proc. *142*, 25 (1978).

5. S.T. Hanley, J.A. Dowling, R.F. Horton, J.A. Curcio, C.O. Gott, M. Woytko, and J. Storvick, "Atmospheric Transmission Measurement at White Sands Missile Range, August 1978," NRL Report 8422, July 1980.

6. K.M. Haught and J.A. Dowling, "Long-Path High Resolution Field Measurements of Absolute Transmission in the 3.8-4.0 μm Atmospheric Window," Optics Letters *1*, 121-123 (1977).

7. K.M. Haught, J.A. Curcio, J.A. Dowling, D.H. Garcia, C.O. Gott, S.T. Hanley, R.F. Horton, J.T. Ulrich, J.W. Walsh, R.J. Bergemann, M.C. Sola, and R.E. Roberts, "Comparison of Low-and-High-Resolution Infrared Propagation Measurements in the 3- to 5-μm Atmospheric Window," NRL Report 8254 (1978).

8. J.A. Dowling, S.T. Hanley, J.A. Curcio, G.O. Gott, and M.A. Woytko, "Laser-Extinction and High-Resolution Atmospheric Transmission Measurements Conducted at White Sands Missile Range, New Mexico, March 1979," NRL Report 8446 (1980).

9. G.L. Trusty and T.H. Cosden, "Optical Extinction Predictions from Measurements on the Open Sea," NRL Report 8260 (1979).

10. G.L. Trusty and T.H. Cosden, "Optical Extinction Predictions from Measurements Aboard a British Weather Ship," NRL Report 8497 (1981).

11. F.X. Kneizys, et. al., "Atmospheric Transmittance/Radiance: Computer Code LOWTRAN 5," AFGL-TR-80-0067 (1980).

12. L.S. Rothman, "AFGL Atmospheric Absorption Line Parameters Compilation: 1980 Version," Applied Optics *20*, 791-795 (1981).

13. W.C. Wells, G. Gal, M.W. Munn, "Aerosol Distributions in Maritime Air and Predicted Scattering Coefficients in the Infrared," Applied Optics *16*, 654-659 (1977).

14. V.R. Noonkester, "Offshore Aerosol Spectra and Humidity Relations Near Southern California," Proceedings of the 2nd Conference on Coastal Meterology, 1981.

15. Operating and Service Manual, EG&G-PAR Model 5204 Lock-In Analyzer, 1979, p. II-4.

16. A.K. Goroch, Naval Environmental Prediction Research Facility, Private Communication.

17. E.C. Crittenden, Jr., A.W. Cooper, E.A. Milne, G.W. Rodeback, S.H. Kalmbach, and R.L. Armstead, "Measured Atmospheric MTF Over the Ocean for Visible to Far IR," OSA Topical Meeting on Optical Propagation through Turbulence, Rain, and Fog, 1977.

18. K.L. Davidson, G.E. Schacher, C.W. Fairall, and A.K. Goroch, "Verification of the Bulk Method for Calculating Overwater Optical Turbulence," Applied Optics *20*, 2919-2924 (1981).

19. K.M. Haught, "High-Resolution Atmospheric Transmission Spectra from 5 to 3 μm," NRL Report 8297, 1979.

20. D.H. Leslie and G.L. Trusty, "Measurements of DF Laser Absorption by Methane Using an Intracavity Spectrophone," Applied Optics *20*, 1941-1947 (1981).

21. D.E. Burch, D.A. Gryvnak, and J.D. Pembrook, "Investigation of the Absorption of Infrared Radiation by Atmospheric Gases: Water, Nitrogen, Nitrous Oxide," AFCRL-71-0124, Hanscom AFB, MASS (1971).

22. W.R. Watkins, K.O. White, L.R. Bower, and B.Z. Sojka, "Pressure Dependence of the Water Vapor Continuum Absorption in the 3.5-4.0 μm Region," Applied Optics *18*, 1149-1160 (1979).

23. H.J.P. Smith, D.J. Dube, M.E. Gardner, S.A. Clough, F.X. Kneizys, L.S. Rothman, FASCODE-Fast Atmospheric Signature Code (Spectral Transmittance and Radiance)," AFGL-TR-78-0081 (1978).

24. K.M. Haught, "REALTRAN: Real-Time Implementation of Atmospheric-Transmittance Codes," *SPIE Technical Proceedings*, Vol. 277, 125-133 (1981).

25. R.A. McClatchey and A.P. D'Agati, "Atmospheric Transmission of Laser Radiation: Computer Code LASER," AFGL-TR-78-0029.

26. B.S. Katz and A.L. Lee, "Statistical Evaluation of Optical Propagation Codes Using San Nicholas Island Transmissometer Measurements," *National IRIS Proceedings*, May, 1981.

27. D.H. Ehhalt, "Vertical Profiles of HTO, HDO, and H_2O in the Troposphere," NCAR Technical Note NCAR-TN/STR-100, National Center for Atmospheric Research, Boulder, CO. (1974).

28. P.B. Ulrich, 'Proceedings of the Tri-Service Lidar Workshop, Tucson, Arizona 3-5 Feb., 1981,' Sponsored by OUSDRE and the EOMET Program.

29. D. Jensen, R. Jeck, G. Trusty, and G. Schacher, "Intercomparison of PMS Particle Size Spectrometers," NOSC Technical Report 555 (1980).

30. A. Guttman, ed., "Data Compendium for Atmospheric Laser Propagation Studies Conducted at Cape Canaveral, Fla.: Feb-May 1977," NRL Memorandum Report 3611 (1977).

31. G.L. Trusty, T.H. Cosden, S. Craig, and P.C. Ashdown, "Measurements of Optical Propagation Parameters Aboard the Aircraft Carrier USS LEXINGTON," NRL Memorandum Report 4716 (1981).

32. J.L. Walsh and P.B. Ulrich, "Thermal Blooming in the Atmosphere," p. 223-318, in *Laser Beam Propagation in the Atmosphere*, J.W. Strohbehn, ed., Springer-Verlag, N.Y. 1978.

33. D.M. Cordray, J.W. Fitzgerald, S.G. Guthman, J.N. Hayes, J.E. Kenney, G.P. Mueller, and R.E. Ruskin, "Meteorological Sensitivity Study of High Energy Laser Propagation," NRL Report 8097 (1977).

34. P.G. Gebhardt, "High Power Laser Propagation," Applied Optics *15*, 1479 (1976).

APPENDICES

Appendix A

PRELIMINARY TRACKER TEST PLAN

In order for PMS/405 and NRL to asses progress on the ship-to-ship measurements program, NRL will perform, during Autumn 1981, an extensive analysis of the tracker performance. The test and measurements will be conducted on the roll-and-pitch platform at NRL's Chesapeake Bay Division. The tracker assembly will be mounted on the platform and exercised to simulate at-sea conditions as are expected aboard LEXINGTON. A fixed beacon will be mounted on a stable mount, probably on the jack-up barge offshore in Chesapeake Bay, together with the tracking equipment (quad-cell, detector, tracking data link, ect.). The following tests and measurements will be performed:

1. The error signal in the servo-electronics will be recorded as the tracker simulates the at-sea motion. Analysis of this data will be used to evaluate the electronics control design.

2. The degree of difficulty of acquiring the target will be measured. Several people will each employ the joystick system for target acquisition, as the system is in motion.

3. The quad-cell signal-to-noise will be measured at several ranges.

4. The beam size and strength of the GaAs laser system will be studied for turbulence effects.

A report discussing the results and conclusions of the above tests will be delivered to PMS/405 on or before 11 January, 1982.

N/H TEST RESULTS AND ANALYSIS OF TRACKING CAPABILITY

Prepared for
Naval Research Laboratory

by

Massachusetts Manufacturing Corporation
308 Pearl Street
Cambridge MA 02139

9 September 1981

Table of Contents

Figures

1. INTRODUCTION

In March 1979, Appendix A, "Mount Control Systems" was written as an addition to "A Shipboard Experiment for DF Laser Propagation Measurements" by R.F. Horton (June 1979). This briefly discussed the N/H tracker in general terms. We calculated ship-based fixed-target tracking errors of 25-100 μrad based on a guess as to the achievable servo unity gain bandwidth.

With considerably more information, we produced a "Nike Hercules Interim Report", dated 24 April 1980. Unfortunately, at that time anomalously high friction was measured on the mount which created uncertainties. Nonetheless, the predicted errors were in the same range.

In December 1980, we installed a position control system on the mount. This used 50 μrad resolution shaft angle encoders to measure the position instead of the beacon tracking silicon quadrant which will come later. In addition, the mount was on stationary dry land and therefore the servo system did not have to handle external perturbations. However, the transient response to step inputs added more information which can be used to predict performance expected in the field.

At this point it seems appropriate to try to tie these together. In addition, a new potential requirement for tracking moving targets makes it worthwhile to look at the possibilitiese there. In response to questions from individuals trying to evaluate progress, we will keep the discussion on a non-specialist level. A general understanding of Laplace transforms will be very useful, however.

We will examine different "types" of servo systems and in particular errors one might expect. Then we will look at a more general system--one that combines two types. This model will be adapted to a "real" system such as the N/H tracker. Lastly, some experimental results and, based on this, projections of future performance will be given.

2. ERRORS FROM DIFFERENT "TYPE" SERVO SYSTEMS--BANDWIDTH

After a basic discussion, we find steady state errors for various inputs and "types", which term is explained. Bandwidth can have a slightly different meaning than the usual -3 dB one, and this is explained below.

2.1 Basics

The need for feedback can be illustrated by Fig. 1. Without it (H=0),

$$C = GE = GR \tag{2.1}$$

If G could be made well behaved, then no feedback would be necessary. Often, however, G includes a power amplifier or motor whose characteristics are not only nonlinear but change with time. The basic feedback operation is to compare the input R with a sample of the output B (or the output C if H=1) to produce an error, E, which drives an amplifier G. The bottom line usually is what is E? We have

$$C = GE = G(R-HC)$$

$$C = \frac{G}{1+GH} R$$

$$E = R - \frac{GH}{1+GH} R = \frac{R}{1+GH} \tag{2.2}$$

when

$$G \to \infty,\ C \to R/H,\ \text{and}\ E \to 0.$$

A desirable system results if G is large and H is the <u>inverse</u> of the desired input to output transfer function. Here the assumption is made that a sufficiently accurate

H element can be built. For instance, a shaft angle encoder to feedback angle information will always be more precise than a 1 Hp motor to control the angle, but even so the desired precision can sometimes tax the capabilities of the feedback sensor (as in the N/H case).

2.2 Unity Feedback, H=1

Without too much loss, we can simplify the discussion by assuming unity feedback, H=1. This means we have a perfect measuring device on the output and want it to be an exact replica of the input. Equation 2.2 becomes

$$\frac{C}{R} = \frac{G}{1+G}$$

$$\frac{E}{R} = \frac{1}{1+G} \qquad (2.3)$$

2.3 Instability

Now it would appear that all we have to do is make G infinite by, for instance, the addition of electronic amplifiers in front of the motor. As is well known, however, the system can become unstable if the gain is made too high. To illustrate, suppose we are not too greedy and are willing to settle for a system which is very accurate at low frequencies only. We will make G large there but let it fall off as frequencies increase. We could try (assuming ideal motors, etc.)

$$G(S) = \frac{G_0}{S^3} \qquad (2.4)$$

G_0 = a constant

Then,

$$\frac{C}{R} = \frac{G}{1+G} = \frac{K}{S^3+K} \tag{2.5}$$

and

$$\frac{E}{R} = \frac{S^3}{S^3+K} \tag{2.6}$$

Thus, the error at zero frequency is zero but it can be shown that the response to an input would be of the form

$$C(t) = \exp(+\sigma t)\ \sin(\sqrt{3}\ \sigma t + \phi) \tag{2.7}$$

$$\sigma = (K/8)^{1/3}$$

ϕ = some phase angle

In other words, the output would grow exponentially (the system is unstable).

The major effort in servo design is to minimize the error but keep the system stable.

2.4 System Type

Quite often the forward open loop gain G can be written in the form

$$G(S) = \frac{G_1}{S^n}\frac{N(S)}{D(S)} \tag{2.8}$$

where

G_1 = a constant

n = 0, 1, 2, 3, etc.

and where

$N(0)/D(0) = 1$

The definition of servo system type is simple:

Type:	0	I	II	III	etc.
n:	0	1	2	3	

We saw above that Type III systems can be unstable and we will, as is usually done, restrict ourselves to Type II or lower.

2.5 Steady State Errors with Algebraic Inputs

One evaluation criteria for a servo system is the residual or steady state error remaining after inputs like steps, ramps, and parabolas. Two of these are the integrals of the previous one and go as t^m, as in the table below.

Kind	r(t)	R(S)	m
step	$u_{-1}(t)$	$1/S$	1
ramp	$tu_{-1}(t)$	$1/S^2$	2
parabola	$1/2\ t^2u_{-1}(t)$	$1/S^3$	3

The simplicity of the Laplace transform, R(S), is helpful because, even without knowing the detailed transient response, one can find steady state values using the final value theorem. For the error, we have

$$e_{ss} \equiv \lim_{t\to\infty} e(t) = \lim_{S\to 0} SE(S) = \lim_{S\to 0} \frac{SR(S)}{1+G(S)}. \qquad (2.9)$$

This can be simplified if we use a low frequency approximation $G(S) = G_1/S^n$. Then for the algebraic inputs,

$$e_{ss} = \lim_{S\to 0} \frac{S^{n+1-m}}{G_1+S^n} \qquad (2.10)$$

with the following results for steady state errors, e_{ss}:

Type	n \ m	step 1	ramp 2	parabola 3
0	0	$(G_1+1)^{-1}$	∞	∞
I	1	0	G_1^{-1}	∞
II	2	0	0	G_1^{-1}

The steady state errors are either infinite, finite, or zero. Since $G_1 \gg 1$ (usually), the finite errors are inversely proportional to gain. Type 0 systems are rarely used in tracking servos because of the non-zero errors, and parabolic inputs are not often encountered. One therefore tends to concentrate on Type I and II systems with step and ramp inputs.

(See Section 2.5R, page 10)

2.6 Steady State Errors with Sinusoidal Inputs

If the tracking system is mounted on a table which oscillates sinusoidally, the equivalent input is an identical sinusoid. Thus,

$$r(t) = \sin \omega_e t \tag{2.11}$$

and

$$R(S) = \frac{\omega_e}{S^2 + \omega_e^2} \tag{2.12}$$

but in the steady state,

$$|e(t)| = \left| \frac{1}{1 + G(j\omega_e)} \right| \tag{2.13}$$

Using $G = G_1/s^n$, we have for errors due to unit sinusoids:

Type	Error Magnitude	Approximate Error ($\omega_e << G_1$)
0	$(1+G_1)^{-1}$	$1/G_1$
I	$(1 + G_1^2/\omega_e^2)^{-1/2}$	ω_e/G_1
II	$(1 - G_1/\omega_e^2)^{-1}$	ω_e^2/G_1

Again, the error is inversely proportional to gain and decreases as the type goes up (since $\omega_e << G_1$).

2.7 Bandwidth

Looking at Eq. 2.13 one might conclude that the 3 dB bandwidth occurs when $G(j\omega) = j$. This is approximately true, but not a useful concept since the transient response can differ considerably from a simple filter.

The more usual frequency characteristic is the similar unity gain crossover frequency, $f_1 = \omega_1/2\pi$, defined by

$$|G(\omega_1)| = 1 \qquad (2.14)$$

or the Type systems discussed so far, ω_1 is:

Type	ω_1	$\lvert G(S)\rvert$
0	-	G_1
I	G_1	ω_1/ω
II	$\sqrt{G_1}$	$(\omega_1/\omega)^2$

where $G(S)$ was assumed to be G_1/s^n

The sinusoidal tracking errors were discussed in the 1979 Appendix. At that time, we anticipated ship rolls of ±2° in 12 sec periods with unity gain crossovers for Type II systems of 1.5 to 3.1 Hz to yield 100 μr to 25 μr errors, respectively. In the Interim Report we discussed more realistic ship's roll rates of 1° in a worst case 16-sec period. This is considerably easier than before, but in December 1980, as we discuss below, we could only achieve an 0.8 Hz unity gain bandwidth.

With these newer results, we have

$$
\begin{aligned}
f_1 &= 0.8 \text{ Hz} \\
\omega_1 &= 2\pi f_1 = 5 \text{ rad/sec} \\
A &= 1^\circ = 17.4 \text{ mrad} \\
\omega_e &= 2\pi/T = 0.4 \text{ rad/sec} \\
\text{Type} &= \text{II} \\
e_{ss} &= A_1(\omega_e/\omega_1)^2 = 111 \text{ μrad}
\end{aligned}
\tag{2.15}
$$

which is slightly higher than we first guessed. Unfortunately, we do not have a pure Type II system and so these results are a lower bound on the error. On the other hand, the 0.8 Hz represents only a 3-day effort with a fully operating mount. Further, typical roll rates are expected to be down by a factor of 4. We will return to this in Section 5.2.

2.5B Steady State Error Coefficients

Another bit of nomenclature involves the so-called error coefficients which are defined for steps, ramps, parabolas, etc. These are a little more general then the error computation given in Section 2.5. Given

$$R(S) = S^{-m} \quad m = 1, 2, 3, \text{ etc.}$$

then

$$e_{ss} = \lim_{S \to 0} \frac{SR(S)}{1+G(S)} = \lim_{S \to 0} \frac{1}{S^{m-1} + S^{m-1}G(S)}$$

$$= \frac{1}{1+K_1} \quad m=1$$

$$= \frac{1}{K_m} \quad m=2,3, \ldots$$

where

$$K_m = \lim_{S \to 0} S^{m-1}G(S)$$

If we identify 1, 2, 3 with a step, ramp, and parabola, then the error coefficients are conventionally identified as related to position, velocity, and acceleration. The following table may help.

m	Input	Designation	Coefficient	Limit	Steady State Error
1	step	position	K_p	$G(S)$	$(1+K_p)^{-1}$
2	ramp	velocity	K_v	$SG(S)$	K_v^{-1}
3	parabola	acceleration	K_a	$S^2G(S)$	K_a^{-1}

This method of finding errors is slightly more general than that of Section 2.5 because one does not need to write $G(S)$ explicitly in the form G_0/S^n.

3. SECOND ORDER SYSTEM RESPONSE

Most systems cannot be described well as a single Type but many can be as a combination of a Type I and Type II over some frequency range. By this we mean the open loop gain is of the form

$$G(S) = \frac{1}{(S/\omega_0)[2\delta + (S/\omega_0)]} \qquad (3.1)$$

where ω_0 = "natural" frequency
δ = damping factor.

For low frequencies $G(S) \approx 1/S$, but at higher ones, $G(S) \approx 1/S^2$. By adjusting δ one can go from Type I to Type II.

The closed loop gain and error transfer functions are

$$\frac{C}{R} = \frac{G}{1+G} = \frac{1}{1 + 2\delta(S/\omega_0) + (S/\omega_0)^2}$$

$$\frac{E}{R} = \frac{1}{1+G} = \frac{2\delta(S/\omega_0) + (S/\omega_0)^2}{1 + 2\delta(S/\omega_0) + (S/\omega_0)^2} \qquad (3.2)$$

The steady state errors for steps, ramps, and low frequency sinusoids are:

Step	0
Ramp	$2\delta/\omega_0$
Sinusoid	$2\delta(\omega_e/\omega_0)$

It appears that one would like to make δ small but this may adversely affect the transient response even though steady state error is improved. The remainder of Section 3 discusses this tradeoff.

3.1 Response to a Step

If $r(t) = u_{-1}(t)$, then using Eq. (3.1) and inverse Laplace transforms, one can find (see Fig. 2)

$$C(T) = 1 - \frac{e^{-\delta\omega t}}{\sqrt{1-\delta^2}} \sin(\sqrt{1-\delta^2}\omega_0 t + \phi) \tag{3.3}$$

where

$$\phi = \cos^{-1}\delta = \sin^{-1}\sqrt{1-\delta^2} \tag{3.4}$$

One can see from the figure that as $\delta \to 0$, the transient response has a great deal of overshoot and zero average error but large instantaneous error, even in the steady state. As $\delta \to \infty$, instantaneous errors become small but this takes a long time to achieve. Because of the slow response, values of $\delta > 1$ are generally not used. The lowest total rms error is achieved when $\delta = 1/2$.

Because it is easy to understand and measure on a strip chart recorder, the first (peak) overshoot and time to reach it are of some interest. Setting $dC/dt = 0$, one finds

$$C_{max} = 1 + \exp[-\pi\delta/(1-\delta^2)^{1/2}] \tag{3.5}$$

at

$$t_{max} = \frac{\pi}{\omega_0}\left(\frac{1}{1-\delta^2}\right)^{1/2} \tag{3.6}$$

The maximum error occurs at t_{max} also and is given simply by

$$e_{max} = C_{max} - 1 = \exp(-\pi\delta/\sqrt{1-\delta^2}) \equiv P \quad \text{for } 0<\delta<1 \qquad (3.7)$$

Since the input is a unit step, this is a fraction called "overshoot", P. Note that for $\delta>1$ there is no overshoot.

Given P and t_{max}, one can find

$$\delta = \left(\frac{\ln^2 P}{\pi^2 + \ln^2 P}\right)^{1/2} \qquad (3.8)$$

and

$$\omega_0 = \frac{(\pi^2 + \ln^2 P)^{1/2}}{t_{max}} \qquad (3.9)$$

3.2 Response to a Ramp Input

For a ramp, $r(t) = tu_{-1}(t)$, $R(S) = 1/s^2$, and we can use inverse Laplace transforms or note that a ramp is the integral of a step and so are the responses. We find

$$C(t) = t - \frac{2\delta}{\omega_0} + \frac{e^{-\delta\omega t}}{\omega_0(1-\delta^2)^{1/2}} \sin(\sqrt{1-\delta^2}\,\omega_0 t + \psi) \qquad (3.10)$$

$$\psi = \cos^{-1}(2\delta^2 - 1) = \sin^{-1} 2\delta\sqrt{1-\delta^2} \qquad (3.11)$$

which is illustrated in Fig. 3.

The error is

$$e(t) = C(t) - t = \frac{2\delta}{\omega_0} + \frac{e^{-\delta\omega t}}{\omega_0(1-\delta^2)^{1/2}} \sin(\sqrt{1-\delta^2}\,\omega_0 t + \psi) \qquad (3.12)$$

This has a steady state value, $2\delta/\omega_0$, as we found previously, and a decaying sinusoid. Again, if $\delta=0$, the average error equals zero but the sinusoid never decays. If $0<\delta<1$ the error reaches a peak undershoot on the first cycle, which occurs at

$$t_{max} = \frac{\pi - \cos^{-1}\delta}{\omega_0(1-\delta^2)^{1/2}} \tag{3.13}$$

at which point

$$e_{max} = -\left(\frac{2\delta + \exp\left(\frac{-\delta(\pi-\cos^{-1}\delta)}{(1-\delta^2)^{1/2}}\right)}{\omega_0}\right) \tag{3.14}$$

Since this is the maximum error, it tells us whether we can keep a target that suddenly appears within the field of view.

We could also find ω_0 and δ from t_{max} and e_{max} but ramp inputs are harder to produce and not as convenient to interpret for test and measurement purposes.

3.3 Response to a Sinusoidal Input--Unity Gain Bandwidth

The amplitude response to a sinusoidal input $\sin \omega_e t$ is

$$|C| = \frac{1}{1 + 2\delta j(\omega_e/\omega_0) + (j\omega_e/\omega_0)^2}$$

$$= \left([1 - (\omega_e/\omega_0)^2]^2 + (2\delta\omega_e/\omega_0)^2\right)^{-1/2} \tag{3.15}$$

The magnitude of the error is

$$|e| = [\quad\quad]^{2,1/2}|a| \qquad (3.16)$$

When the input frequency is low, the error is

$$|E| \approx 2\delta \frac{\omega_e}{\omega_0} \tag{3.17}$$

which contrasts with a pure Type II system, where the error was

$$|E| = (\omega_e/\omega_1)^2 \tag{3.18}$$

In this system, the magnitude of the open loop gain decreases to 1 at a frequency

$$\omega_1' = \omega_0[(1+4\delta^2)^{1/2} - 2\delta^2]^{1/2} \tag{3.19}$$

ω_1' varies from ω_0 to $.49\omega_0$ as δ increases from 0 to 1. Thus ω_1' is close to ω_0 in value and for small δ, ω_1' can replace ω_0 in Eq. (3.17). In order to keep the same error for the same bandwidth as a pure ype II, one needs to keep

$$\delta << \frac{1}{2}\left(\frac{\omega_e}{\omega_0}\right) \tag{3.20}$$

As an example, if $\omega_1 = 5$ rad/sec and $\omega_e = .4$ rad/sec as in Section 2, then we need $\delta << .04$. This is very low and indicates for a system with good transient response we will need a larger bandwidth than the pure Type II.

4. MOTOR DRIVEN ANGULAR POSITION SERVO

Having laid the basic mathematical groundwork, we can start to look at slightly more realistic situations. We will find, however, that a second order (in S) model can still be useful.

4.1 Motors

The prime movers in most tracking systems are motors. The minimum model is one which takes into account inertia and viscous friction. The equation of motion is

$$T = BN + J\,dN/dt \qquad (4.1)$$

or

$$T(S) = (B+JS)N(S)$$

where

T = torque
J = moment of inertia
B = viscous friction coefficient
N = motor shaft speed.

The motor torque can usually be expressed approximately as a linear function of a control voltage or current, depending on the type of motor. The transfer function is therefore of the form

$$\frac{N(S)}{V(S)} = \frac{K}{B+JS} \qquad (4.2)$$

where K = torque constant
V = voltage applied to motor.

4.2 General Angle Control Loop

The simple angle control servo, Fig. 4, is typical of both the N/H and 60" systems. This has unity position feedback to an angle error amplifier A. The H(S) block is a new feature, an internal feedback or minor loop. It will provide compensation for part of the servo by feeding back a function of the angular velocity to the velocity error amplifier G.

Note that shaft angle, θ, is mathematically the integral of shaft speed, N, so the 1/S term is exact. One tends therefore to have at least a Type I system.

4.3 Rate (Tachometer) Feedback Compensation

If all servo system components were ideal, then the tach loop would not be useful or could be accomplished in some other way. However, because motors and their associated power amplifiers are not well behaved, it has been found beneficial to control the motor shaft speed with this type of internal feedback, H(S). We will assume H(S) is necessary but still use a linear motor model for further discussion.

It might be assumed that the ideal form would be H(S)=1. In other words, try to make N=M and go from there for the position loop. This is the case when operating a joystick which has inputs connected at point M and the desired controlled variable is N. However, when embedded in a position loop, this is usually not the case. The transfer function

$$\frac{N}{M} = \frac{\frac{GK}{B+SJ}}{1 + \frac{GK}{B+SJ} H} = \frac{GK}{B + SJ + GKH} \qquad (4.3)$$

already contains a term in the denominator, B, which is not zero at low frequencies. This keeps the open loop gain small at low frequencies, something we have been trying to avoid. Adding another constant term, GK (if H=1, G = constant), does not help. Making G=S would fix that, but would cause problems in the numerator.

A possibility is to make A(S) = 1/S, but now we have S's in three denominators, raising possibilities of instability. The usual choice is to make

$$H(S) = DS \tag{4.4}$$

where

D = tachometer feedback constant.

With this choice, angular acceleration, dN/dt, is fed back. Then,

$$\frac{N}{M} = \frac{GK}{B + S(J+GKD)} \tag{4.5}$$

$$= \frac{GK/B}{1+ST}$$

where

T = J/B + GKD/B, a time constant.

By varying D, one can swamp out the motor time constant J/B. Additionally, if D and S are large,

$$\frac{N}{M} \approx \frac{1}{DS} \tag{4.6}$$

In this approximation we would have a Type II positioning system if A is a constant.

4.4 Position Control

Using the rate loop compensation discussed in the last section, the open loop (forward) gain is

$$A_{ol} = A \times \frac{GK/B}{1+ST} \times \frac{1}{S} = \frac{a/B}{S + S^2T} \tag{4.7}$$

where

$a = AGK$, a constant, and

$$\frac{\theta}{R} = A_{cl} = \frac{A_{ol}}{1+A_{ol}} = \frac{a/B}{a/B + S + S^2T} \tag{4.8}$$

$$= \frac{1}{1 + SB/a + S^2TB/a} = \frac{1}{1 + 2\delta S/\omega_0 + (S/\omega_0)^2}$$

where

$$\omega_0 = \left(\frac{a}{TB}\right)^{1/2} = \left(\frac{AGK}{J + GKD}\right)^{1/2}$$

and

$$\delta = \frac{\omega}{2}\frac{B}{a} = \frac{B}{2}\left(\frac{1}{AGK(J+GKD)}\right)^{1/2}$$

When D is large, we have

$$\omega_0 \approx (A/D)^{1/2} \tag{4.9}$$

$$\delta \approx \frac{B}{2GK}\left(\frac{1}{AD}\right)^{1/2}$$

We have a second order control system identical to the kind discussed in Section 3. The "natural frequency", ω_0, and damping, δ, can be adjusted with A, G, and D.

We found in Section 3 that the steady state error due to a unit ramp was

$$e_{ss} = \frac{2\delta}{\omega_0} = \frac{B}{AGK} \tag{4.10}$$

and due to a unit sinusoid was

$$|e| = \frac{2\delta}{\omega_0}\left(\frac{\omega_e}{\omega_0}\right) = \frac{B}{AGK}\left(\frac{\omega_e(J+GKD)}{AGK}\right)^{1/2} \tag{4.11}$$

In both cases higher gain is needed to overcome friction.

5.1 N/H Servo Experiments

In December 1980, a preliminary servo system electronics package was connected to the N/H mount. This package consisted of

a) a joystick
b) a trackball
c) thumbwheel switches
d) LCD displays
e) analog displays
f) servo electronics.

The joystick could be used for velocity control and the trackball for position control. A more useful position control device was the set of thumbwheel switches for each axis. These and the LCD were 17-bit binary devices matching the 50 urad resolution of the shaft encoders installed on the mount. Since tracking quad cells were not installed, the shaft encoders were the only means of position feedback.

The servo electronics implemented a tachometer feedback compensated position loop similar to that described in Section 4. They were a bit more complicated, but those details are not necessary here. After some adjustment of gains and filters, we obtained reasonably stable control of the azimuth axis.

Experiments were performed in which one of the levers on the thumbwheel switch was advanced one position and the error transient recorded on a strip chart. The results for steps of 400 urad, 3 mrad, 24 mrad, 200 mrad, and 1.6 rad are shown in Figs. 5.1 through 5.5. Note that the initial size of the error equals the step so the absolute vertical scale is not required.

Ignoring for the moment the 400 μrad case, Fig. 5.1, one can see in Figs. 5.2 and 5.3 a reasonably behaved transient response for the 3 mr and 24 mr steps. Using Eqs. (3.8) and (3.9), we find

$$\delta = 0.5$$
$$\omega = 5 \text{ rad/sec}$$

Looking back at the 400 μrad case, one can discern transients obscured by apparent noise. Although the reproduction does not make it obvious, examination of the original strip chart suggests that the noise consists of 50, 100, 150, 200 μrad, etc. steps corresponding to one or more bits of the shaft encoder. This could be reduced using higher gain but then the transient response became oscillatory. It is expected that the chatter can be reduced later by reducing the gear backlash and motor amplifier deadzones.

The 200 mr and 1.6 rad responses are progressively slower and less damped. If the system were linear, their shapes would be identical to the lower amplitude transient responses. If it were simply a case of lower gain, the frequency would be lower but the damping would be higher. When response time slows down with amplitude, it is usually a sign of saturation inside the control loop, but this needs further investigation.

5.2 Projected Errors

Making the assumption that we can obtain a second order servo with an $\omega_0 = 5$ rad/sec (corresponding to a unity gain bandwidth of .76 Hz), we have prepared Table 5.1 of errors to be expected from steps and sinusoids for

Table 5.1

Normalized Errors for ω_0 = 5 rad/sec

	1 rad step		1 rad/sec ramp			1 rad sinusoid at 0.4 rad/sec	0.25° sinusoid at 0.4 rad/sec
δ	e_{max} (rad)	t_{max} (sec)	e_{max} (rad)	t_{max} (sec)	e_{ss} (rad)	(rad)	(μrad)
0	1.00	.628	.20	.314	0	.0064	28
.1	.73	.63	.21	.34	.04	.017	74
.2	.53	.64	.22	.36	.08	.033	144
.5	.16	.73	.26	.48	.20	.081	353
.707	.04	.89	.30	.67	.28	.113	493
.9	.002	1.44	.37	1.23	.36	.144	628
1.00	0.0	∞	.40	∞	.40	.160	698

Table 5.2

Normalized Errors for ω_0 = 10 rad/sec

	1 rad step		1 rad/sec ramp			1 rad sinusoid at 0.4 rad/sec	0.25° sinusoid at 0.4 rad/sec
δ	e_{max} (rad)	t_{max} (sec)	e_{max} (rad)	t_{max} (sec)	e_{ss} (rad)	(rad)	(μrad)
0	1.00	.314	.10	.157	0	.0072	31
.1	.73	.316	.16	.17	.02	.0082	36
.2	.53	.32	.11	.18	.04	.016	70
.5	.16	.36	.13	.24	.10	.040	175
.707	.04	.44	.15	.33	.14	.057	24
.9	.002	.72	.18	.62	.18	.072	-
1.00	0.0	∞	.20	∞	.20	.080	349

δ's from 0 to 1. Since it is conceivable, we have made Table 5.2 for ω_0 = 10 rad/sec.

One can see that up to δ = 0.707, the response time is not appreciably lengthened. The overshoot becomes appreciable when δ=.2 so that 0.2<δ<0.7 is a preferred range, but there the error due to ship's motion is appreciable unless δ=0.2 and ω_0 = 10 rad/sec. Using Eq. (3.9), ω_1' = 9.99 rad/sec or f_1 = 1.6 Hz. This is not an unreasonable hope.

Another alternative is to dynamically vary δ depending on the situation. It is not unusual to use a Type I system (δ large) to give small overshoots and switch to a Type II system (δ small) to reduce the residual error. This will be investigated in the future.

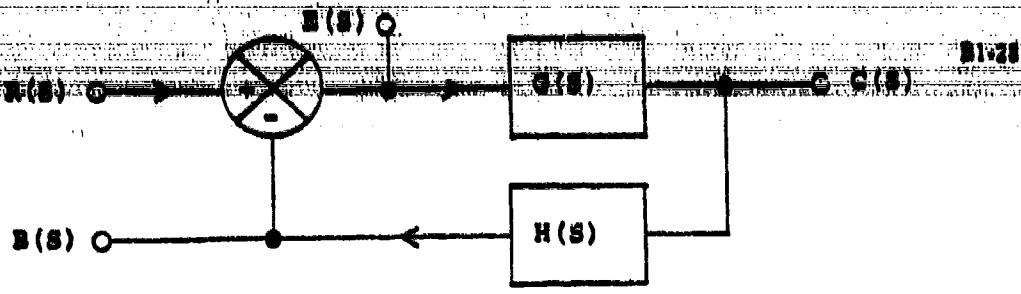

R = input
C = output
B = sample of output
E = error
G = forward (open loop) gain
S = Laplace transform frequency variable

Fig. 1. Basic Servo Block Diagram.

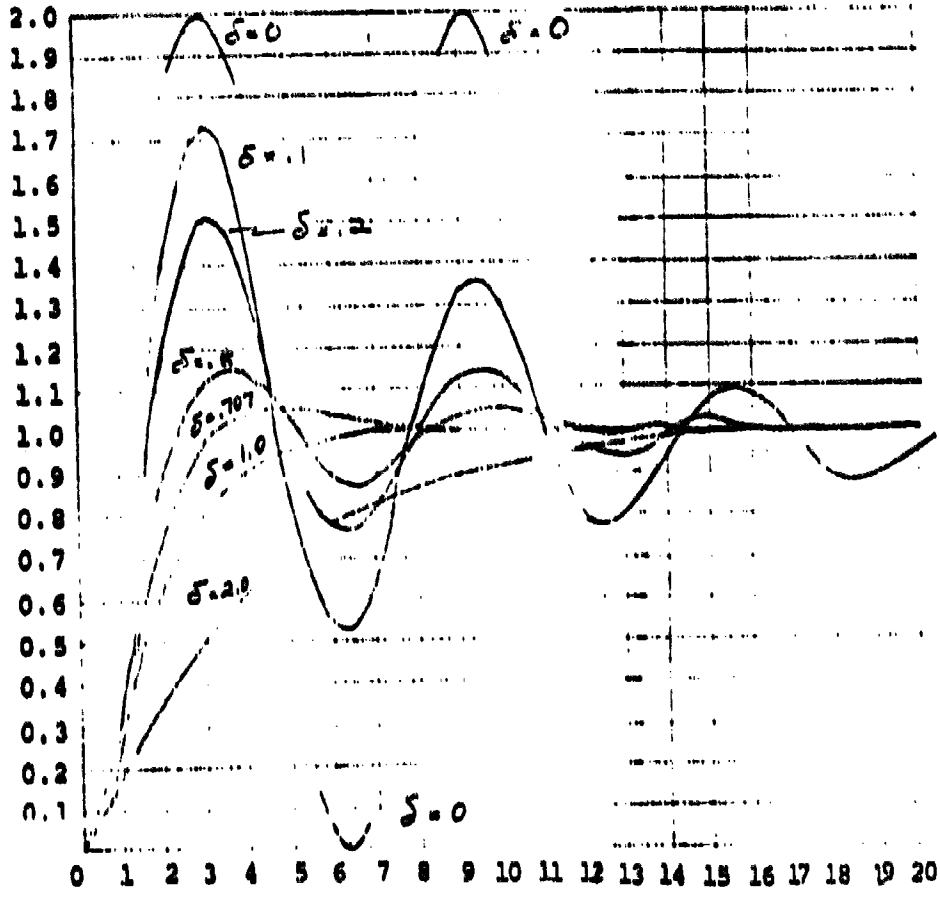

Fig. 2. Unit Step Transient Response.

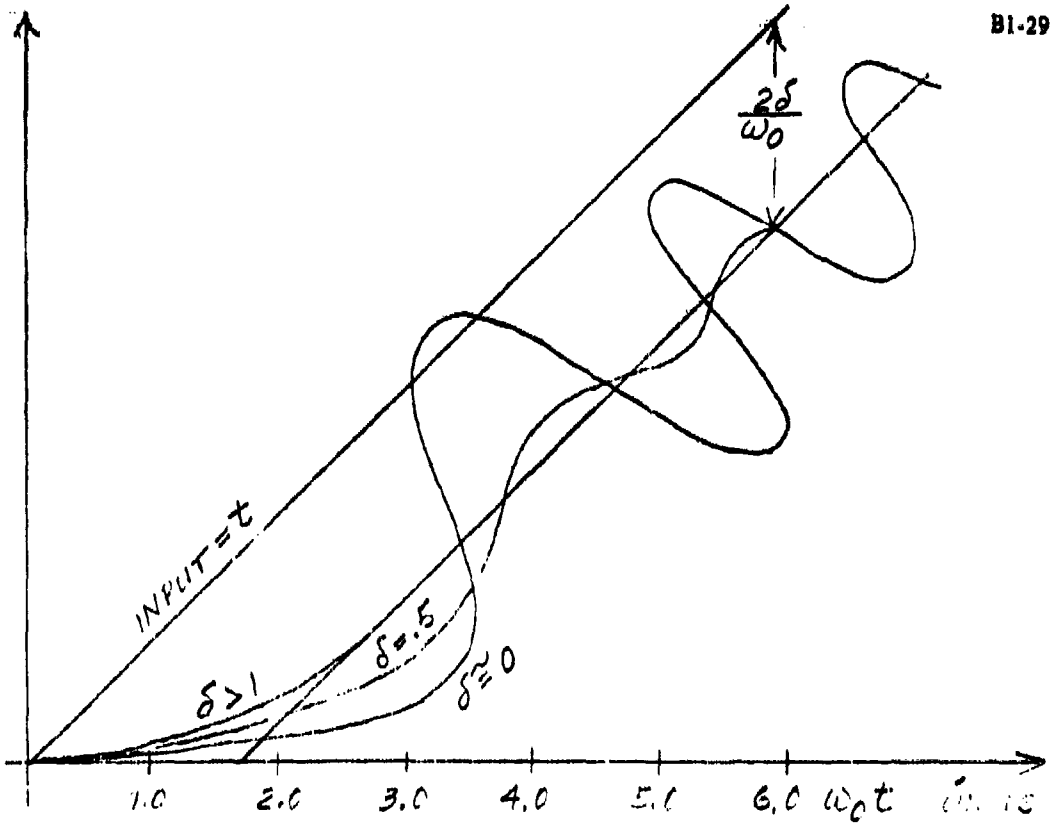

Fig. 3. Unit Ramp Transient Response.

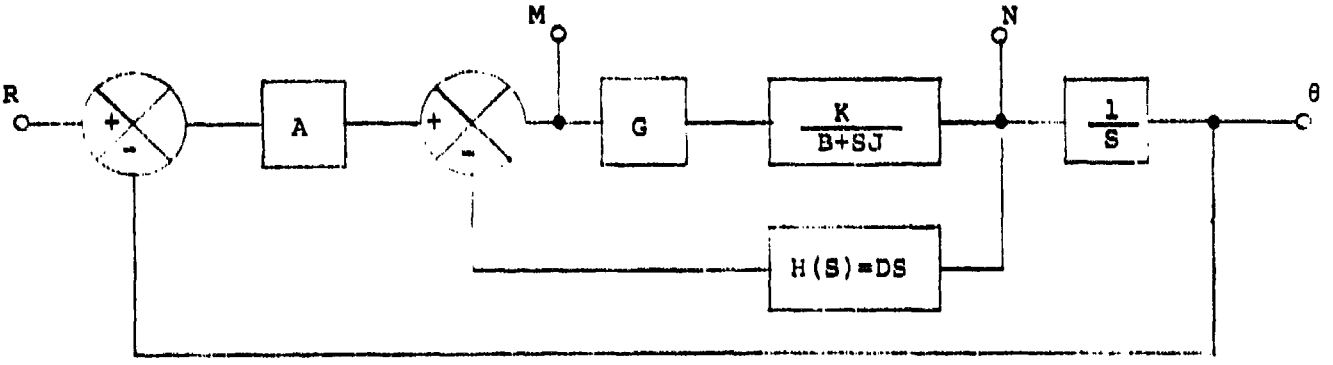

Fig. 4. Simple Angle Control Servo.

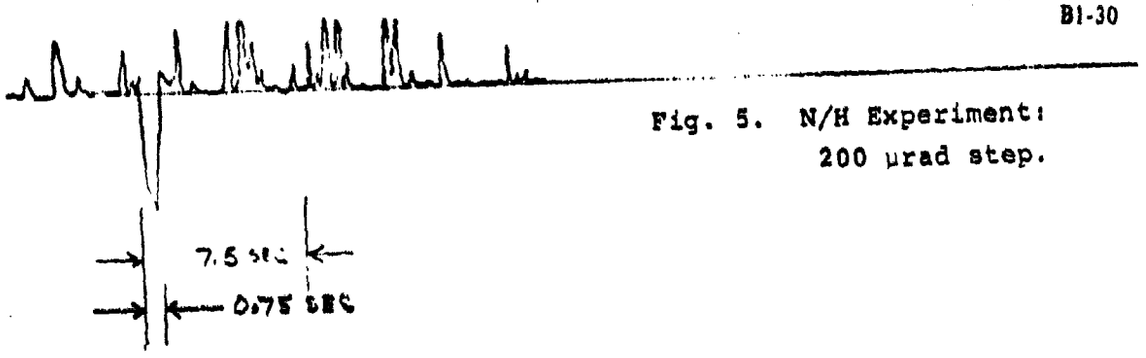

Fig. 5. N/H Experiment: 200 μrad step.

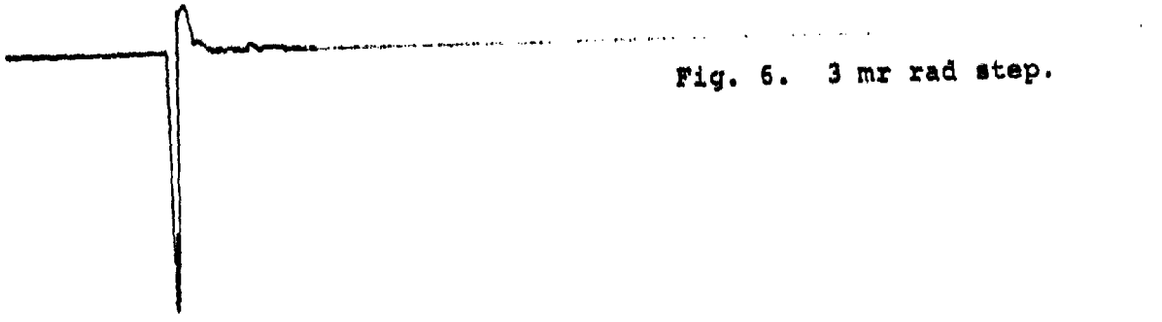

Fig. 6. 3 mr rad step.

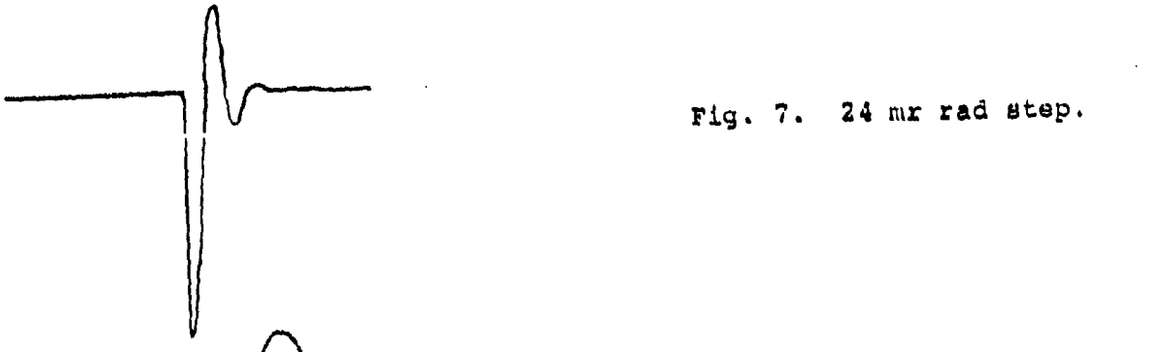

Fig. 7. 24 mr rad step.

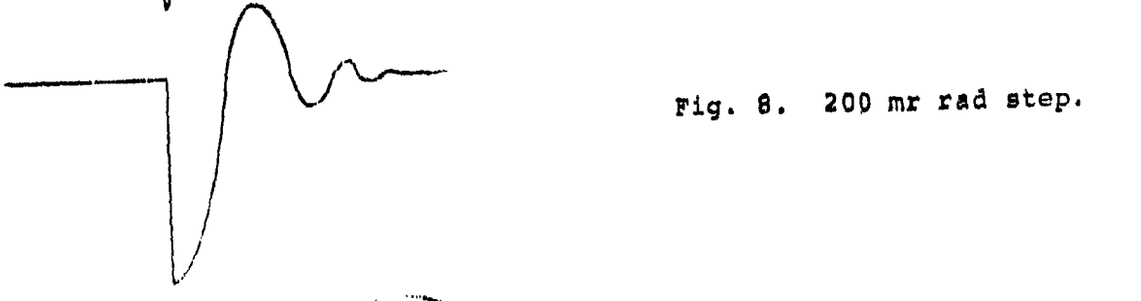

Fig. 8. 200 mr rad step.

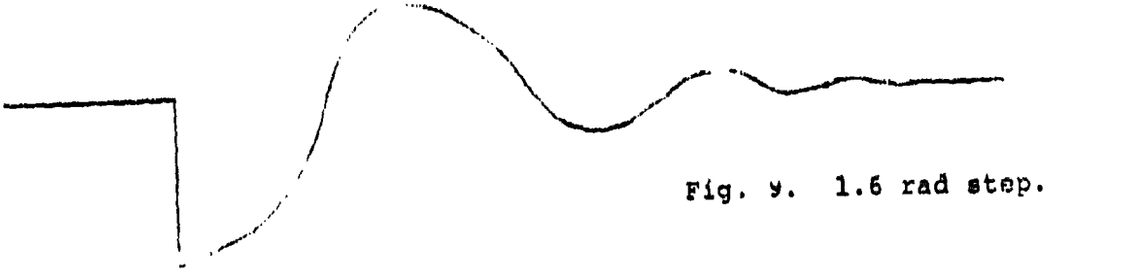

Fig. 9. 1.6 rad step.

SYSTEM ANALYSIS OF SHIP-TO-SHIP TRANSMITTANCE MEASUREMENTS AND ASSOCIATED ELECTRONICS

INTERIM REVIEW

APRIL 1981

MASSACHUSETTS MANUFACTURING CORPORATION

1. INTRODUCTION

In 1977, the Naval Research Laboratory (NRL) began investigating the possibility of placing its heretofore land-based Infrared Mobile Optical Radiation Laboratory (IMORL)[1] on large naval ships.[2] The purpose would be to extend its measurement of the atmosphere from conditions obtained on land or at the seacoast to those which might obtain at sea. The primary measurement would be of atmospheric transmission in the 2-12 μm wavelength range. This would require two ships to act as sender and receiver. For reasons of stability, ease of emplacement, and availability, an aircraft carrier used as a training vessel was proposed to house the major part of the equipment.

NRL started procuring optical mirrors for the new 32" telescope which would be required and, in July 1979, Massachusetts Manufacturing Corporation (MMC) started designing a servo control system to point it. This telescope would use a U.S. government surplus Nike/Hercules (N/H) radar mount with the optical mirrors substituted in place of the radar receiving dish. Cost and availability were major reasons for taking this approach. Work progressed on a very low level, but progress was made. The telescope optical design was finished[3] and the servo control aspects of the N/H mount began to be understood.[4] Finally, in December 1980, the mount was brought under closed loop velocity and position control. The position control used digital shaft angle encoders only; infrared tracking sensors were to be installed in the third and final phase of MMC's contract.

By January 1981, confidence in the likelihood of achieving the initial objective had increased and some new tasks had been thought of. These new ones centered primarily on using the N/H tracking telescope to follow aircraft from the carrier or in some cases basing the telescope on land and following ships or aircraft. The purpose would still be to make atmospheric transmission measurements, at least on a relative basis, and to measure radiation from a variety of sources. Because the potential usefulness seemed greater than before, NRL decided to pursue the program on a stepped-up level.

The following proposal from MMC is directed toward achieving what we take to be NRL's two main objectives of:

1) making absolute atmospheric transmission measurements between two ships at sea over ranges up to 5 km, and

2) to the largest extent possible, using the N/H telescope alone to track and measure sources other than used in the transmission measurements. This will include helicopters, aircraft, and the like.

The remainder of this document discusses what is now named the IMORTAL system. Most of the discussion centers on the first objective, since the second one will be realized later in time and will depend on experience in realizing the first. It should be stated that the second objective will be pursued as much as possible from the beginning, however.

We will discuss the transmission measurements, the servo controls, and the measurement system electronics. A work statement, list of deliverables, and schedule follow. It is assumed the reader has some familiarity with the references above and progress to date.

Although the overall problem is addressed, MMC's part is limited to the electronics and electro-optical elements. Many parts of the system will be furnished by NRL.

2. TRANSMISSION MEASUREMENTS

In order to understand the requirements on the tracking servos and other electronics, it is necessary to know how the system will be used to make measurements. A typical IMORTAL system deployment between two ships, Fig. 1, would make an absolute transmission measurement in two steps--absolute at a few fixed wavelengths used to calibrate relative measurements over a broad range.

2.1 Absolute Transmission

For this measurement, a laser is used which, in conjunction with the N/H telescope, produces a well-collimated beam. To make absolute transmission measurements from one ship to another, all the energy in this beam, except that absorbed by the atmosphere, must be captured by another optical telescope on the receiving end. The major technical problem is to steer the beam into the light bucket, which task is aided by using the largest possible bucket. The one proposed is a modified NRL surplus anti-aircraft searchlight with a 60" mirror.

The 60" telescope need not produce a high quality image, since light gathering is all that is required, but there are other requirements. If a 3" beam from the N/H impinges on the bucket, then at most 3.4" of central obscuration can be allowed before 1% of the beam is lost. Thus, in addition to the primary IR detector

(DET #1), a secondary one (DET #2) is required, since the secondary of the 60" must be larger than 3.4". The obscuration due to XMTR B (whose use is explained below) must be less than 3.4" in diameter.

Assuming the fields of view (FOV) θ_{60_1} and θ_{60_2} are equal, IR DET #2 will be less sensitive since it has the smallest collector. For 1% transmission measurement accuracy, a signal-to-noise ratio (SNR) greater than 100:1 is required. A rough calculation (Appendix, section 2.1) shows this can be achieved with pyroelectric detectors and a ±5 mr FOV.

In terms of the control systems, if a 32" beam is to be kept in a 60" bucket and no turbulence exists, then less than 116 μr of error is allowed on the N/H control system at 5 km separation. The 60" control system must point at the N/H, keeping cos θ less than 1%, in other words, θ less than 140 mr (8°). In addition, the N/H must always be within the FOV of the IR detectors and so ±5 mr could become the real requirement.

2.2 Scanning Michelson Interferometer (SMI) Measurements

In this case, IR DET #1 is replaced by a light source and the laser at the N/H is replaced by an NRL SMI. Now the N/H must keep the 60" within the SMI's FOV (300 μr). The 60" control system must keep the SMI source beam pointed at the N/H. In order to keep the SMI SNR high, the source beam divergence should be as small as possible--on the order of 10 mr (0.5°) or less.

3. CONTROL SYSTEMS

Both the N/H and 60" systems will have servo control systems which point their respective telescopes. Usually manual (joystick) control of velocity will be used for acquisition followed by optical tracking of IR beacons.

3.1 Quad Sensors

Steering is accomplished via silicon quadrant angular position sensors (QUADs A and B) which track GaAs 0.9 μm laser diode transmitters (XMTRs A and B). The N/H must direct its beam precisely down the 60" boresight and so XMTR B must be located there. QUAD A likewise must be on the boresight of the N/H. Since 60" steering is much more relaxed, XMTR A and QUAD B can be off axis.

An earlier configuration used the laser in place of XMTR A and a quad IR detector as DET #2 in place of QUAD B. The change here is suggested because it uncouples some aspects of the measurement from the control systems so that

a) we can separately optimize tracking and measurement,

b) we will not have to wait for relatively expensive laser sources and IR detectors before closing the 60" control loop,

c) the money spent on a quadrant IR detector can be spent elsewhere,

d) XMTR A can be used as a data link from the N/H to the 60".

There are some disadvantages as well:

a) Two transmitters and receivers are needed--but these can be identical and development costs are only for one,

b) XMTR A may be picked up by IR DET 1 & 2. This can be a problem at close range (Appendix, section 2.2), but can be almost eliminated (see below).

c) XMTR B backscatter may be picked up by DET 1 & 2. Based on an experiment at NRL, backscatter in clear air at least should be negligible, but should be kept in mind.

The Appendix (section 1.1) indicates that SNR would be quite good for a reasonable quad sensor/IR beacon system.

3.2 N/H Control System

This has been discussed in detail elsewhere and will not be here.[4]

3.3 60" Control System

The original 60" searchlight consisted of

a) transmitter synchros driving
b) control synchros driving
c) vacuum tube amplifiers driving
d) Amplidynes® driving
e) DC motors driving
f) the searchlight.

The transmitter synchros could be hand driven at a control station connected via cable or by an automatic locator. In order to use the searchlight with a quad cell, we would need linear to synchro converters to simulate the transmitter synchro. Since these are 110V synchros, this is not easy.

® General Electric Co.

It appears that the easiest place to break into the chain is at the Amplidyne field control winding. This requires 10W approx (100VDC at 0.1A) and is a simple control point since motor torque will be a fairly linear function of applied voltage.

This also eliminates a tremendous number of cables and interconnections that would have to be checked and possibly refurbished.

In order to have reasonably accurate tracking, QUAD B's FOV cannot be too big. This means some sort of manual control would be desireable. For initial pointing, a joystick velocity control is probably best. The DC motor's back EMF can be used for velocity feedback.

The control loops would then be similar to the N/H but trackballs, shaft position encoders, position displays, and thumbwheel switches would be left out. Looser requirements and better behaved main power actuators here (Amplidyne-motor) should make the design less critical.

3.4 Detector Ring Array

In making absolute transmission measurements, it is essential that the beam not wander out of the light bucket. One straightforward way of checking this is to put a ring of perhaps eight detectors around the circumference of the 60" mirror (Fig. 2). In order to be cost effective, each sensor must use small optics and inexpensive detectors. This precludes using pyroelectric detectors, but allows silicon or possibly lead salt detectors. As shown, eight are used, but if the approximately 3% area lost in the worst case is too severe, 16 would reduce it to less than 1%.

In order to use silicon, a HeNe laser would have to be added to the transmitted beam. The SMI uses such a laser to measure its internal mirror position already, and possibly would find use in this mode.

In any case, if 1 mW is available, we show in the Appendix (section 3.1) that the SNR would be very high with 1" optics and silicon detectors.

Given that this is the case, one might try to use the ring detectors for not only checking but also controlling beam wander. This might be useful in the initial acquisition stages, but if employed instead of the XMTR A - QUAD B com ination, the resulting on-off type control system would only keep the average position of the beam in the center of the bucket. Quite a bit of wander and small excursions outside the bucket would result.

4. IMORTAL Measurement Systems

The system for transmission measurement is shown in more detail in Fig. 3. In the approach illustrated, the beacon tracking subelements XMTR A,B and QUAD B,A form a duplex communication link which will be discussed in detail below. Assuming the link, we will first discuss the N/H and 60" subsystems.

4.1 60" Subsystem

The receiver contains fewer elements and will be described first. At the top (Fig. 3) are the two IR DET's whose signals are appropriately weighted and summed together. A variable gain amplifier is controlled by an automatic gain control (AGC) loop which looks at the output of a phase sensitive detector (PSD). (PSD's are also called

synchronous rectifiers or lock-in amplifiers.) The reference for the PSD is obtained by decoding the sum output of the QUAD B tracker which picked up the encoded signal from XMTR A.

Previous approaches have used asynchronous detection, but it is thought signals in the future may be smaller than heretofore. Narrow-band passive filters can be used but since these are fixed, the chopping frequency must be fairly stable. Once PSD techniques are employed, the ultimate SNR is obtainable and chopper stability is no longer a problem. Commercial lock-ins can be used or simple dedicated ones can be constructed using about 10 sq. in. of board space.

Following conversion to DC, either a V-to-F or 16-bit* A-to-D converter changes the analog to digital. At first glance the V-to-F looks simpler, but in the long run the A-to-D may be. Its parallel output would allow us to use commercial encoders which convert 8-bit bytes into serial transmission signals complete with parity bits. This information is the numerator, N, in the ratio of transmission. Other information could also be sent, e.g., whether the beam has wandered as determined by the ring array.

In the SMI mode, IR DET's 1 and 2 are not used, but the rest of the system is. In this mode, the source could be monitored at the 60" and this amplitude sent back since the communications link would still be open.

*24 bits is obtained by automatic gain changing and digital scaling of the A-to-D output.

4.2 N/H Subsystem

This consists of a 2-12 μm laser source which is alternately transmitted and reflected to a local IR DET. Detection and conversion to binary form is accomplished as in the 60" system.

A chopper pick-off drives a phase lock loop (PLL) which drives the PSD, and after encoding sends a reference to the 60" system via XMTR A.

The signal from the 60" is received by QUAD A, decoded, and becomes the denominator of the ratio N/D which is the transmission.

4.3 Data Handling

In the past, analog dividers (ratiometers) were used because high accuracy A-to-D converters and digital computation were expensive. The analog approach required closely matched filters and some care to achieve 0.2% (9-bit) accuracy. In the intervening 8? years, digital techniques have become much less expensive. In fact so much so that a general purpose digital data handler has become the most cost effective current method.

An example of this is the Hewlett-Packard HP-85 system. Using keyboard commands, one can enter information, process it, including digital division, and display the information on both a CRT and a small strip printer. For later use the information can be sent to a digital tape recorder such as NRL's Digidata.

The major advantage to this approach in addition to low first cost is flexibility. More variables than those shown can be input and more complicated calculations performed if needed. Considering the high cost of arranging ships for measurements, it is essential the operators have immediate feedback on the system and whether it is producing sensible results. As these requirements are understood, changes are readily made with such a system. As an example, in addition to absolute transmission, if the range is known, the value for extinction can be calculated and compared to the expected value.

4.4 Duplex Data Link

The XMTR A,B plus QUAD A,B, in addition to providing servo tracking, also function as a duplex (simultaneous bi-directional) data link, Fig. 4. In this application the data sent and received has been specialized but more flexible use could be made in the future.

For now, in the absolute transmission mode we would like to send information on the phase of the laser beam chopper (top of Fig. 4). At the same time we need to minimize the signal picked up by IR DETs 1 and 2 and decoded by the PSD.

The approach we use is to send the same number of pulses in the (+) and (-) phases of the reference. These are arranged at approximately the same density but in the (-) phase half the pulses are shifted slightly. If one can imagine a real pulse density five times that shown and a detector with a response time extending over

many pulses, it should be reasonable that the difference between the (+) and (-) phases will be small. Since the PSD subtracts the signal in the (-) half from the (+) half, the residual signal will also be small. This should be good for the two orders of magnitude reduction in pickup required if no visible filters are used on IR DET's 1 and 2. (See Appendix, section 2.2, for further discussion of pickup.)

On the return path, XMTR B is shown sending a number of pulses corresponding to an 8-bit word plus parity and a check bit. Identical pulses are sent in each half of the chopper cycle so that any backscatter pickup is effectively cancelled. Additionally, sending duplicate transmissions allows one to reduce errors if necessary.

4.5 Transmission Error Rates

From a tracking standpoint one needs SNR's from the QUAD's of greater than 100:1 in order to track with an accuracy of 1% of the QUAD's FOV. The bit error rate in this case is infinitesimally small. It is possible to operate tracking systems with much lower SNR's. As an example, 5:1 would imply an equivalent random angle noise of 20% of the FOV. This may still be useful but the bit error rate will go up by exp(+40).

The error rate for one 100 ns pulse would be

$$\left.\frac{e^{-x^2/2}}{\sqrt{2\pi}\,x}\right|_{x=5} = 3 \times 10^{-7}$$

With unsophisticated processing 10^7 times this would occur every second. If we transmit a word every .005 seconds, the word error rate is $.005 \times 10^7 \times 3 \times 10^{-7} = .015$, which is large enough to require error correction but small enough to be feasible.

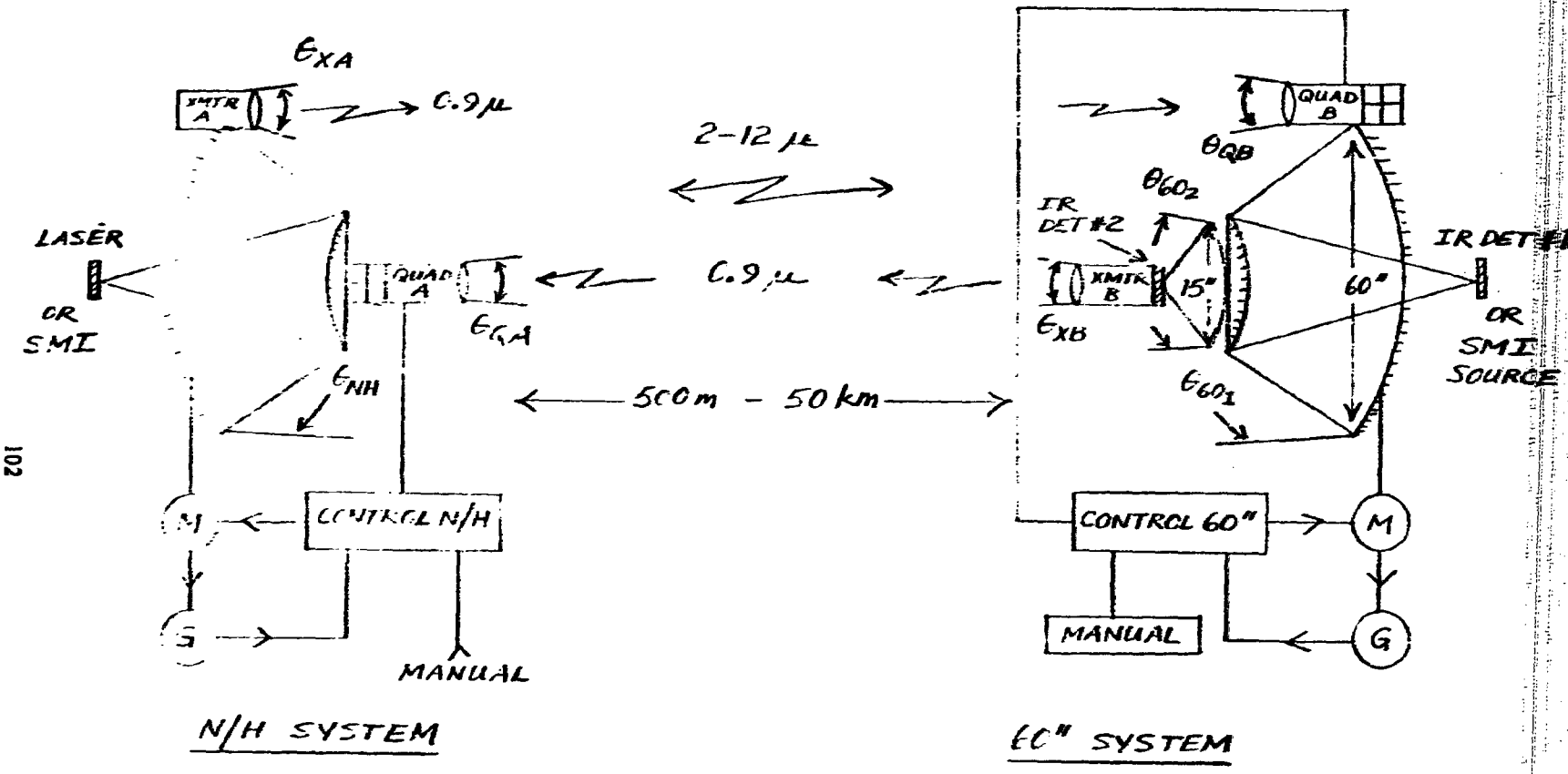

Fig. 1. IMORTAL Servo Control Systems

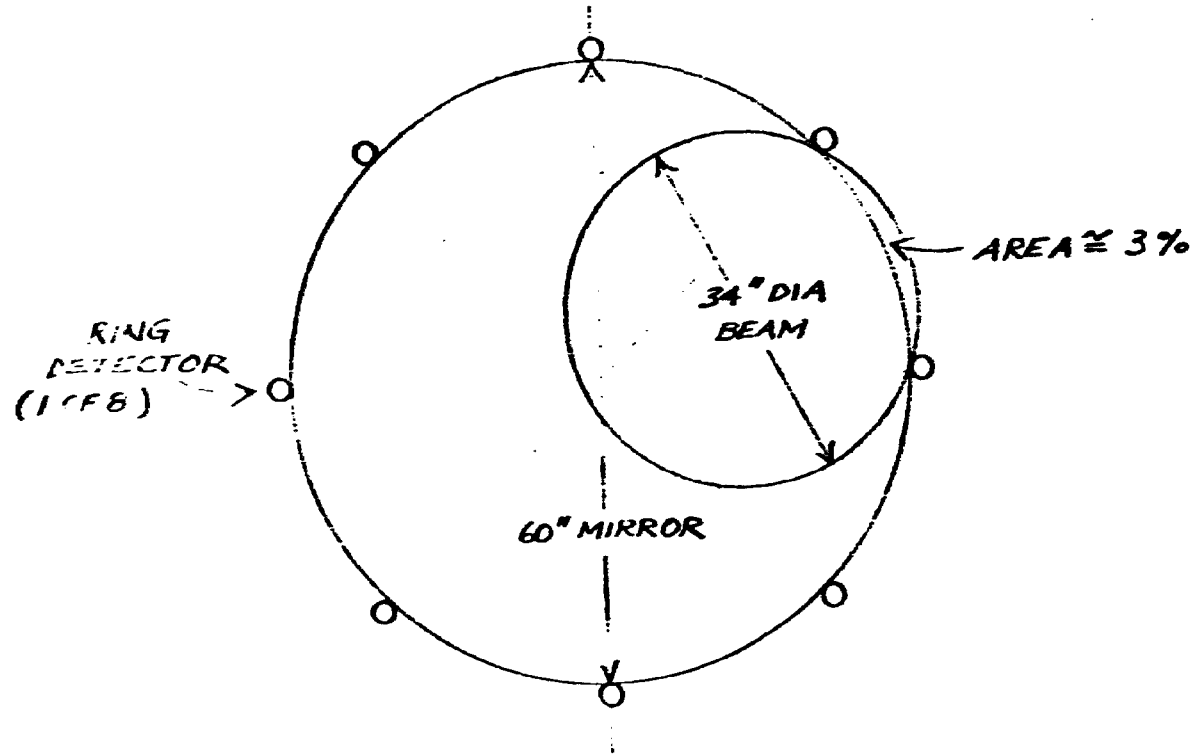

Fig. 2. Ring Array of Eight Detectors.

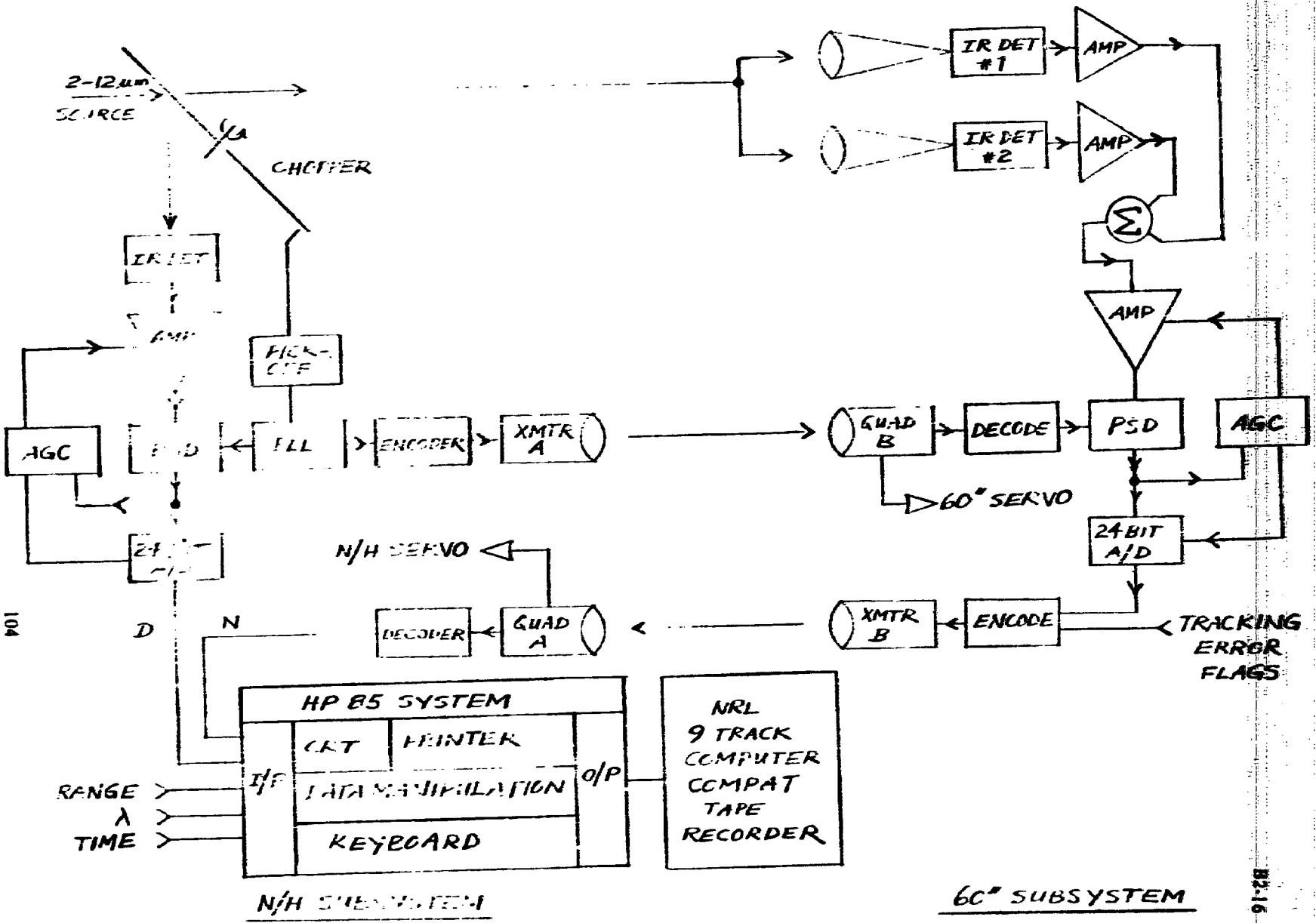

Fig. 3. IMORTAL Transmission Measurement System.

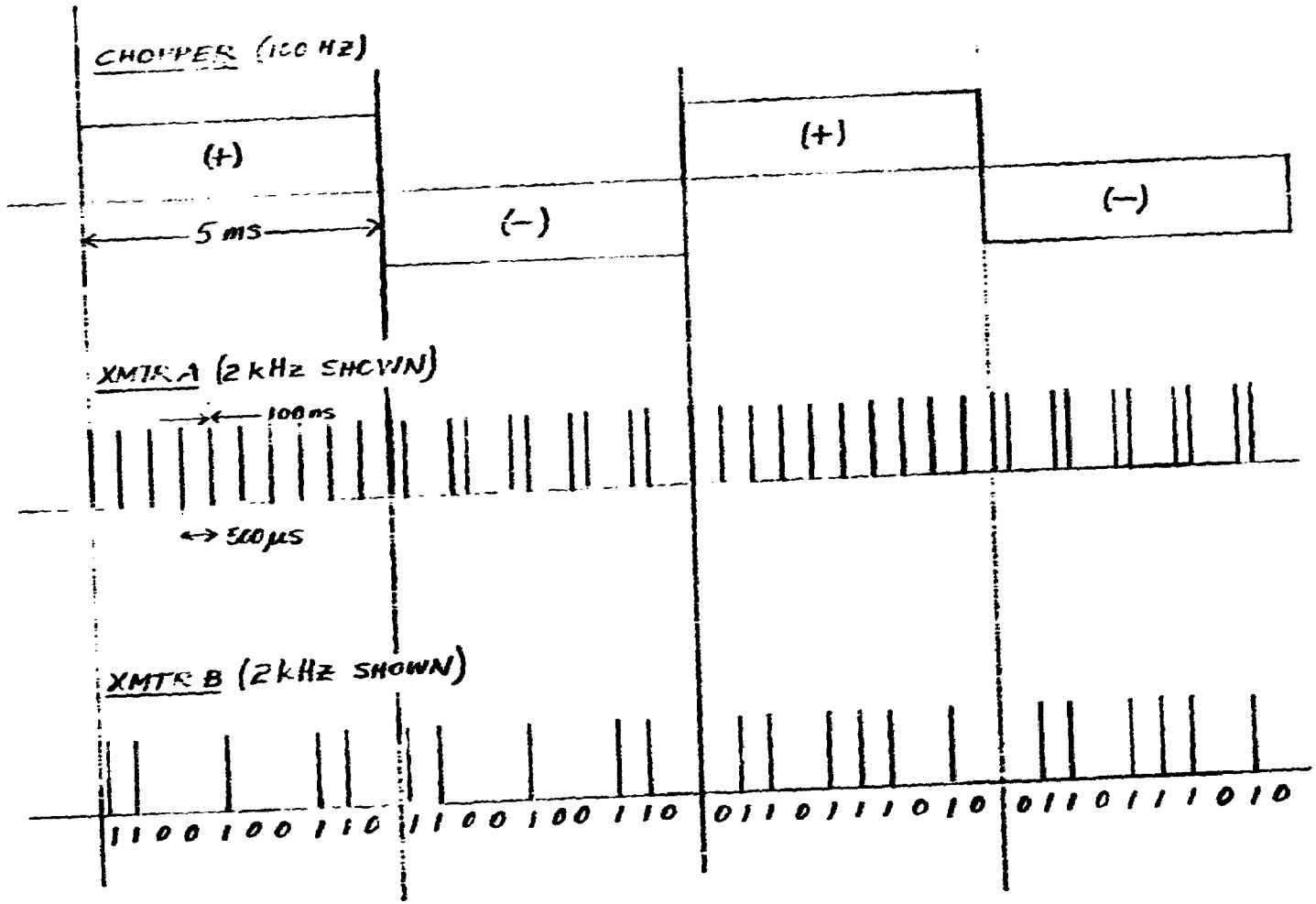

Fig. 4. Transmitter Pulse Train Coding

References

1. NRL Report 8059. "Atmospheric Transmission Measurement Program and Field Test Plan." Nov. 30, 1977.

2. NRL Report 0000. "A Shipboard Experiment for DF Laser Propogation Measurements." June 1979, Revised 24 September 1979.

3. R.F. Horton. "An 0.8 Meter Infrared Tracking Optical System Design." SPIE Proceedings, Vol. 237, International Lens Design Conference. Oakland, Calif., June, 1980. p. 412.

4. Nike Hercules Interim Report, prepared for NRL Contract #N00173-79-C-0221 by Mass. Manufacturing Corp., 24 April 1980.

Appendix: FIRST CUT ANALYSIS OF EXPECTED SIGNAL-TO-NOISE

We will work out numerical examples for three detection cases:

1) Silicon quadrant tracking GaAs beacon
2) Pyroelectric detector measuring 2-12 μm laser transmission
3) Silicon single detector detecting HeNe laser beam.

Also we will look at the possibility of crosstalk among them. Transmission and optical efficiencies will be assumed to be 100%. Sunlight backgrounds will be neglected.

1.1 Silicon quadrant tracking GaAs beacon

For the beacon we assume

peak power: 1W
pulse width: 100 ns
rep rate: 10 kHz
divergence angle (after lens): ±10 mr (±.57°)
(Note: average power = 1 mW)

For the silicon quadrant, we assume

overall diameter: 1 cm
D*: 10^{12} cm-cps$^{1/2}$-W^{-1}

For 100 ns pulses the optimum bandwidth is 1.6 MHz, and so at best, for one pulse the NEP is 1.3×10^{-9} watts, but more pessimistically,

NEP per pulse: 10^{-8} watts.

We assume

receiver optics: 500 mm, f/8.

Therefore,

receiver area: 30 cm^2

We compute

irradiance at receiver: 1.3×10^{-8} W/cm^2 peak.

Therefore,

power on detector: 3.8×10^{-7}

signal to noise (one pulse): 38 to 1.

This may not seem large, but from a communications standpoint,

probability of false alarm: $\exp_{10}(-314)$.

From the standpoint of a tracker, we can average over 10 pulses and still not introduce a delay greater than 1 ms in the servo loop, so

tracking signal to noise ratio: 120 to 1.

Therefore,

random angle noise: ±42 μrad.

1.2 Effects of 2-12 μm laser transmission on Si quad

During transmission measurements, the quad cell will be irradiated by 2-12 μm radiation. This should have no effect except heating and this should be less than 1 mW.

1.3 Effects on HeNe laser on Si quad

See Section 3. The HeNe irradiance is 4 times the GaAs irradiance, but a combination of optical and electronic filters can eliminate it.

2.1 Pyroelectric detector measuring 2-12 μm laser

Several lasers could be used in the transmission measurements. The worst case we can imagine is 1 mW spread over 60" at the receiver; thus,

irradiance: 5.5×10^{-8} watts/cm^2.

For the receiver, we assume

Collector: 31" (787 mm) F.L., f/2.

Therefore,

collector area: 1100 cm^2

watts on detector: 6.1×10^{-5} watts.

Further,

detector size: 5 mm dia.

Therefore,

field of view: ±3 mr.

Pyroelectric detector NEP's are non-simple functions of bandwidth. The one we use depends on laser chopping frequencies and the fidelity required. For now we assume

bandwith: 100 Hz.

Therefore,

NEP (10.6 μm, 1-100 Hz): 1.5×10^{-7} watts

signal-to-noise: 400 to 1.

This is adequate for 1% accuracy when transmission is 100%. Higher laser powers may be useful, however.

2.2 Pyroelectric pickup of GaAs beacon

The 100 Hz bandwidth is so slow that the 10 kHz beacon can be modeled as a DC source with a corresponding average power. We have

duty cycle: 100ns x 10kHz = 10^{-3}
average power: 1W x 10^{-3} = 10^{-3}W.

Therefore,

irradiance at collector: 1.3 x 10^{-11}W/cm^2 at 5 km
watts on detector: 1.5 x 10^{-8}W at 5 km.

Also we have

ratio to 2-12 μm laser: 2.5 x 10^{-3} at 5 km.

This is reasonably small but at 500 m range, the GaAs source would be 25% of the 2-12 μm laser. More powerful lasers or non-interference chopping schemes would be required to make accurate transmission measurements.

3.1 Silicon single detector detecting HeNe laser

Because eight of these are envisioned, small simple receivers will be used. We assume

detector size: 1 mm
D*: 10^{12}cm-Hz$^{1/2}$-W^{-1}

Therefore,

NEP: $\sim 10^{-13}$W-Hz$^{-1/2}$.

For now,

bandwidth: Δf
collector: 100mm F.L. f/4.

Therefore,

collector area: 5.9 cm^2
field of view: ±5 mr.

We further assume

source: 1 mW HeNe laser spread over 60".

Therefore,

irradiance: 5.5×10^{-8} W/cm^2

watts on detector: 2.7×10^{-7}

signal to noise: $\frac{2.7 \times 10^{-6}}{\sqrt{\Delta f}}$

The signal to noise is very high unless the bandwidth is also high. If a fixed chopper is used, the bandwidth will be low. When the SMI is used as an interference "chopper," the frequency is variable, but the maximum is

$$\Delta f = 4 \text{ cm/sec} \div 1.2 \text{ m/cycle} = 33 \text{ kHz}.$$

Therefore,

signal to noise: 1.5×10^4.

All of the radiation will not be available from the SMI, but this is still high.

3.2 Pickup from GaAs beacon

The GaAs beacon will be picked up but it would be attenuated by the smaller collector and lower bandwidth. We have

irradiance at receiver: 1.3×10^{-8} W/cm^2 peak.

Therefore,

power on detector: 6.4×10^{-8} W peak.

Also

33 kHz low pass filter attenuation: .02

effective watts on detector: 1.3×10^{-9}.

This is less than 1% of the HeNe signal and so could be discriminated against.

3.3 Pickup from 2-12 μm laser

The 2-12 μm laser should generate at most a little heating of the detector.

WORK STATEMENT

1. N/H Control System

*1. Analyze NRL December tests.

2. Redesign and build servo to (a) handle moving targets, and (b) reduce backlash on fixed targets.

3. Add 17 bit input port to allow programmed tracking.

*4. Change outer electronics package to fit trailer.

5. Procure small modern trackball.

6. Design and build new trackball interface card.

7. Test new designs at CBD on static N/H mount against tracking test source.

8. Finalize servo design.

9. Test at CBD on roll table against fixed test sources.

10. Test at CBD on roll table against moving test sources.

11. Write up informal manual.

12. Write up ship-based field test plans.

13. Test on carrier against helicopter-borne Hg lamp.

2. 60" Control System

*1. Measure open-loop Amplidyne motor characteristics at CBD.

*2. Analyze control servo requirements.

3. Design control electronics.

4. Build control electronics.

5. Package control electronics to mount in 19" rack.

---

*To be done as part of an earlier phase.

6. Test Amplidyne/motor combination at MMC (primarily joystick mode).

7. Assemble and test 60" system at CBD.

8. Test on roll table at CBD.

9. Write informal manual.

10. Write up field test plan.

3. GaAs Transmitters/Si Quad Receivers

1. Analyze FOV-SNR range tradeoff.

2. Design electro-optics.

3. Procure (a) GaAs laser diode and optics
(b) Si quadrant detector and optics

4. Design, breadboard, and test
(a) GaAs LED pulse driver
(b) Si quad front end.

5. Produce PC boards.

6. Build transmitter and receiver cases.

7. Test at MMC for (a) SNR and (b) tracking accuracy.

8. Help install at CBD on (a) N/H and (b) 60".

9. Write up informal manual.

4. Data Acquisition System (Amp/PSD/AGC A-to-D)

1. Determine resolution and accuracy requirements.

2. Design electronics.

3. Procure parts.

4. Build board(s).

5. Debug and test at MMC for
   (a) Dynamic range
   (b) Absolute accuracy
   (c) Signal-to-noise referred to input.

6. Package.

7. Test at CBD.

8. Write informal manual.

5. Communications Link

1. Determine requirements vis-a-vis
   (a) Type and amount of data
   (b) Phasing to avoid interference with IR detectors
   (c) General I/O compatibility.

2. Find off-the-shelf UART (universal asynchronous receiver/transmitter) IC if possible.

3. Design and build on wirewrap boards.

4. Test without optical link at MMC.

5. Test with optical link at MMC.

6. Test with optical link at CBD.

7. Write informal manual.

6. Data Manipulation

1. Determine required data inputs from each end.

2. Determine output displays and storage media.

3. Design special interfaces, if unavailable.

4. Procure parts and equipment.

5. Build special interfaces, if any.

6. Determine data manipulation routines.

7. Test with com links at MMC.

8. Document.

9. Test at CBD.

7. IR Detectors

1. Analyze sensitivity and dynamic range requirements.
2. Procure detectors.
3. Test at MMC using 500°K black body.
4. Help install and check out on N/H at CBD.
5. Help install and check out on 60" at CBD.

8. Field Test: Test all systems at CBD

Appendix C

Reprinted from SPIE Vol. 237 - 1980 International Lens Design Conference (OSA)

An 0.8 meter infrared tracking optical system design

Richard F. Horton
Optical Sciences Division, Naval Research Laboratory, Washington, D.C. 20375

Abstract

An 0.8 meter Cassegrain, reflecting relay and matching optics comprise a system which incorporates a Nike Hercules pedestal for an infrared tracking system. Optical design criteria and performance will be discussed.

Introduction

The Field Measurements Section of NRL's Optical Sciences Division has been making in situ atmospheric propagation measurements for several years.[1] The scope and accuracy of these measurements has been paced by the development of the required optical systems. In 1975, an optical transmitter and receiver system was reported which accomplished DF laser transmission measurements over a stationary 5 km path.[2] In 1976, a new receiver system was reported which added laser calibrated high resolution atmospheric spectroscopy to the capability of HeNe, Nd-YAG, HF, DF, CO, and CO_2 laser transmission measurements.[3]

Currently we are building an optical system to extend our measurement capability from stationary path measurements to tracking situations, of which, a ship to ship measurement of laser transmissions, high resolution atmospheric transmission and atmospheric turbulence is of interest.

A recent study[4] concluded that a ship to ship measurement was feasible, based upon reciprocal optical tracking from a "high resolution" tracking transmitter, (50 μr), to a "low resolution" tracking receiver, (5 mr). To keep costs low the transmitter system is based on a surplus Nike Hercules radar mount capable of the required tracking accuracy.[5]

The design study which this paper presents is the result of the design problem of matching the most capable optical system practical to the existing Nike Hercules mount.

General Design Considerations

The Nike Hercules mount appears well suited for our use as an optical mount. It is an altazimuth mount, with a trunnion ring which can accommodate a 32" Cassegrain telescope. The base appears well suited to the mounting of our Scanning Michelson Interferometer, (SMI), which requires stability and accessibility. In addition, laser systems which require vacuum, high voltage, water cooling, etc. require a stable platform. Specific requirements of the SMI and laser sources will be discussed later.

Practical Considerations

As this is going to be a field system, it will reside in a semi-trailer, to be transported to an experimental field site and set up as quickly as possible. The optical system should be "built to take it" and be realigned quickly, precisely, and repeatably. The optical system may be used under conditions of large thermal variations, and should either be insensitive to these variations or quickly adjusted to them. A maximum telescope tube length, required by the trailer layout, is 60" from the mount center. This, along with moment of inertia considerations, makes a compact telescope desirable.

We require the optical system to have good performance over a wavelength range of 1 to 20 microns. This precludes the use of refractive elements in the design. To facilitate tracking and the use of a boresight TV, a field of $1/2^{0}$ is desired. Field curvature should be minimal. The optical system should be able to focus from infinity to 1 km, and closer focusing is desirable. The turbulent atmosphere will usually limit performance of the optical system in the visible, however later atmospheric propagation studies will require the system to be diffraction limited beyond 3 microns. Alignment will be done with a HeNe laser, so alignment toleranceing for the wavelength must be compatible with performance criteria in the infrared. Special fixtures to aid in alignment will be designed during the optical installation, designing in this capability is useful.

Cost is, of course, an important consideration, but also important is procurement time, set up time, initially and in the field, an overall versatility. Five years from now the system may be engaged in experiments of a totally unforeseen nature.

Nike Hercules Mount

In most optical systems the mounting of the telescope is designed along with or after the optics. Here, because of costs, the converse is true. A photograph of the refurbished mount appears as Figure 1. The mount has had several modifications made to it to facilitate the installation of optics:

1. The entire radar system and its supporting electronics were removed from the mount.
2. The Elevation shaft was cut off just beyond the bearing to allow approximately 8" clearance for optics in the "data side" of the Azimuth yoke.
3. The "Nike pots" were removed from the encoder gearboxes and unnecessary cabling was removed from the "data side" of the yoke.
4. The 100 channel slip ring was removed from the center of the Azimuth axis, to be replaced by a cable wrap allowing a 6.125" central opening along the axis.
5. Holes were cut in the central webbing of the yoke to allow the passage of light.
6. All power supplies, motor controls, etc. were removed from approximately 2/3 of the "front" of the base to allow installation of optical benches, etc.
7. A shock absorber and stop was fitted to the Azimuth axis to allow motions of from -10° to 370°. This precludes damage to the cable wrap and protects the optics from severe angular deceleration of the Azimuth axis.

The resulting mount, ready for optics is depicted schematically in Figure 2. The trunnion ring inner diameter is 34" with some minor projections which limit the unobscured diameter to 32". The width of the trunnion ring is 17", which will allow mounting of the telescope tube and spider on one face and the primary mirror cell on the other. A turning flat will be required to direct light from along the optic axis of the Cassegrain through the Elevation shaft. This mirror can be supported from the rear, possibly through the central perforation in the primary, aiding in the inherent baffling of the system.

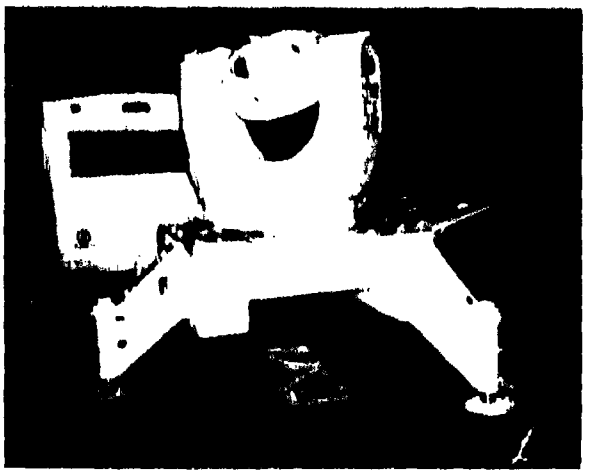

Figure 1 (above) Nike Hercules Mount, Ready for Optics.

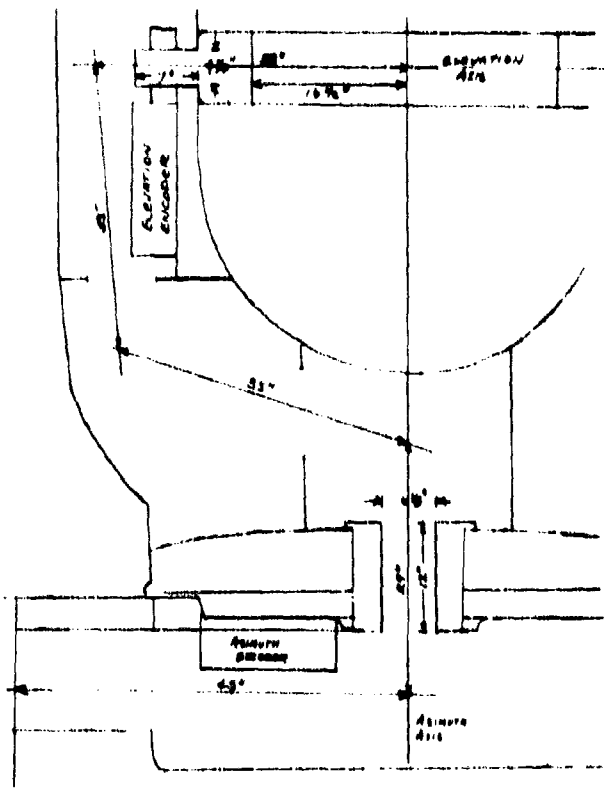

Figure 2 (right) Schematic of Mount Layout and Possible Light Path.

The 4 1/4" inner diameter of the hollow Elevation shaft is a significant aperture affecting the design of the system. This diameter must be held for approximately 7" until the light emerges in the "data" compartment of the yoke. The yoke is webbed for structural strength, effectively compartmenting the yoke. The optical system will be contained in three compartments. The first is shared with the Elevation encoder package. The second is empty save cabling to the Elevation encoders. The third is situated over the Azimuth axis hole, and is empty except for the tail of the cable wrap which goes to the "motor side" of the yoke. Since the webbing may allow mounting of mirror supports, etc. and is required for structural integrity, it has been left intact until the optical design is finished. There are access holes and covers for all of these compartments, so providing for access to adjustment of optical mounts does not appear to be a problem. The three compartments are very small, and "shoe-horning" of a workable optical system into this space is a reasonable task.

The 6 1/8" hole down the Azimuth axis is the next major constraint on the optical design. This diameter must be held for about 12". After passing this axis, the light enters a relatively open area in the base of the mount, which connects to the "front" of the base by an opening approximately 12" x 13 1/2". Optical benches supporting the instrumentation will be attached to the "front" of the base.

The Elevation axis and Azimuth axis force another constraint on the system design. This has to do with the rotational symmetry of the beams as they pass along these two axes. Obviously non-axially symmetric designs, which might have field tilts or asymmetries about the axis should be avoided.

Instrumentation Requirements

The requirements of the desired instrumentation fall into three categories; full field, collimated narrow field, and focused narrow field.

The boresight TV system will be used for fine tracking adjustments, and needs access to the full 1/2° focal plane, for initial acquisition of the target and alignment checks. During other measurements, the region being sampled may be subtracted from the field, and in its place a dot be superimposed. Call this the field hole.

The SMI and laser sources would be working through the focal point not used by the TV. The laser sources will want to enter the system as focused beams centered on the field hole, matched in f/ number and exit pupil obscurations to the output pupil of the telescope system. The alignment laser could work through the system in the same way that the laser sources do.

The Scanning Michelson interferometer requires a collimated beam of 2" diameter as its input beam. The angle over which this beam is defined in object space is 6.6 mr. An off axis parabola would be used to form the 16 power telescope required. The system would then sample .41 mr in the telescopes object space. This could couple through the field hole mentioned previously, allowing simultaneous boresight TV to record the object point. A schematic of this system is shown in Figure 3. Notice that it does require a stationary focal plane. This means focusing must be accomplished prior to this point. Two possible ways of achieving this are the use of a "trombone" section of the optical path, which adds reflections and possible misalignment, and the moving of one optical element along its optic axis.

Generalized Solution

Afocal Systems

It would be simple to devise a Galilein telescope of 16 power. This would form the 2" collimated beam required by the SMI. The field of view for this system would be very small. With the apparent field of view defined by the two axial apertures, it would only be about 14 degrees. The true field of the system would be 1/16 th of that, about 1.5 mr. This is just large enough to do both the laser experiments and the SMI work, but there would be no field left over for any tracking offsets, or to even see the target. This might be adequate in some situations, however this system would be too constraining for our needs. See Figure 4.

Systems With Real Foci

The field of view of any system coming to a focus after going through the Elevation axis is a function of the f/ number of the Cassegrain and the distance of the focus from the 4 1/4" aperture, (ε), as shown in Figure 5. A 1/2° field of view, without vignetting is possible only for distances up to 12" away from the end of the elevation shaft. A relay system of some type is required to relay this focus to a point at the appropriate

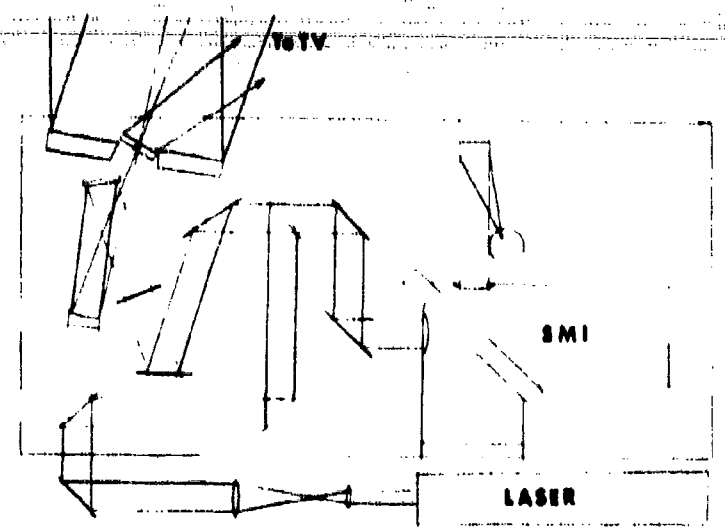

Figure 3. Instrument Matching Optical Layout.

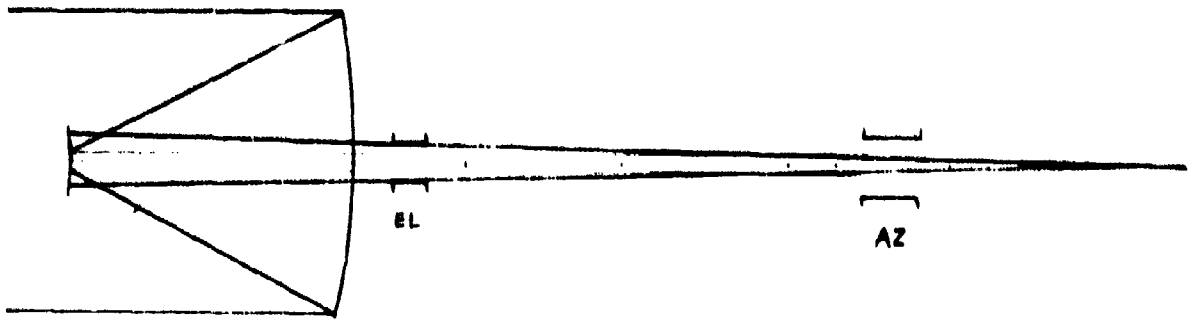

Figure 4. Simple 16 Power Afocal System Showing Maximum Aparent Field.

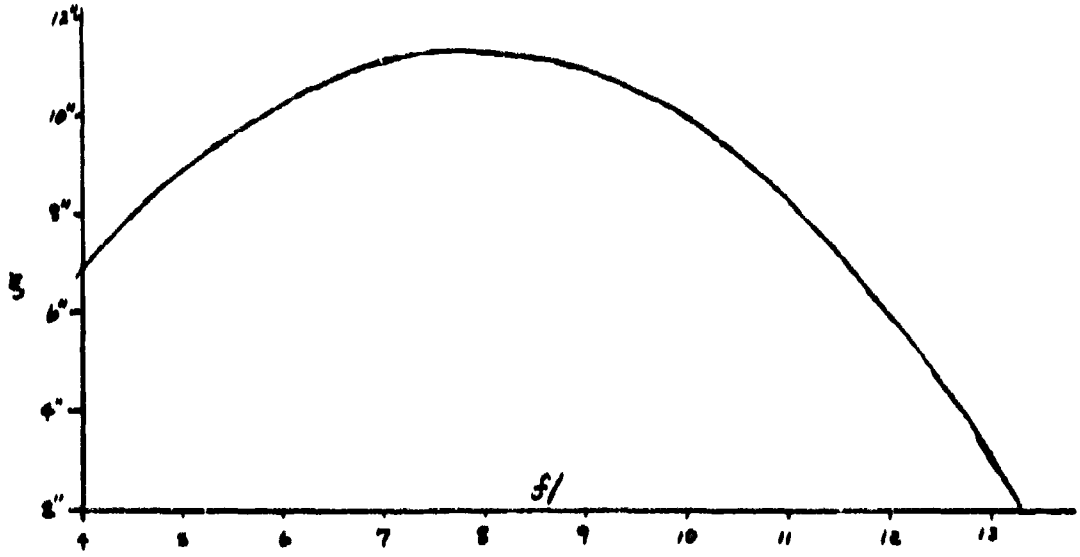

Figure 5. Variation of f (distance from End of Elevation Shaft to First Focus) Vs. Cassegrain f/no.

place in the base. This would be very simple with refractive optical elements, and a series of field lenses could be used. With reflective optics, however, the solutions to this problem fall into two categories, axially symmetric along the chief ray, and off axis systems.

Off axis relay systems. Off axis relay systems would generally be comprised of sections of spherical surfaces, since conic sections would be too expensive to fabricate for low f/ number systems. This necessitates a design in which the aberrations balance, giving the desired degree of correction. Remembering that the aberrations induced by the optics must be axially symmetric when the light passes through the Azimuth bearing, implies that any off axis relay system must be fully corrected within the confines of the three compartments of the yoke. This is the major problem with off axis relay systems. The Offner autocollimator[6,7] showed great promise, but was very difficult to shoe-horn into the boundaries of the yoke for any practical field. A second system, with more problems in correction, but with a field lens like element, was also looked at. High f/ numbers required for aberration balancing lead naturally to many reflections and small useful fields. These two systems are shown in Figures 6a and 6b.

Axially symmetric systems. A great advantage to axially symmetric systems is the use of conic sections to balance aberrations. The disadvantage is that Newtonian flats or their complements must be used liberally to fold the system back onto itself. This is not true in a concentric relay of the "clamshell" type[8], shown in Figure 6c or a similar system shown in 6d. The latter showed promise since the midpoint of the relay is about one half the diameter of the mirrors. This looked like a good way to pass through the 6 1/8" diameter aperature at the Azimuth bearing. Unfortunately the use of two (or three) folding mirrors to fit this into the confines of the yoke, etc. resulted in the penalty of six (or nine) extra reflections.

The relay system which the final design is based upon is shown in Figure 6e. Two perforated flats are used to gain access to the focal planes from two ellipses which share the central focal plane between them. This focal plane is magnified by a factor of 3 in this case. When this focal plane is situated near the Azimuth bearing hole, a reasonable field can be accommodated. One drawback to this relay system is, lacking a field lens, the second ellipse must be a larger diameter than the first. Another is that the hole in the first flat does not map onto the hole in the second flat, except at very small angles. This causes an oddly shaped kink in the vignetting function, which is a minor drawback, and must be taken into account if radiometric measurements are ever made over a wide field. This will be elaborated upon later. Advantages of this relay system are minimum number of reflections and focusing is readily accomplished by moving E 1 along its optic axis.

f/6 Cassegrain and Relay System

The best optical system design matches a classic Cassegrain with the double elliptical relay system just described. The layout of the optical surfaces is shown in isometric projection in Figure 7. A drawing indicating the fit in the Nike Hercules mount is shown in Figure 8. The system has a useful field of 1/2° which will interface directly to the instrument matching optical layout described above. The f/2.5 parabola and a 11 1/4" diameter secondary with a magnification of 2.4 result in a classic Cassegrain of f/6. The 1/2° field of view is defined by the 1.686" hole in the first perforated flat, PF 1. The diameter of PF 1 and E 1 are consistent with mounting in the "data" compartment of the yoke. E 1 will be the focusing element of the system. Ray tracings indicate that focusing at 300 meters is possible without severe image degradation over the field. The systems second focus, approximately 5" in diameter is positioned just above the Azimuth axis hole. This will allow the positioning of an alignment aperture, concentric with the hole for alignment checks. The second ellipse, E 2, must be 13" in diameter but is positioned in the open base. The second perforated flat, PF 2, will be situated just outside the base at the front.

Ray Traces

The system was optimized for image quality in the 1/2° field of view using ray tracing techniques. Ray traces were made using 18 rays about the chief ray in a hexagonal pattern. Input parameters were spacings and surface radii of curvature. Conic constants of mirrors E 1 and E 2 were allowed to vary, with the primary and secondary held at both classic Cassegrian and Ritchey-Chrétien values. It was found that the optimum conic constant for E 2 was -.51 and that E 1 would like to be an oblate spheroid (K -1). Since E 2 dominates the final performance of the system and "best focus" field curvature, it was decided to halt E 1 at a sphere to minimize costs. The use of a classic Cassegrain allows the system some extra versatility, without the first turning flat it is a stand alone telescope.

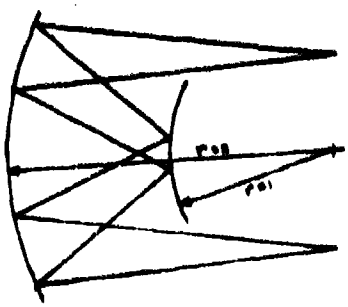

6a. Offner Relay.

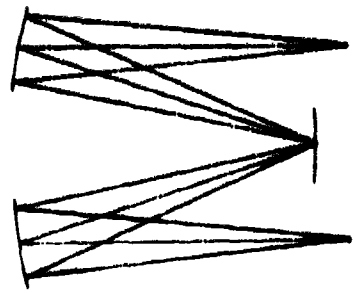

6b. Off Axis Relay with "Field lens".

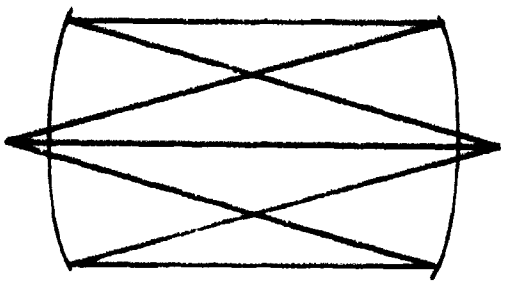

6c. "Glassshell" Relay.

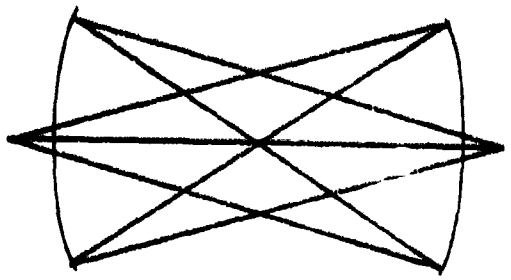

6d. Relays With Internal Focus.

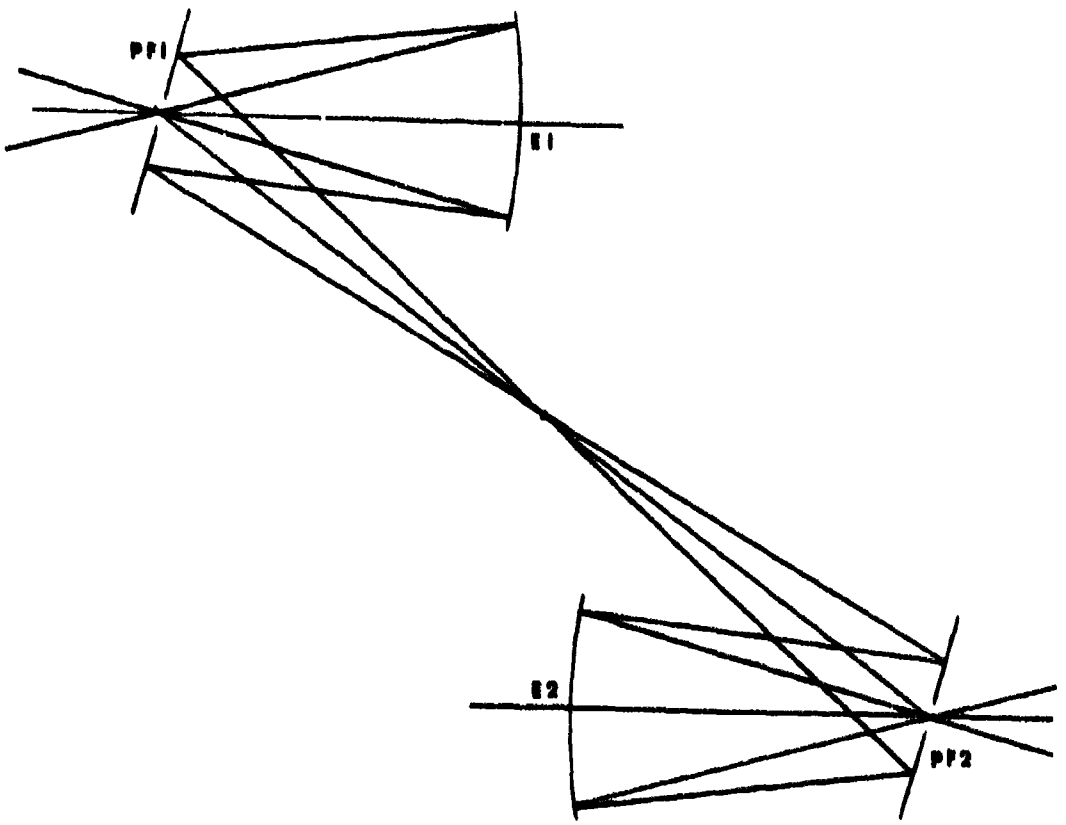

6e. Relay System Using 2 Ellipses and 2 Perforated Plate.

Table 1

Surfaces		Inches	Meters
Primary	Parabola	M = 0	
	(Hyperbola)	(M = .232)	
	R Curvature	160.00	4.0640
	Diameter	32.00	.8128
Secondary	Hyperbola	M = 4.90	
	(Hyperbola)	(M = 7.82)	
	R Curvature	109.92	2.7919
	Diameter	13.25	.3366
E1	Spheer	M = -1	
	R Curvature	54.00	1.3716
	Diameter	7.00	.1778
PF1	Diameter	4.25	.1080
	Perforation	1.68	.0426
PF2	Diameter	12.00	3.048
	Perforation	1.68	.0426
E2	Ellipse	M = -.53	
	R Curvature	54.00	1.3716
	Diameter	13.00	.3302

Separations

Primary	Secondary	47.94	1.2177
Secondary	E1	112.94	2.8687
E1	E2	216.00	5.4864
Back focal length		29.00	.7366
E2	final focus	36.00	.9144
E1	PF1	36.00	.9144
PF2	E2	36.00	.9144

Primary f/no 2.50 Obscuration Ratio .414
System f/no 6.00 Full Field .50°

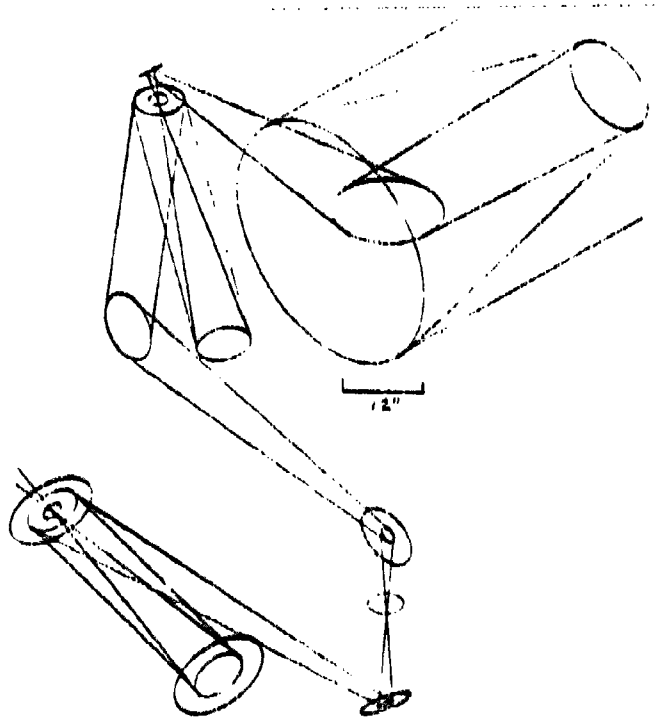

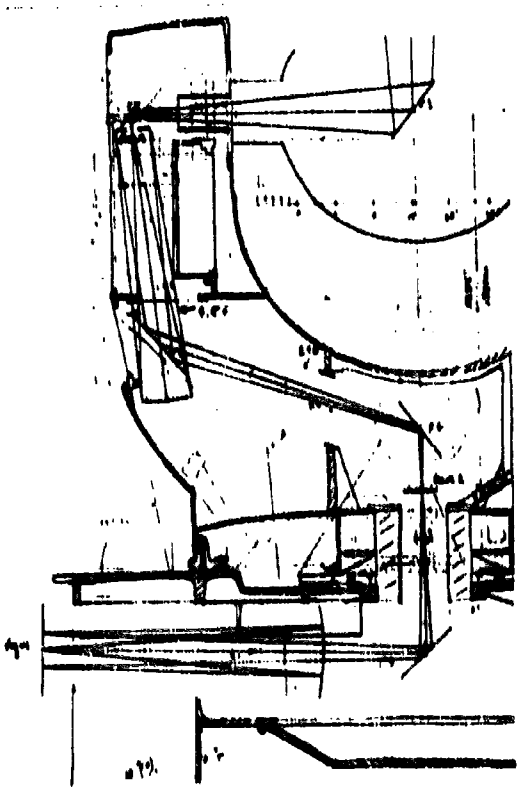

Figure 7 (above) Isometric Layout.
Figure 8 (right) Optical System in Mike Hercules Mount.

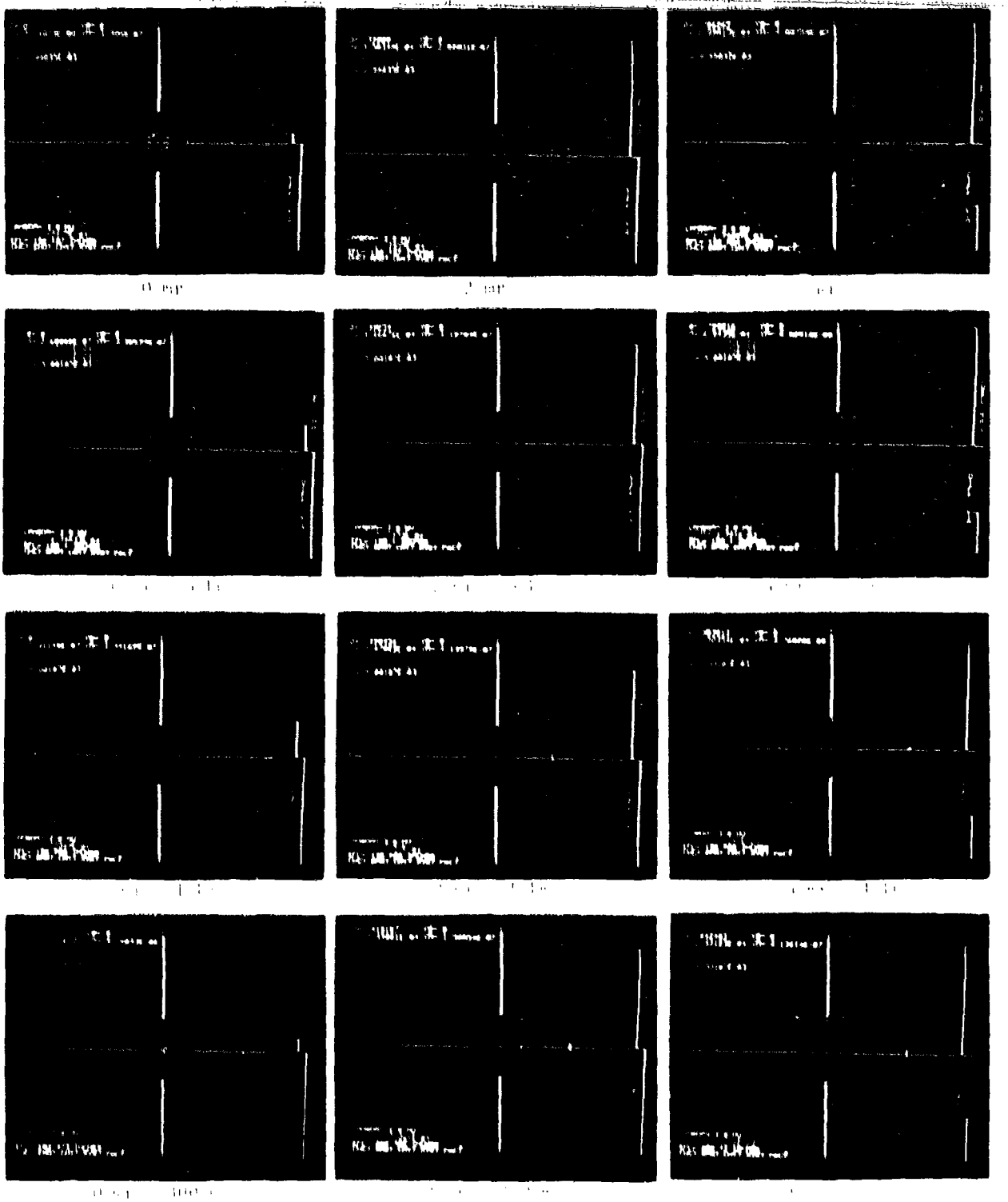

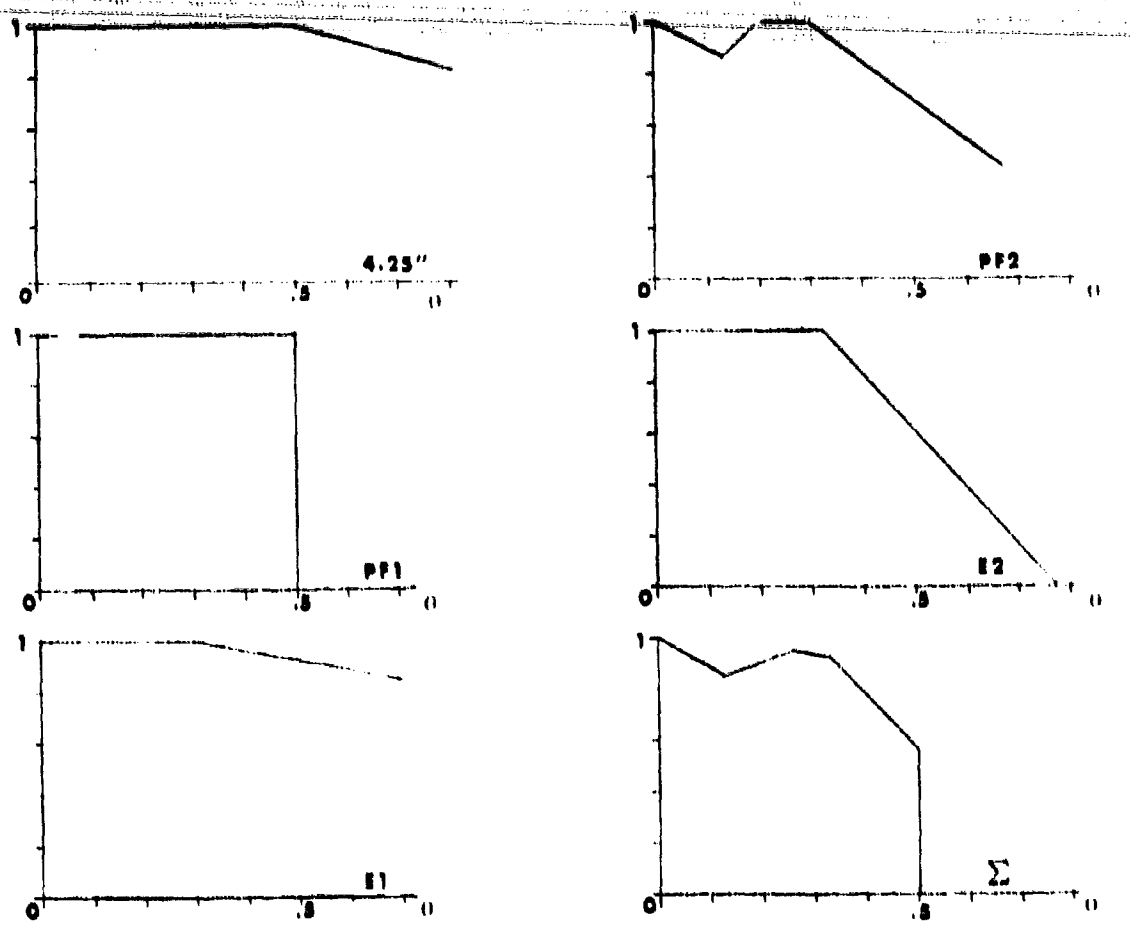

Figure 10. Vignetting Function Plotted vs. Field Angle for Various Surfaces and System C-1.

A listing of the pertinent diameters, spacings, radii of curvature and conic constants is given in Table I. Results of system ray traces are shown in Figure 9 for field angles of 0, 2 and 4 mr, with object distances of 300, 1000, 3000 and 10^{20} meters.

Vignetting Functions

Approximate vignetting functions with varying field angle are shown in Figure 10 for the major reflecting surfaces in the relay system. Of these the one corresponding to E-2 has the nasty kink at .075° field angle which was mentioned previously. If necessary, the vignetting function may be "smoothed" by a specially designed aperture, however it seems most useful to see if any problems arise first.

Conclusions

The design study was successful. The design goals were met by a slightly simpler system than had been expected. Ray traces indicate that the system performance will be good. Perhaps this use of a surplus radar mount for a tracking system will be repeated.

Acknowledgments

This work was sponsored by Naval Sea Systems Command PMS-405. The author wishes to thank Mrs. Barbara Eckert for her careful and patient typing of the manuscript.

References

1. J. A. Dowling, R. F. Horton, S. T. Hanley, and K. M. Haught, "High Resolution Field Measurement of Atmospheric Transmission," SPIE Proceedings, Vol. 142, OPTICAL PROPERTIES OF THE ATMOSPHERE, (1978), p 25.

2. R. F. Horton, J. A. Curcio, and T. A. Cosden, "Optics for a 5 km DF Laser Extinction Experiment," OSA Annual Meeting Paper, ThD16, Boston, Oct. 1975.

3. R. F. Horton, "Optics for Laser-Calibrated High Resolution Atmospheric Transmission Studies," OSA Annual meeting paper TuO11, Tucson, Oct. 1976.

4. R. F. Horton, "At Sea Measurement," - White Paper to be published as an NRL Technical Report.

5. T. H. Johnson, H. H. Plotkin, and P. L. Spadin, "A Laser Satellite Ranging System - Part I: Equipment Description," JQE Vol. QE-3, No. 11 (Nov. 1967), p 435.

6. A Offner, "New Concepts in Projection Mask Aligners," Opt. Eng., 14, 131 (1975).

7. R. Kingslake, Lens Design Fundamentals, Academic Press, New York, 1978, p 321.

8. The Infrared Handbook - William L. Wolfe and George J. Zissis, editors, Environmental Research Institute of Michigan, 1978, p 9-23.

NRL INFRARED TRACKER

Ray Trace Analysis

PERFORMED BY

RESEARCH OPTICS, INC.

9411 Flagstone Drive
Baltimore, Maryland 21234

1. INTRODUCTION.

This document describes the results of an optical system ray trace analysis. The optical system is an Infrared tracker which uses a Nike Hercules pedestal. NAVAL RESEARCH LABORATORY letter #2412-429 (8-21-80) and several papers by R. Horton contain a complete system description.

The tracking system has a focal length of 192 inches and an f/6 aperture. It operates at object ranges from 0.3 Km to infinity at a full field of view equal to 0.5 degrees. The system itself comprises a pure Cassegranian telescope followed by a relay system consisting of a Sphere and an Ellipse.

This report describes in detail the optical elements: four focussing elements and seven optical flats. Ray trace results are included for various object ranges from 0.3 Km to 10,000 Km. and for two object angles: object on thr optical axis and 0.25 degrees off the optical axis. The results show that the optical design goals have been met.

2.SYSTEM DESCRIPTION.

The optical system comprises four focussing mirrors and seven flats. In the order in which an input beam would strike them they are:

1. Parabola
2. Hyperbola
3. Folding Flat
4. Folding Flat 2
5. Sphere
6. Perforated Folding Flat 1
7. Folding Flat 3
8. Folding Flat 4
9. Folding Flat 5
10. Perforated Folding Flat 2
11. Ellipse

The Parabola and Hyperbola form a pure Cassegranian telescope; the sphere and ellipse constitute a relay system which together with the folding flats transfers the image to a convenient location. Figure 1, which is extracted from the NAVAL RESEARCH LABORATORY letter to the Muffoletto Optical Company, shows schematically the optical system layout. The specific element parameters, also extracted from the same document are as follows.

Primary Mirror	Concave Parabola
Diameter	32.00 ±0.05 inches
Focal length	80.00 ±0.10 inches
Perforation Diameter	8.00±0.05inches
Material	NRL supplied

Secondary Mirror	Convex Hyperbola
Diameter	13.25 ± 0.05 inches
Thickness	2.25 inches minimum
Figure	R curvature = 109.9 ± 0.05 inches
	Conic constant, M= 4.90
Material	Precision annealed Pyrex

Turning Mirror (F1)	Flat
Material	NRL supplied 12 inch diameter x 2 inch thick glass or precision annealed Pyrex.

Turning Mirror (F2)	Flat
Diameter	4.30 ± 0.05 inches
Thickness	0.75 inches minimum
Material the same as in the previous item.	

Relay Mirror (E1)	Concave Sphere
Diameter	7.00 ± 0.05 inches
Figure	R curvature 54.00 ± 0.10 inches
	Conic constant M = -1.0
Material	Same as previous item.

Perforated Relay Mirror (PF1) Flat

Diameter	4.25 + 0.05 inches
Thickness	0.75 inches minimum
Perforation Diameter	1.62 + 0.02 inches
Perforation Cone 1/2 Angle	20 degrees

Turning Flat (F3)
NRL supplied Newtonian Diagonal from 36 inch system to be stripped and add/chrome coated only.

Turning Flats (F4) and (F5)

Diameter	12.0 + 0.05 inches
Thickness	2.00 + 0.05 inches
Material	Same as Flat (F1)

Perforated Relay Mirror (PF2) Flat

Diameter	12.00 + 0.05 inches
Thickness	2.00 inches minimum
Perforation Diameter	1.68 + 0.02 inches
Perforation Cone 1/2 Angle	20 degrees

Relay Mirror (E2)

Diameter	13.00 + 0.05 inches
Thickness	2.25 inches minimum
Figure	R curvature 54.00 + 0.10 inches Conic Constant M = -.53
Material	Precision annealed Pyrex

The effective focal length of the optical system is the focal length of the Cassegranian telescope formed by the primary Parabola and the Hyperbola. The Sphere and Elippse constitute a relay system and donot change the effective system focal length.

The above stated mirror curvatures together with the following spacings between the focussing elements determine effective focal length and the final image position. The spacings are as follows.

Primary to Secondary	47.94 inches
Secondary to E1 (sphere)	112.94 inches
E1 to E2 (Ellipse)	216.00 inches
E2 to final Focus	36.00 inches

The system effective focal Length is 192.00 inches. This value and the 32.00 inch Primary Diameter determine the [redacted] f number to be 6.00. The Obscuration Ratio is .414.

3. SYSTEM PERFORMANCE.

System performance has been evaluated by means of a trigonometric ray trace for the following (point) object distances: 1, 5, 10, 50, 100, 500, 1000, 5000, and 10000 kilometers. At each range the object is on-axis and 0.25 degrees off axis. Results are also shown for the object at 300 meters in order to demonstrate how movement of the relay sphere maintains the image in the proper focal plane.

In each case a fan of forty rays emanating from the object point scans the primary mirror in a four inch by four inch grid. The results show the focal plane coordinates in terms of the grid points on the primary. The coordinate system is one in which the Z axis is the optical axis. Positive X is horizontal toward the right when looking toward the primary mirror. Positive Y is up. . XP and YP denote the primary mirror coordinates; XF and YF denote the focal plane coordinates. For each case the X and Y focal plane coordinates are separately averaged to determine the mean and standard deviation for focal plane X and Y coordinates. In each case the focal plane is located 36 inches behind the final Ellipse.

4. RAY TRACE RESULTS.

The focal plane coordinates for all cases even for the object as near as one Kilometer and 0.25 degrees off axis stay within an angular spread of 0.4 milliradians. Note that all mirror and focal plane locations remained constant over the entire object range from one to 10,000 kilometers. As the object distance increases the focal plane spot size decreases and eventually exceeds the Physical Optics Diffraction limit. The larger spot sizes at short ranges result from out-of-focus conditions but the focussing elements were not altered during the traces from one to 10,000 Kilometers purposely in order to demonstrate the acceptable optical system performance without the need for adjustment

The final trace shows the focal plane coordinates for the point object at only 0.3 Kilometers. Here the third focussing element (Sphere) moved 3.66 inches backward (toward the Focal Plane) while not changing the other locations. The spot size for optimum adjustment of the sphere exceeds the Airy Diffraction Limit Criteria (Wavelength = 0.6 micrometers) both for the object on-axis and 0.25 degrees off-axis.

RESEARCH OPTICS, INC.

By: _____
C. Verne Muffoletto, President
8/24/81

Range is: 1 Kilometer
Image is on the axis
The following dimensions are in inches

XP	YP	XF	YF
0	-16	0	-.0779393
-8	-12	-.0390106	-.0585166
-4	-12	-.0195202	-.0585583
0	-12	0	-.0586065
4	-12	.0195202	-.0585583
8	-12	.0390106	-.0585166
-12	-8	-.0585207	-.039013
-8	-8	-.0390698	-.0390698
-4	-8	-.0195561	-.0391122
0	-8	0	-.0391299
4	-8	.0195561	-.0391122
8	-8	.0390698	-.0390698
12	-8	.0585207	-.039013
-12	-4	-.0585583	-.0195202
-8	-4	-.0391122	-.0195561
8	-4	.0391122	-.0195561
12	-4	.0585583	-.0195202
-16	0	-.0779393	0
-12	0	-.0586065	0
-8	0	-.0391299	0
8	0	.0391299	0
12	0	.0586065	0
16	0	.0779393	0
-12	4	-.0585583	.0195202
-8	4	-.0391122	.0195561
8	4	.0391122	.0195561
12	4	.0585583	.0195202
-12	8	-.0585207	.039013
-8	8	-.0390698	.0390698
-4	8	-.0195561	.0391122
0	8	0	.0391299
4	8	.0195561	.0391122
8	8	.0390698	.0390698
12	8	.0585207	.039013
-8	12	-.0390106	.0585166
-4	12	-.0195202	.0585583
0	12	0	.0586065
4	12	.0195202	.0585583
8	12	.0390106	.0585166
0	16	0	.0779393

Average X Value is: 0
Mean X Spread is .0420898

Average Y Value is: 0
Mean Y Spread is .0420894 (Inches)

Range is: 1 Kilometer
Image Height is 4.36332 meters off the axis
The following dimensions are in inches

XP	YP	XF	YF
0	-16	0	-.923574
-8	-12	-.0392576	-.90476
-4	-12	-.0196468	-.904979
0	-12	0	-.905091
4	-12	.0196468	-.904979
8	-12	.0392576	-.90476
-12	-8	-.0591582	-.885524
-8	-8	-.0395014	-.885867
-4	-8	-.019774	-.886084
0	-8	0	-.886152
4	-8	.019774	-.886084
8	-8	.0395014	-.885867
12	-8	.0591582	-.885524
-12	-4	-.0594723	-.866284
-8	-4	-.0397272	-.866608
8	-4	.0397272	-.866608
12	-4	.0594723	-.866284
-16	0	-.0795169	-.846323
-12	0	-.0597912	-.846716
-8	0	-.0399261	-.847002
8	0	.0399261	-.847002
12	0	.0597912	-.846716
16	0	.0795169	-.846323
-12	4	-.060016	-.826863
-8	4	-.0400907	-.8271
8	4	.0400907	-.8271
12	4	.060016	-.826863
-12	8	-.0602357	-.806735
-8	8	-.0402225	-.806953
-4	8	-.0201337	-.807082
0	8	0	-.807128
4	8	.0201337	-.807082
8	8	.0402225	-.806953
12	8	.0602357	-.806735
-8	12	-.040342	-.786581
-4	12	-.0201873	-.786701
0	12	0	-.786708
4	12	.0201873	-.786701
8	12	.040342	-.786581
0	16	0	-.766134

Average X Value is: 0 Average Y Value is:-.846278
Mean X Spread is .0429425 Mean Y Spread is .0425057 (Inches)

Range is: 5 Kilometers
Image is on the axis
The following dimensions are in inches

XP	YP	XF	YF
0	-16	0	-.015691
-8	-12	-7.87628E-03	-.0118134
-4	-12	-3.94398E-03	-.0118313
0	-12	0	-.0118649
4	-12	3.94398E-03	-.0118313
8	-12	7.87628E-03	-.0118134
-12	-8	-.0118134	-7.87628E-03
-8	-8	-7.90596E-03	-7.90596E-03
-4	-8	-3.96723E-03	-7.93445E-03
0	-8	0	-7.94721E-03
4	-8	3.96723E-03	-7.93445E-03
8	-8	7.90596E-03	-7.90596E-03
12	-8	.0118134	-7.87628E-03
-12	-4	-.0118313	-3.94398E-03
-8	-4	-7.93445E-03	-3.96723E-03
8	-4	7.93445E-03	-3.96723E-03
12	-4	.0118313	-3.94398E-03
-16	0	-.015691	0
-12	0	-.0118649	0
-8	0	-7.94721E-03	0
8	0	7.94721E-03	0
12	0	.0118649	0
16	0	.015691	0
-12	4	-.0118313	3.94398E-03
-8	4	-7.93445E-03	3.96723E-03
8	4	7.93445E-03	3.96723E-03
12	4	.0118313	3.94398E-03
-12	8	-.0118134	7.87628E-03
-8	8	-7.90596E-03	7.90596E-03
-4	8	-3.96723E-03	7.93445E-03
0	8	0	7.94721E-03
4	8	3.96723E-03	7.93445E-03
8	8	7.90596E-03	7.90596E-03
12	8	.0118134	7.87628E-03
-8	12	-7.87628E-03	.0118134
-4	12	-3.94398E-03	.0118313
0	12	0	.0118649
4	12	3.94398E-03	.0118313
8	12	7.87628E-03	.0118134
0	16	0	.015691

Average X Value is: 0
Mean X Spread is 8.50527E-03

Average Y Value is: 0
Mean Y Spread is 8.50527E-03 (Inches)

Range is: 5 Kilometers
Image Height is 21.8166 meters off the axis
The following dimensions are in inches

XP	YP	XF	YF
0	-16	0	-.859218
-8	-12	-7.74634E-03	-.856506
-4	-12	-3.87877E-03	-.856673
0	-12	0	-.85677
4	-12	3.87877E-03	-.856673
8	-12	7.74634E-03	-.856506
-12	-8	-.0118935	-.853379
-8	-8	-7.96402E-03	-.853664
-4	-8	-3.99673E-03	-.853845
0	-8	0	-.85391
4	-8	3.99673E-03	-.853845
8	-8	7.96402E-03	-.853664
12	-8	.0118935	-.853379
-12	-4	-.012202	-.850231
-8	-4	-8.1768E-03	-.850504
8	-4	8.1768E-03	-.850504
12	-4	.012202	-.850231
-16	0	-.0165601	-.846421
-12	0	-.012512	-.846775
-8	0	-8.38113E-03	-.84703
8	0	8.38113E-03	-.84703
12	0	.012512	-.846775
16	0	.0165601	-.846421
-12	4	-.0127656	-.843025
-8	4	-8.55422E-03	-.843261
8	4	8.55422E-03	-.843261
12	4	.0127656	-.843025
-12	8	-.0130246	-.839003
-8	8	-8.72123E-03	-.839226
-4	8	-4.37325E-03	-.839354
0	8	0	-.839384
4	8	4.37325E-03	-.839354
8	8	8.72123E-03	-.839226
12	8	.0130246	-.839003
-8	12	-8.87644E-03	-.834923
-4	12	-4.44823E-03	-.835048
0	12	0	-.83508
4	12	4.44823E-03	-.835048
8	12	8.87644E-03	-.834923
0	16	0	-.830552

Average X Value is: 0 Average Y Value is:-.846316
Mean X Spread is 8.97838E-03 Mean Y Spread is 7.76659E-03 (Inches)

Range is: 10 Kilometers
Image is on the axis
The following dimensions are in inches

XP	YP	XF	YF
0	-16	0	-7.90453E-03
-8	-12	-3.98004E-03	-5.96929E-03
-4	-12	-1.9967E-03	-5.9886E-03
0	-12	0	-6.01959E-03
4	-12	1.9967E-03	-5.9886E-03
8	-12	3.98004E-03	-5.96929E-03
-12	-8	-5.96929E-03	-3.98004E-03
-8	-8	-4.0077E-03	-4.0077E-03
-4	-8	-2.0166E-03	-4.03321E-03
0	-8	0	-4.04418E-03
4	-8	2.0166E-03	-4.03321E-03
8	-8	4.0077E-03	-4.0077E-03
12	-8	5.96929E-03	-3.98004E-03
-12	-4	-5.9886E-03	-1.9967E-03
-8	-4	-4.03333E-03	-2.01666E-03
8	-4	4.03333E-03	-2.01666E-03
12	-4	5.9886E-03	-1.9967E-03
-16	0	-7.90453E-03	0
-12	0	-6.01959E-03	0
-8	0	-4.04418E-03	0
8	0	4.04418E-03	0
12	0	6.01959E-03	0
16	0	7.90453E-03	0
-12	4	-5.9886E-03	1.9967E-03
-8	4	-4.03333E-03	2.01666E-03
8	4	4.03333E-03	2.01666E-03
12	4	5.9886E-03	1.9967E-03
-12	8	-5.96929E-03	3.98004E-03
-8	8	-4.0077E-03	4.0077E-03
-4	8	-2.0166E-03	4.03321E-03
0	8	0	4.04418E-03
4	8	2.0166E-03	4.03321E-03
8	8	4.0077E-03	4.0077E-03
12	8	5.96929E-03	3.98004E-03
-8	12	-3.98004E-03	5.96929E-03
-4	12	-1.9967E-03	5.9886E-03
0	12	0	6.01959E-03
4	12	1.9967E-03	5.9886E-03
8	12	3.98004E-03	5.96929E-03
0	16	0	7.90453E-03

Average X Value is: 0
Mean X Spread is 4.30413E-03

Average Y Value is: 0
Mean Y Spread is 4.30412E-03 (Inches)

Range is 10 Kilometers
Image Height is 43.6332 meters off the axis
The following dimensions are in inches

XP	YP	XF	YF
0	-16	0	-.851206
-8	-12	-3.79801E-03	.850464
-4	-12	-1.91182E-03	-.850652
0	-12	0	-.850719
4	-12	1.91182E-03	-.850652
8	-12	3.79801E-03	-.850464
-12	-8	-5.97191E-03	-.849357
-8	-8	-4.02844E-03	-.849647
-4	-8	-2.02841E-03	-.849822
0	-8	0	-.849882
4	-8	2.02841E-03	.849822
8	-8	4.02844E-03	-.849647
12	-8	5.97191E-03	-.849357
-12	-4	-6.28614E-03	-.848231
-8	-4	-4.2361E-03	-.848492
8	-4	4.2361E-03	-.848492
12	-4	6.28614E-03	-.848231
-16	0	-8.68964E-03	-.846442
-12	0	-6.5968E-03	-.846788
-8	0	-4.43411E-03	-.847034
8	0	4.43411E-03	-.847034
12	0	6.5968E-03	-.846788
16	0	8.68964E-03	-.846442
-12	4	-6.85215E-03	-.84506
-8	4	-4.62079E-03	-.845277
8	4	4.62079E-03	-.845277
12	4	6.85215E-03	-.84506
-12	8	-7.1156E-03	-.843056
-8	8	-4.77994E-03	-.843262
-4	8	-2.39944E-03	-.843392
0	8	0	-.843425
4	8	2.39944E-03	-.843392
8	8	4.77994E-03	-.843262
12	8	7.1156E-03	-.843056
-8	12	-4.93717E-03	-.840992
-4	12	-2.48098E-03	-.841102
0	12	0	-.841138
4	12	2.48098E-03	-.841102
8	12	4.93717E-03	-.840992
0	16	0	-.838642

Average X Value is: 0
Mean X Spread is 4.73449E-03

Average Y Value is: -.846329
Mean Y Spread is 3.40049E-03 (Inches)

Range is: 100 Kilometers
Image is on the axis
The following dimensions are in inches

XP	YP	XF	YF
0	-16	0	-9.09567E-04
-8	-12	-4.78506E-04	-7.19547E-04
4	-12	2.40982E-04	-7.25985E-04
0	-12	0	-7.65085E-04
4	-12	2.40982E-04	-7.25985E-04
8	-12	4.78506E-04	-7.19547E-04
-12	-8	-7.19547E-04	-4.78506E-04
-8	-8	-5.08666E-04	-5.08666E-04
-4	-8	-2.62856E-04	-5.25713E-04
0	-8	0	-5.38588E-04
4	-8	2.62856E-04	-5.25713E-04
8	-8	5.08666E-04	-5.08666E-04
12	-8	7.19547E-04	-4.78506E-04
-12	-4	-7.25985E-04	-2.40982E-04
-8	-4	-5.25713E-04	-2.62856E-04
8	-4	5.25713E-04	-2.62856E-04
12	-4	7.25985E-04	-2.40982E-04
-16	0	-9.09567E-04	0
-12	0	-7.65085E-04	0
-8	0	-5.38588E-04	0
8	0	5.38588E-04	0
12	0	7.65085E-04	0
16	0	9.09567E-04	0
-12	4	-7.25985E-04	2.40982E-04
-8	4	-5.25713E-04	2.62856E-04
8	4	5.25713E-04	2.62856E-04
12	4	7.25985E-04	2.40982E-04
-12	8	-7.19547E-04	4.78506E-04
-8	8	-5.08666E-04	5.08666E-04
-4	8	-2.62856E-04	5.25713E-04
0	8	0	5.38588E-04
4	8	2.62856E-04	5.25713E-04
8	8	5.08666E-04	5.08666E-04
12	8	7.19547E-04	4.78506E-04
-8	12	-4.78506E-04	7.19547E-04
-4	12	-2.40982E-04	7.25985E-04
0	12	0	7.65085E-04
4	12	2.40982E-04	7.25985E-04
8	12	4.78506E-04	7.19547E-04
0	16	0	9.09567E-04

Average X Value is: 0
Mean X Spread is 5.27961E-04

Average Y Value is: 0
Mean Y Spread is 5.27961E-04 (Inches)

Range is 50 kilometers
Image is on the grid
The following dimensions are in inches

xP	yP	yF	yF
0	-16	0	1.69773E+03
-8	-12	-8.64864E-04	-1.29652E-03
-4	-12	-4.36783E-04	-1.31321E-03
0	-12	0	-1.34659E-03
4	-12	4.36783E-04	-1.31321E-03
8	-12	8.64864E-04	-1.29652E-03
-12	-8	-1.29652E-03	-8.64864E-04
-8	-8	-8.89778E-04	-8.89778E-04
-4	-8	-4.59313E-04	-9.18627E-04
0	-8	0	-9.28403E-04
4	-8	4.59313E-04	-9.18627E-04
8	-8	8.89778E-04	-8.89778E-04
12	-8	1.29652E-03	-8.64864E-04
16	-8	1.31321E-03	-4.36783E-04
-16	-4	-9.18627E-04	-4.59313E-04
8	-4	9.18627E-04	-4.59313E-04
12	-4	1.31321E-03	-4.36783E-04
-16	0	-1.69773E-03	0
16	0	-1.34659E-03	0
8	0	9.28403E-04	0
8	0	9.28403E-04	0
12	0	1.34659E-03	0
16	0	1.69773E-03	0
-12	4	-1.31321E-03	4.36783E-04
-8	4	-9.18627E-04	4.59313E-04
8	4	9.18627E-04	4.59313E-04
12	4	1.31321E-03	4.36783E-04
12	8	1.29652E-03	8.64864E-04
-8	8	-8.89778E-04	8.89778E-04
-4	8	-4.59313E-04	9.18627E-04
0	8	0	9.28403E-04
4	8	4.59313E-04	9.18627E-04
8	8	8.89778E-04	8.89778E-04
12	8	1.29652E-03	8.64864E-04
-8	12	-8.64864E-04	1.29652E-03
-4	12	-4.36783E-04	1.31321E-03
0	12	0	1.34659E-03
4	12	4.36783E-04	1.31321E-03
8	12	8.64864E-04	1.29652E-03
0	16	0	1.69773E-03

Average X Value is 0
Mean X Spread is 9.4704E-04

Average Y Value is 0
Mean Y Spread is 9.4704E-04 (Inches)

Range Test on Parameters
Energy Output in 100,000 meters with Time Axis
Box-Cox Power Transformations are in Inches

Obs	Y	X1	X2
1	1.00	0	-.0464115
2	1.00	-2.32441E-04	.0470636
3	-12	-3.42071E+04	-.0458647
4	-12	0	-.0458692
5	-12	3.42071E+04	-.0458642
6	-12	6.13704E+04	.0456536
7	12	-1.22669E+05	-.0461461
8	-11	-8.80957E+04	-.0461439
9	-11	-4.16358E+04	-.0462596
10	-11	0	-.0466665
11	11	4.46857E+04	.0462996
12	11	8.80957E+04	-.0464039
13	11	1.22669E+05	.0461461
14	9	1.56308E+05	-.0462531
15	9	1.88349E+05	.0460891
16	9	2.18049E+05	-.0460891
17	9	2.46357E+05	.0460531
18	6	-2.39943E+05	-.0460501
19	6	-1.97688E+05	.0462999
20	6	-1.57971E+05	.0462035
21	6	-1.19E+05	.0461035
22	6	-8.13604E+04	-.0460999
23	6	-4.36024E+04	-.0460458
24	4	-1.02603E+04	-.0460035
25	4	1.46357E+05	.0460501
26	4	4.36357E+04	-.0460501
27	4	7.13523E+04	.0460966
28	4	9.80042E+04	-.0462692
29	8	-1.62784E+05	-.0464973
30	8	-1.05511E+04	-.0466615
31	8	0	.0466604
32	8	1.05511E+04	-.0466615
33	8	1.62784E+05	.0464973
34	8	2.20044E+05	-.0462692
35	12	1.78350E+05	.0458576
36	12	9.01043E+04	-.0459916
37	12	0	-.0459914
38	12	-9.01043E+04	.0459916
39	12	-1.78350E+05	-.0460036
40	16	0	-.0460069

Average X Value (m) = 0
Mean X Spread (s) = 1.36861E+05

Average Y Value (m) = -.0462541
Mean Y Spread (s) = 4.10820E-04 (Inches)

Range is: 100 Kilometers
Image Height is 436.332 meters off the axis
The following dimensions are in inches

XP	YP	XF	YF
0	-16	0	-.84399
-8	-12	-2.64525E-04	-.845064
-4	-12	-1.45733E-04	-.845243
0	-12	0	-.845308
4	-12	1.45733E-04	-.845243
8	-12	2.64525E-04	-.845064
-12	-8	-6.68049E-04	-.845759
-8	-8	-4.8089E-04	-.846031
-4	-8	-2.49386E-04	-.846191
0	-8	0	-.846256
4	-8	2.49386E-04	-.846191
8	-8	4.8089E-04	-.846031
12	-8	6.68049E-04	-.845759
-12	-4	-9.95159E-04	-.846434
-8	-4	-6.85692E-04	-.846688
0	-4	6.85692E-04	-.846688
12	-4	9.95159E-04	-.846434
-16	0	-1.61338E-03	-.846463
-12	0	-1.28698E-03	-.846798
-8	0	-8.85248E-04	-.847036
8	0	8.85248E-04	-.847036
12	0	1.28698E-03	-.846798
16	0	1.61338E-03	-.846463
-12	4	-1.55902E-03	-.846873
-8	4	-1.07837E-03	-.847098
8	4	1.07837E-03	-.847098
12	4	1.55902E-03	-.846873
-12	8	-1.80769E-03	-.846686
-8	8	-1.23298E-03	-.846901
-4	8	-6.26385E-04	-.847024
0	8	0	-.847066
4	8	6.26385E-04	-.847024
8	8	1.23298E-03	-.846901
12	8	1.80769E-03	-.846686
-8	12	-1.39189E-03	-.846442
-4	12	-7.05481E-04	-.846564
0	12	0	-.846603
4	12	7.05481E-04	-.846564
8	12	1.39189E-03	-.846442
0	16	0	-.845887

Average X Value is: 0
Mean X Spread is 9.62894E-04

Average Y Value is: -.846343
Mean Y Spread is 2.44141E-04 (Inches)

Range is: 500 Kilometers
Image is on the axis
The following dimensions are in inches

XP	YP	XF	YF
0	-16	0	-2.94924E-04
-8	-12	-1.62005E-04	-2.41041E-04
-4	-12	-8.76784E-05	-2.63214E-04
0	-12	0	-2.93493E-04
4	-12	8.76784E-05	-2.63214E-04
8	-12	1.62005E-04	-2.41041E-04
-12	-8	-2.41041E-04	-1.62005E-04
-8	-8	-1.94311E-04	-1.94311E-04
-4	-8	-1.05739E-04	-2.11477E-04
0	-8	0	-2.31028E-04
4	-8	1.05739E-04	-2.11477E-04
8	-8	1.94311E-04	-1.94311E-04
12	-8	2.41041E-04	-1.62005E-04
-12	-4	-2.63214E-04	-8.76784E-05
-8	-4	-2.11477E-04	-1.05739E-04
8	-4	2.11477E-04	-1.05739E-04
12	-4	2.63214E-04	-8.76784E-05
-16	0	-2.94924E-04	0
-12	0	-2.93493E-04	0
-8	0	-2.31028E-04	0
8	0	2.31028E-04	0
12	0	2.93493E-04	0
16	0	2.94924E-04	0
-12	4	-2.63214E-04	8.76784E-05
-8	4	-2.11477E-04	1.05739E-04
8	4	2.11477E-04	1.05739E-04
12	4	2.63214E-04	8.76784E-05
-12	8	-2.41041E-04	1.62005E-04
-8	8	-1.94311E-04	1.94311E-04
-4	8	-1.05739E-04	2.11477E-04
0	8	0	2.31028E-04
4	8	1.05739E-04	2.11477E-04
8	8	1.94311E-04	1.94311E-04
12	8	2.41041E-04	1.62005E-04
-8	12	-1.62005E-04	2.41041E-04
-4	12	-8.76784E-05	2.63214E-04
0	12	0	2.93493E-04
4	12	8.76784E-05	2.63214E-04
8	12	1.62005E-04	2.41041E-04
0	16	0	2.94924E-04

Average X Value is: 0
Mean X Spread is 1.91891E-04

Average Y Value is: 0
Mean Y Spread is 1.91891E-04 (Inches)

Range is: 500 Kilometers
Image Height is 2181.66 meters off the axis
The following dimensions are in inches

XF	YF	XF	YF
0	-16	0	-.84337
-8	-12	4.13656E-05	-.844596
-4	-12	1.5974E-05	-.844751
0	-12	0	-.844815
4	-12	-1.5974E-05	-.844751
8	-12	-4.13656E-05	-.844596
-12	-8	-2.04325E-04	-.84545
-8	-8	-1.7488E-04	-.845722
-4	-8	-1.01626E-04	-.845886
0	-8	0	-.845941
4	-8	1.01626E-04	-.845886
8	-8	1.7488E-04	-.845722
12	-8	2.04325E-04	-.84545
-12	-4	-5.26905E-04	-.846274
-8	-4	-3.7837E-04	-.846526
8	-4	3.7837E-04	-.846526
12	-4	5.26905E-04	-.846274
-16	0	-9.81331E-04	-.84647
-12	0	-8.14676E-04	-.846801
-8	0	-5.78523E-04	-.847039
8	0	5.78523E-04	-.847039
12	0	8.14676E-04	-.846801
16	0	9.81331E-04	-.84647
-12	4	-1.09386E-03	-.847036
-8	4	-7.56025E-04	-.847266
8	4	7.56025E-04	-.847266
12	4	1.09386E-03	-.847036
-12	8	-1.33181E-03	-.847014
-8	8	-9.1207E-04	-.847232
-4	8	-4.69565E-04	-.847345
0	8	0	-.847383
4	8	4.69565E-04	-.847345
8	8	9.1207E-04	-.847232
12	8	1.33181E-03	-.847014
-8	12	-1.07396E-03	-.846935
-4	12	-5.486e1E-04	-.84704
0	12	0	-.847098
4	12	5.486e1E-04	-.84704
8	12	1.07396E-03	-.846935
0	16	0	-.84655

Average X Value is: 0
Mean X Spread is 6.52511E-04

Average Y Value is: -.846348
Mean Y Spread is 4.88281E-04 (Inches)

Range is: 1000 Kilometers
Image is on the axis
The following dimensions are in inches

XP	YP	XF	YF
0	-16	0	-2.10047E-04
-8	-12	-1.20878E-04	-1.80721E-04
-4	-12	-6.92606E-05	-2.05278E-04
0	-12	0	-2.33412E-04
4	-12	6.92606E-05	-2.05278E-04
8	-12	1.20878E-04	-1.80721E-04
-12	-8	-1.80721E-04	-1.20878E-04
-8	-8	-1.56403E-04	-1.56403E-04
-4	-8	-8.54135E-05	-1.70827E-04
0	-8	0	-1.90735E-04
4	-8	8.54135E-05	-1.70827E-04
8	-8	1.56403E-04	-1.56403E-04
12	-8	1.80721E-04	-1.20878E-04
-12	-4	-2.05278E-04	-6.92606E-05
-8	-4	-1.70827E-04	-8.54135E-05
-4	-4	1.70827E-04	-8.54135E-05
0	-4	2.05278E-04	-6.92606E-05
4	-4	-2.10047E-04	0
8	-4	-2.33412E-04	0
12	-4	-1.90735E-04	0
-16	0	1.90735E-04	0
-12	0	2.33412E-04	0
-8	0	2.10047E-04	0
-4	0	-2.05278E-04	6.92606E-05
0	0	-1.70827E-04	8.54135E-05
4	0	1.70827E-04	8.54135E-05
8	0	2.05278E-04	6.92606E-05
12	0	-1.80721E-04	1.20878E-04
16	0	-1.56403E-04	1.56403E-04
-12	4	-8.54135E-05	1.70827E-04
-8	4	0	1.90735E-04
-4	4	8.54135E-05	1.70827E-04
0	4	1.56403E-04	1.56403E-04
4	4	1.80721E-04	1.20878E-04
8	4	-1.20878E-04	1.80721E-04
12	4	-6.92606E-05	2.05278E-04
-8	8	0	2.33412E-04
-4	8	6.92606E-05	2.05278E-04
0	8	1.20878E-04	1.80721E-04
4	8	0	2.10047E-04
8	8		
12	8		
-8	12		
-4	12		
0	12		
4	12		
8	12		
0	16		

Average X Value is: 0
Mean X Spread is: 1.4921E-04

Average Y Value is: 0
Mean Y Spread is: 1.4921E-04 (Inches)

Range is: 5000 Kilometers
Image is on the axis
The following dimensions are in inches

XP	YP	XF	YF
0	-16	0	1.4782E-04
-8	-12	-8.92878E-05	-1.34945E-04
-4	-12	-5.33462E-05	-1.60933E-04
0	-12	0	-1.89781E-04
4	-12	5.33462E-05	-1.60933E-04
8	-12	8.92878E-05	-1.34945E-04
-12	-8	-1.34945E-04	-8.92878E-05
-8	-8	-1.24574E-04	-1.24574E-04
-4	-8	-7.00951E-05	-1.4019E-04
0	-8	0	-1.58668E-04
4	-8	7.00951E-05	-1.4019E-04
8	-8	1.24574E-04	-1.24574E-04
12	-8	1.34945E-04	-8.92878E-05
-12	-4	-1.60933E-04	-5.33462E-05
-8	-4	-1.4019E-04	-7.00951E-05
8	-4	1.4019E-04	-7.00951E-05
12	-4	1.60933E-04	-5.33462E-05
-16	0	-1.4782E-04	0
-12	0	-1.89781E-04	0
-8	0	-1.58668E-04	0
8	0	1.58668E-04	0
12	0	1.89781E-04	0
16	0	1.4782E-04	0
-12	4	-1.60933E-04	5.33462E-05
-8	4	-1.4019E-04	7.00951E-05
8	4	1.4019E-04	7.00951E-05
12	4	1.60933E-04	5.33462E-05
-12	8	-1.34945E-04	8.92878E-05
-8	8	-1.24574E-04	1.24574E-04
-4	8	-7.00951E-05	1.4019E-04
0	8	0	1.58668E-04
4	8	7.00951E-05	1.4019E-04
8	8	1.24574E-04	1.24574E-04
12	8	1.34945E-04	8.92878E-05
-8	12	-8.92878E-05	1.34945E-04
-4	12	-5.33462E-05	1.60933E-04
0	12	0	1.89781E-04
4	12	5.33462E-05	1.60933E-04
8	12	8.92878E-05	1.34945E-04
0	16	0	1.4782E-04

Average X Value is: 0 Average Y Value is: 0
Mean X Spread is 1.16848E-04 Mean Y Spread is 1.16848E-04 (Inches)

Range is: 1000 Kilometers
Image Height is 4363.32 meters off the axis
The following dimensions are in inches

XP	YP	XF	YF
0	-16	0	-.847274
-8	-12	8.15392E-05	-.844535
-4	-12	3.54648E-05	-.844692
0	-12	0	-.844757
4	-12	-3.54648E-05	-.844692
8	-12	-8.15392E-05	-.844535
-12	-8	-1.42574E-04	-.845405
-8	-8	-1.33634E-04	-.845683
-4	-8	-8.05855E-05	-.845848
0	-8	0	-.845902
4	-8	8.05855E-05	-.845848
8	-8	1.33634E-04	-.845683
12	-8	1.42574E-04	-.845405
-12	-4	-4.55856E-04	-.846261
-8	-4	-3.44753E-04	-.846516
8	-4	3.44753E-04	-.846516
12	-4	4.55856E-04	-.846261
-16	0	-9.10282E-04	-.84647
-12	0	-7.56025E-04	-.846798
-8	0	-5.3525E-04	-.847039
8	0	5.3525E-04	-.847039
12	0	7.56025E-04	-.846798
16	0	9.10282E-04	-.84647
-12	4	-1.01972E-03	-.847064
-8	4	-7.1764E-04	-.847282
0	4	7.1764E-04	-.847282
12	4	1.01972E-03	-.847064
-12	8	-1.26529E-03	-.847061
-8	8	-8.83937E-04	-.847256
-4	8	-4.51326E-04	-.847382
0	8	0	-.847432
4	8	4.51326E-04	-.847382
8	8	8.83937E-04	-.847256
12	8	1.26529E-03	-.847061
-8	12	-1.03426E-03	-.846993
-4	12	-5.28038E-04	-.847102
0	12	0	-.847162
4	12	5.28038E-04	-.847102
8	12	1.03426E-03	-.846993
0	16	0	-.846606

Average X Value is: 0
Mean X Spread is 6.14625E-04

Average Y Value is: -.846348
Mean Y Spread is 8.45728E-04 (Inches)

Range is: 5000 Kilometers
Image Height is 21816.6 meters off the axis
The following dimensions are in inches

XP	YP	XF	YF
0	-16	0	-.843052
-8	-12	1.20044E-04	-.844406
-4	-12	4.44651E-05	-.844673
0	-12	0	-.844732
4	-12	-4.44651E-05	-.844673
8	-12	-1.20044E-04	-.844486
-12	-8	-1.09911E-04	-.845385
-8	-8	-1.03712E-04	-.845656
-4	-8	-6.1214E-05	-.845823
0	-8	0	-.845881
4	-8	6.1214E-05	-.845823
8	-8	1.03712E-04	-.845656
12	-8	1.09911E-04	-.845385
-12	-4	-4.21763E-04	-.846263
-8	-4	-3.18289E-04	-.846517
8	-4	3.18289E-04	-.846517
12	-4	4.21763E-04	-.846263
-16	0	-8.33273E-04	-.846474
-12	0	-7.20501E-04	-.846801
-8	0	-5.03778E-04	-.847043
8	0	5.03778E-04	-.847043
12	0	7.20501E-04	-.846801
16	0	8.33273E-04	-.846474
-12	4	-9.82523E-04	-.847079
-8	4	-6.84619E-04	-.847303
8	4	6.84619E-04	-.847303
12	4	9.82523E-04	-.847079
-12	8	-1.23286E-03	-.847081
-8	8	-8.533E-04	-.847286
-4	8	-4.3416E-04	-.847416
0	8	0	-.847453
4	8	4.3416E-04	-.847416
8	8	8.533E-04	-.847286
12	8	1.23286E-03	-.847081
-8	12	-1.00482E-03	-.847042
-4	12	-5.11348E-04	-.847157
0	12	0	-.847182
4	12	5.11348E-04	-.847157
8	12	1.00482E-03	-.847042
0	16	0	-.846672

Average X Value is: 0 Average Y Value is: -.846354
Mean X Spread is 5.88692E-04 Mean Y Spread is 6.90534E-04 (Inches)

Range is: 10000 Kilometers
Image is on the axis
The following dimensions are in inches

XP	YP	XF	YF
0	-16	0	-1.43766E-04
-8	-12	-8.70228E-05	-1.30177E-04
-4	-12	-5.16176E-05	-1.54018E-04
0	-12	0	-1.80721E-04
4	-12	5.16176E-05	-1.54018E-04
8	-12	8.70228E-05	-1.30177E-04
-12	-8	-1.30177E-04	-8.70228E-05
-8	-8	-1.22309E-04	-1.22309E-04
-4	-8	-6.83069E-05	-1.36614E-04
0	-8	0	-1.56522E-04
4	-8	6.83069E-05	-1.36614E-04
8	-8	1.22309E-04	-1.22309E-04
12	-8	1.30177E-04	-8.70228E-05
-12	-4	-1.54018E-04	-5.16176E-05
-8	-4	-1.36614E-04	-6.83069E-05
8	-4	1.36614E-04	-6.83069E-05
12	-4	1.54018E-04	-5.16176E-05
-16	0	-1.43766E-04	0
-12	0	-1.80721E-04	0
-8	0	-1.56522E-04	0
8	0	1.56522E-04	0
12	0	1.80721E-04	0
16	0	1.43766E-04	0
-12	4	-1.54018E-04	5.16176E-05
-8	4	-1.36614E-04	6.83069E-05
8	4	1.36614E-04	6.83069E-05
12	4	1.54018E-04	5.16176E-05
-12	8	-1.30177E-04	8.70228E-05
-8	8	-1.22309E-04	1.22309E-04
-4	8	-6.83069E-05	1.36614E-04
0	8	0	1.56522E-04
4	8	6.83069E-05	1.36614E-04
8	8	1.22309E-04	1.22309E-04
12	8	1.30177E-04	8.70228E-05
-8	12	-8.70228E-05	1.30177E-04
-4	12	-5.16176E-05	1.54018E-04
0	12	0	1.80721E-04
4	12	5.16176E-05	1.54018E-04
8	12	8.70228E-05	1.30177E-04
0	16	0	1.43766E-04

Average X Value is: 0 Average Y Value is: 0
Mean X Spread is: 1.13185E-04 Mean Y Spread is: 1.13185E-04 (Inches)

Range is: 100000 Kilometers
Image is on the axis
The following dimensions are in inches

XP	YP	XF	YF
0	-16	0	-1.33514E-04
-8	-12	-8.24928E-05	-1.24693E-04
-4	-12	-4.94123E-05	-1.46627E-04
0	-12	0	-1.75238E-04
4	-12	4.94123E-05	-1.46627E-04
8	-12	8.24928E-05	-1.24693E-04
-12	-8	-1.24693E-04	-8.24928E-05
-8	-8	-1.1754E-04	-1.1754E-04
-4	-8	-6.63996E-05	-1.32799E-04
0	-8	0	-1.51753E-04
4	-8	6.63996E-05	-1.32799E-04
8	-8	1.1754E-04	-1.1754E-04
12	-8	1.24693E-04	-8.24928E-05
-12	-4	-1.46627E-04	-4.94123E-05
-8	-4	-1.32799E-04	-6.63996E-05
8	-4	1.32799E-04	-6.63996E-05
12	-4	1.46627E-04	-4.94123E-05
-16	0	-1.33514E-04	0
-12	0	-1.75238E-04	0
-8	0	-1.51753E-04	0
8	0	1.51753E-04	0
12	0	1.75238E-04	0
16	0	1.33514E-04	0
-12	4	-1.46627E-04	4.94123E-05
-8	4	-1.32799E-04	6.63996E-05
8	4	1.32799E-04	6.63996E-05
12	4	1.46627E-04	4.94123E-05
-12	8	-1.24693E-04	8.24928E-05
-8	8	-1.1754E-04	1.1754E-04
-4	8	-6.63996E-05	1.32799E-04
0	8	0	1.51753E-04
4	8	6.63996E-05	1.32799E-04
8	8	1.1754E-04	1.1754E-04
12	8	1.24693E-04	8.24928E-05
-8	12	-8.24928E-05	1.24693E-04
-4	12	-4.94123E-05	1.46627E-04
0	12	0	1.75238E-04
4	12	4.94123E-05	1.46627E-04
8	12	8.24928E-05	1.24693E-04
0	16	0	1.33514E-04

Average X Value is: 0 Average Y Value is: 0
Mean X Spread is 1.08599E-04 Mean Y Spread is 1.08599E-04 (Inches)

Range is: 10000 Kilometers
Image Height is 43633.2 meters off the axis
The following dimensions are in inches

XP	YP	XF	YF
0	-16	0	-.843243
-8	-12	1.06931E-04	-.844563
-4	-12	4.19617E-05	-.844731
0	-12	0	-.844794
4	-12	-4.19617E-05	-.844731
8	-12	-1.06931E-04	-.844563
-12	-8	-1.11341E-04	-.845432
-8	-8	-1.15514E-04	-.845709
-4	-8	-6.83069E-05	-.845865
0	-8	0	-.845917
4	-8	6.83069E-05	-.845865
8	-8	1.15514E-04	-.845709
12	-8	1.11341E-04	-.845432
-12	-4	-4.22239E-04	-.846281
-8	-4	-3.22461E-04	-.846537
8	-4	3.22461E-04	-.846537
12	-4	4.22239E-04	-.846281
-16	0	-8.44956E-04	-.846473
-12	0	-7.06196E-04	-.846814
-8	0	-4.9293E-04	-.847053
8	0	4.9293E-04	-.847053
12	0	7.06196E-04	-.846814
16	0	8.44956E-04	-.846473
-12	4	-9.74417E-04	-.847082
-8	4	-6.81162E-04	-.847304
8	4	6.81162E-04	-.847304
12	4	9.74417E-04	-.847082
-12	8	-1.24145E-03	-.847076
-8	8	-8.53096E-04	-.84729
-4	8	-4.36544E-04	-.847421
0	8	0	-.84745
4	8	4.36544E-04	-.847421
8	8	8.53096E-04	-.84729
12	8	1.24145E-03	-.847076
-8	12	-1.00982E-03	-.847027
-4	12	-5.15759E-04	-.847135
0	12	0	-.847184
4	12	5.15759E-04	-.847135
8	12	1.00982E-03	-.847027
0	16	0	-.846666

Average X Value is: 0
Mean X Spread is 5.89136E-04

Average Y Value is: -.846371
Mean Y Spread is 5.45915E-04 (Inches)

Range is: 100000 Kilometers
Image Height is 436332 meters off the axis
The following dimensions are in inches

XP	YP	XF	YF
0	-16	0	-.843983
-8	-12	1.80006E-05	-.845089
-4	-12	-3.21865E-06	-.84526
0	-12	0	-.845314
4	-12	3.21865E-06	-.84526
8	-12	-1.80006E-05	-.845089
-12	-8	-2.44617E-04	-.845842
-8	-8	-1.98483E-04	-.846101
-4	-8	-1.08898E-04	-.846259
0	-8	0	-.846316
4	-8	1.08898E-04	-.846259
8	-8	1.98483E-04	-.846101
12	-8	2.44617E-04	-.845842
-12	-4	-5.43594E-04	-.846553
-8	-4	-3.95775E-04	-.846797
8	-4	3.95775E-04	-.846797
12	-4	5.43594E-04	-.846553
-16	0	-1.00017E-03	-.84665
-12	0	-8.13723E-04	-.846979
-8	0	-5.79357E-04	-.847208
8	0	5.79357E-04	-.847208
12	0	8.13723E-04	-.846979
16	0	1.00017E-03	-.84665
-12	4	-1.09124E-03	-.847116
-8	4	-7.56025E-04	-.847337
8	4	7.56025E-04	-.847337
12	4	1.09124E-03	-.847116
-12	8	-1.21617E-03	-.847093
-8	8	-8.43048E-04	-.847295
-4	8	-4.30465E-04	-.847426
0	8	0	-.847469
4	8	4.30465E-04	-.847426
8	8	8.43048E-04	-.847295
12	8	1.21617E-03	-.847093
-8	12	-1.07443E-03	-.846827
-4	12	-5.4072E-04	-.846934
0	12	0	-.846987
4	12	5.4072E-04	-.846934
8	12	1.07443E-03	-.846827
0	16	0	-.846358

Average X Value is: 0
Mean X Spread is 6.385418E-04

Average Y Value is: -.846549
Mean Y Spread is

Range is: .3 Kilometer
Image is on the axis
The following dimensions are in inches

XP	YP	XF	YF
0	-16	0	-3.12328E-05
-8	-12	6.65188E-05	1.01805E-04
-4	-12	7.52211E-05	2.27213E-04
0	-12	0	2.55585E-04
4	-12	-7.52211E-05	2.27213E-04
8	-12	-6.65188E-05	1.01805E-04
-12	-8	1.01805E-04	6.65188E-05
-8	-8	2.03967E-04	2.03967E-04
-4	-8	1.46389E-04	2.92778E-04
0	-8	0	3.06726E-04
4	-8	-1.46389E-04	2.92778E-04
8	-8	-2.03967E-04	2.03967E-04
12	-8	-1.01805E-04	6.65188E-05
-12	-4	2.27213E-04	7.52211E-05
-8	-4	2.92778E-04	1.46389E-04
8	-4	-2.92778E-04	1.46389E-04
12	-4	-2.27213E-04	7.52211E-05
-16	0	-3.12328E-05	0
-12	0	2.55585E-04	0
-8	0	3.06726E-04	0
8	0	-3.06726E-04	0
12	0	-2.55585E-04	0
16	0	3.12328E-05	0
-12	4	2.27213E-04	-7.52211E-05
-8	4	2.92778E-04	-1.46389E-04
8	4	-2.92778E-04	-1.46389E-04
12	4	-2.27213E-04	-7.52211E-05
-12	8	1.01805E-04	-6.65188E-05
-8	8	2.03967E-04	-2.03967E-04
-4	8	1.46389E-04	-2.92778E-04
0	8	0	-3.06726E-04
4	8	-1.46389E-04	-2.92778E-04
8	8	-2.03967E-04	-2.03967E-04
12	8	-1.01805E-04	-6.65188E-05
-8	12	6.65188E-05	-1.01805E-04
-4	12	7.52211E-05	-2.27213E-04
0	12	0	-2.55585E-04
4	12	-7.52211E-05	-2.27213E-04
8	12	-6.65188E-05	-1.01805E-04
0	16	0	3.12328E-05

Average X Value is: 0
Mean X Spread is: 1.73498E-04

Average Y Value is: 0
Mean Y Spread is: 1.73498E-04 (Inches)

Range is: .5 Kilometer
Image Height is 1.308899 meters off the axis
The following dimensions are in inches

XP	YP	XF	YF
0	-16	0	-.829702
-8	-12	4.3416E-04	-.831041
-4	-12	2.61128E-04	-.831103
0	-12	0	-.831153
4	-12	-2.61128E-04	-.831103
8	-12	-4.3416E-04	-.831041
-12	-8	2.60592E-04	-.832088
-8	-8	3.08871E-04	-.83228
-4	-8	1.96397E-04	-.832396
0	-8	0	-.832436
4	-8	-1.96397E-04	-.832396
8	-8	-3.08871E-04	-.83228
12	-8	-2.60592E-04	-.832088
-12	-4	-1.43051E-06	-.833023
-8	-4	1.26481E-04	-.833295
8	-4	-1.26481E-04	-.833295
12	-4	1.43051E-06	-.833023
-16	0	-8.66652E-04	-.833171
-12	0	-3.7694E-04	-.833649
-8	0	-1.09434E-04	-.833985
8	0	1.09434E-04	-.833985
12	0	3.7694E-04	-.833649
16	0	8.66652E-04	-.833171
-12	4	-7.96795E-04	-.83387
-8	4	-3.94702E-04	-.834284
8	4	3.94702E-04	-.834284
12	4	7.96795E-04	-.83387
-12	8	-1.3361E-03	-.833592
-8	8	-7.49707E-04	-.834072
-4	8	-3.32356E-04	-.834363
0	8	0	-.834465
4	8	3.32356E-04	-.834363
8	8	7.49707E-04	-.834072
12	8	1.3361E-03	-.833592
-8	12	-1.15609E-03	-.833292
-4	12	-5.33462E-04	-.833628
0	12	0	-.833733
4	12	5.33462E-04	-.833628
8	12	1.15609E-03	-.833292
0	16	0	-.832357

Average X Value is: 0
Mean X Spread is 5.58981E-04

Average Y Value is: -.833003
Mean Y Spread is 8.80262E-04 (Inches)

Appendix E

IMPROVED LIDAR MEASUREMENTS BEARING ON SHIP-TO-SHIP LASER TRANSMISSION

T. D. Wilkerson

Institute for Physical
Science and Technology
University of Maryland

The test program for DF laser transmission between ships at sea could greatly benefit from the application of the full complement of lidar techniques that have been developed to date. These include humidity, temperature, aerosol abundance, wind, concentrations of air pollutants, and all of these as functions of time and distance along the range between ships. The principles and capabilities of lidar for atmospheric measurements have been reviewed in the Proceedings of the DoD Lidar Workships (Tucson, 1981), by R. M. Measures in Analytical Laser Spectroscopy (Ch. 6), Wiley (1979), and by E. D. Hinkley et al. in Laser Monitoring of the Atmosphere, Springer-Verlag (1976).

Unfortunately very few of the appropriate lidar devices are available for the Lexington measurement program in the summer of 1982, because on a nationwide average basis the levels of lidar funding have not been such as to keep a number of transportable systems running, or to permit a dedicated multipurpose installation to be built. A few possibilities exist for the summer of 1982, and these include the SRI Queen-Air - based NdYAG system for aerosols and the NASA-Langley Electra that contains aerosol, H_2O and ozone profiling systems (Nd:YAG + DIAL using dye lasers) though it may be attractive for the project to make use of these lidars, one should bear in mind that a decent measurement program for each is bound to cost $70,000 - $90,000 and the useful information output will likely be marginal in terms of the atmospheric variables and the space- and time-scales important for the DF propagation experiment.

In view of the general capabilities of lidar outlined below it is unfortunate that we cannot wait until summer of 1983, by which time a comprehensive, multi-purpose lidar system could be setup for about $400,000 - $500,000. It could also then be used for a number of other remote sensing applications of interest to the Navy.

An alternative exists that we will describe in this proposal, namely that a relatively novel lidar concept involving pulsed, low power HF and DF lasers

can be implemented quickly to give truly useful data in the 1982 tests - and perhaps then become the basis for more highly evolved versions to be used in subsequent years. The cost and other details of this concept are discussed below. The pulsed DF laser is advantageous for the measurements because the lidar returns will give light scattering and H_2O absorption information right in the band region of interest, and the lidar is eyesafe. We estimate that range resolutions for $[H_2O]$ of under 100-250 meters will be attainable and that ultimate ranges = 2 - 10 km will usually be possible. At first the main goals of the lidar will be to measure aerosols and $[H_2O]$.

General Lidar Capabilities - Comments

For airborne lidar systems used to define the state of the atmosphere during the Lexington tests, one needs to be concerned not only about the accuracy of measuring, say, the humidity but also about the spatial resolution of the measurements - both along the lidar beam direction and along the direction of aircraft flight. For downlooking humidity and temperature measurements, using DIAL methods in the near IR, height resolutions of order 100 m are typical. Given that 20 $\pm$ 10 Joules of optical output are needed by adding up lidar returns, one can expect a horizontal resolution along the flight track of order 1 $\pm$ 1/2 km. This horizontal resolution is just barely good enough relative to the need to document variations along the DF laser transmission range or across the ship's smokestack plume.

The spatial resolutions describing downlooking Nd:YAG measurements of aerosols are in better shape, say 10 meters vertically and 10 meters horizontally along the flight track. What these observations provide, however, is a relative concentration profile of aerosols. This may be useful for depicting local or regional airflows, inversions, etc., and is probably of very limited value for the HEL transmission experiment in question.

One might consider the possibility of using the SRI or NASA-Langly types of equipment actually on the ship with the lidar beam direction along the DF laser transmission direction. While this would provide some measurement advantages over the airborne mode, these laser systems are not eye safe and therefore could not be used in this way in the Lexington environment.

Proposed DF Lidar Measurement

One's attention is naturally drawn to the middle infrared for lidar measurements of atmospheric properties in tests such as the Lexington transmission experiment. In particular the DF regions can be used for range-resolved measurements of at least water vapor concentration and aerosol backscatter in the DF band. Other possibilities such as temperature and air pollutants are also under consideration, and there is some prospect of cross-check measurements using restricted parts of the HF laser line system.

We are proposing the rapid adaptation of existing equipment at NRL, to bring on-line a pulsed, single-mode line-selectable DF laser for atmospheric ranging work during the Lexington tests in 1982. This system will time-share optics with the DF transmission laser, and will make use of some of the same plumbing and gas-handling equipment. Still under study are technical questions involving the repetition rate of the pulsed DF system and the possibility of shortening the pulses to 0.1 μsec (from the present level of ∿ 1 μsec).

A preliminary study indicates that:

(a) sufficient aerosol backscatter will be available for DIAL measurements in the DF band, considering the typical transmitted pulse energy, ranges up to 10 km, and signal-to-noise considerations for the appropriate detectors.

(b) HDO can safely be used as a "spectroscopic surrogate" for H_2O in the DF band because the isotopic abundance ratio is fairly constant (0.03%) near sea level.

(c) The spectral match of high power DF lines with the absorption line spectrum of HDO is good as regards wavelengths, absorption strength, and temperature - insensitivity of the absorption (e.g., see the attached figure).

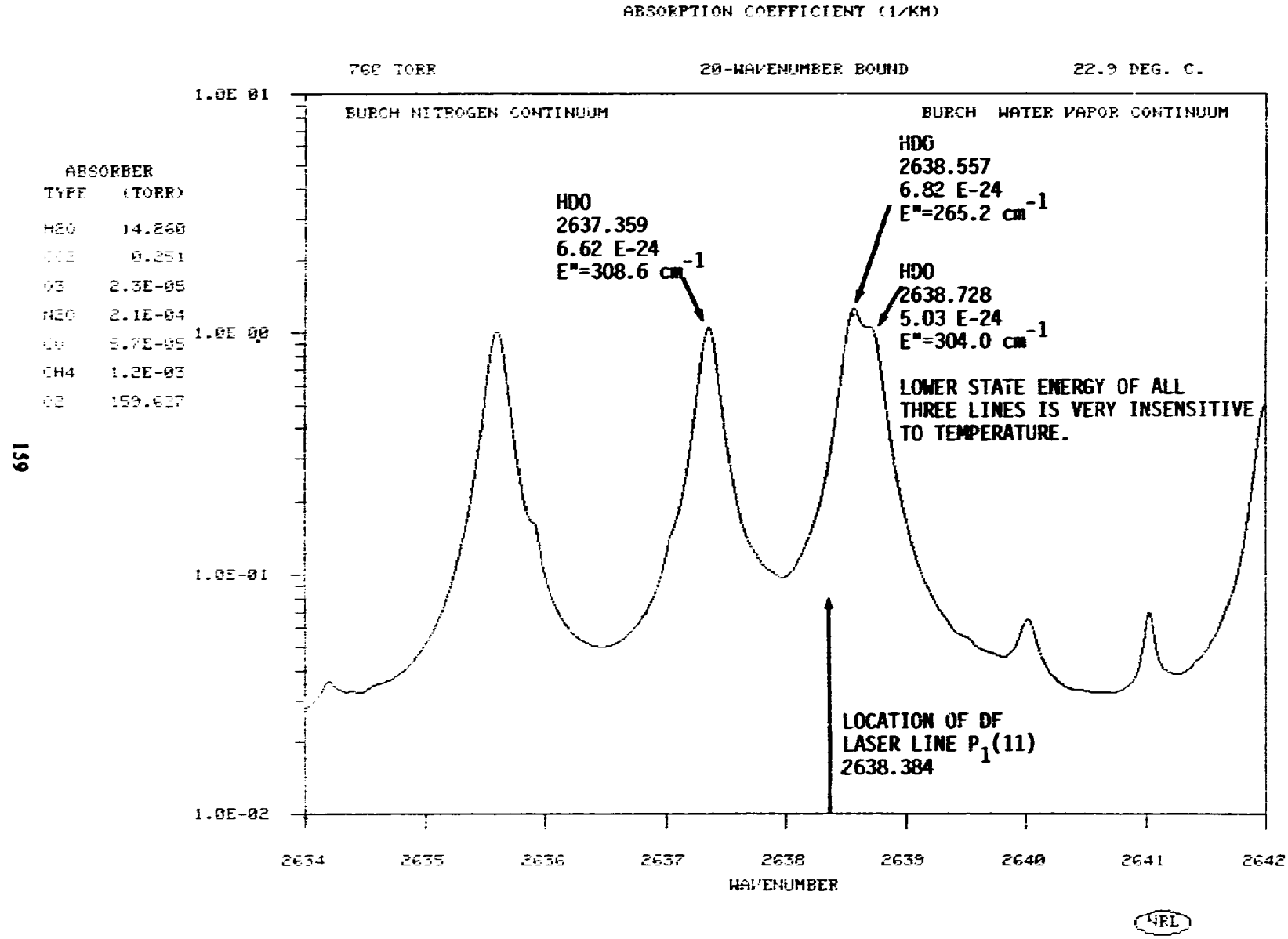
ABSORPTION COEFFICIENT (1/KM)
760 TORR
20-WAVENUMBER BOUND
22.9 DEG. C.
BURCH NITROGEN CONTINUUM
BURCH WATER VAPOR CONTINUUM
ABSORBER
TYPE (TORR)
H2O 14.260
CO2 0.251
O3 2.3E-05
N2O 2.1E-04
CO 5.7E-05
CH4 1.2E-03
O2 159.637
HDO
2637.359
6.62 E-24
E"=308.6 cm-1
HDO
2638.557
6.82 E-24
E"=265.2 cm-1
HDO
2638.728
5.03 E-24
E"=304.0 cm-1
LOWER STATE ENERGY OF ALL THREE LINES IS VERY INSENSITIVE TO TEMPERATURE.
LOCATION OF DF LASER LINE P1(11) 2638.384
1.0E 01
1.0E 00
1.0E-01
1.0E-02
2634
2635
2636
2637
2638
2639
2640
2641
2642
WAVENUMBER
NRL